



Jimma University
Jimma Institute of Technology
School of Graduate Studies
Faculty of Mechanical Engineering
Chair of Thermal System Engineering

*An Optimized Design of Heat Pipe Based Evacuated Tube Solar Water Heater
with Thermal Storage
(Case Study : - Wonji-Shoa Sugar Factory)*

By: Daniel Shitaye

*A Research Report Submitted to the School of Graduate Studies, Jimma
University; in Partial Fulfillment for the Requirement of Degree of Masters in
Thermal System Engineering*

June 2019
Jimma, Ethiopia



Jimma University
Jimma Institute of Technology
School of Graduate Studies
Faculty of Mechanical Engineering
Chair of Thermal System Engineering

*An Optimized Design of Heat Pipe Based Evacuated Tube Solar Water Heater
with Thermal Storage*

(Case Study : - Wonji-Shoa Sugar Factory)

*A Research Report Submitted to the School of Graduate Studies, Jimma
University; in Partial Fulfillment for the Requirement of Degree of Masters in
Thermal System Engineering*

By: Daniel Shitaye Lemma

Main Advisor: Balewgize Amare Zeru (Asst. Prof.)

Co-Advisor: Nebyou Bogale Mereke (Asst. Prof.)

June 2019

Jimma, Ethiopia

Abstract

Solar energy is one of the promising renewable sources in a direct and indirect methods of energy conversion. Solar water heating is simplest and most direct application of solar radiation into heat. The study aims to investigate design of solar water heating system for the case of Wonji-Shoa sugar factory milling plant section and heat transfer enhancement of Heat Pipe-Evacuated Tube Solar collector(HP-ETSc) using nanofluids numerically.

Nanofluids are nanotechnology-based heat transfer fluids that are derived by stably suspending nanometer-sized particles in conventional heat transfer fluid. Heat pipes are effective heat transfer devices in which the nanofluid operates in the two phases, evaporation and condensation; also known as nanofluidic heat pipe. ANSYS/FLUENT powerful CFD package used to compute the complex evaporation and condensation phenomena inside the thermosyphon heat pipe. Transient numerical simulation was used for prediction of heat transfer coefficients and thermal resistance of water, Al and Cu nanofluids in Two Phase Closed Thermosyphon-Heat Pipe (TPCT-HP) with 50% filling ratio of evaporator section at 4kPa initial pressure. The synthesized water nanofluid characterized 0.5 and 4.41vol% of Cu and Al with 25nm and 18nm particle size respectively. The various design parameters are gathered from solar water heater collector manufacturers official site, National Meteorology Agency and case site.

The analytical design parameters of the proposed system gives total number of 10 HP-ETSc modules with 1.15MWh annual sensible thermal energy storage. Annual contribution of solar system to heating load is 2.112MWh. The system save 40,356kg bagasse fuel for alternative use and 28,957.5kgCO₂ emissions to atmosphere is avoided. The economic analysis of the system was done with an initial total investment of 96,761ETBirr with 3.6years payback period. Numerical simulation result showed heat transfer coefficient increases by about 25.2% and 37.9% for Cu and Al nanofluid respectively as compared to water at evaporator section; on the other hand, Cu-water nanofluid is about 30.95% and 78.55% greater than those of Al nanofluid and water respectively. The overall thermal resistance for TPCT-HP is decreased by about 51.86% for Cu nanofluid, whereas it is reduced by 42.75% for Al nanofluid compared with water.

Key Words: *Solar energy, Heat pipe based evacuated tube solar water heater, Two-phase closed thermosyphon, CFD, Heat transfer coefficient, Thermal resistance.*

Acknowledgment

*First of all, I would like to thank to the **Almighty God** then I would like to thank my **Beloved Family and Friends** for giving me their support when I have needed it and having the patience of listening to my complaints and problems.*

*Also I would like to thank my main-advisor **Mr. Balewgize Amare**, my co-advisor **Mr. Nebyou bogale** and **Mr. Abiyou Solomon** for the referee of my thesis report and there help throughout in the stage of my Masters program. Finally, I would like tanks to **Jimma University, JIT** and **Facaluty of Mechanical Engineering** preparing this great chance.*

Table of Contents

Abstract	i
Acknowledgment	ii
Table of Contents	v
List of Tables	vi
List of Figures	viii
Abbreviations	ix
1 INTRODUCTION	1
1.1 Background	3
1.2 Statement of the Problem	5
1.3 Objectives	5
1.3.1 Main objective	5
1.3.2 Specific objectives	5
1.4 Delimitation	6
2 LITERATURE REVIEW	7
2.1 Solar Water Heater	7
2.2 Evacuated tube Collector Modeling	8
2.3 Thermal Storage Modeling	10

2.4	Heat pipe modeling	11
2.5	Nanofluid	13
3	METHODOLOGY	16
3.1	Working principle of HPETSc Solar Water Heater	17
3.2	Component's and Material's HPETSc	17
3.3	Site Assessment	19
3.4	Data Collection and Analysis	20
3.4.1	Solar Data	20
3.4.2	Solar Angles	23
3.4.3	Environmental Data	25
3.4.4	Estimation of Load	26
3.5	Synthesis of Nanofluids	27
3.5.1	Preparation Methods	28
3.5.2	Estimation of Nanofluids Physical Property	29
3.6	Software Programs	33
4	SOLAR THERMAL SYSTEM DESIGN	34
4.1	Thermal Analysis of HPETSc	34
4.1.1	Absorbed Solar Radiation	34
4.1.2	Energy Balance for the Collector components	35
4.1.3	Useful Energy	45
4.1.4	Collector Efficiency	45
4.2	Water Heating System Design	46
4.2.1	System and Component Descriptions	46
4.2.2	Collector Orientation	48
4.2.3	System Sizing	48
4.2.4	Thermal Performance of the System	50
4.2.5	Collector Installation	51
4.2.6	Pressure loss	52

5	TECHNO ECONOMIC ANALYSIS	54
5.1	Techno Economical Indicators	54
5.1.1	Total System Cost	55
5.1.2	Fuel Cost	55
5.1.3	Payback Period	56
5.2	Emission Estimation	57
6	MATHEMATICAL MODELING AND HEAT PIPE CFD ANALYSIS	58
6.1	General Governing Equation	58
6.1.1	Continuity Equation	59
6.1.2	Momentum Equation	59
6.1.3	Energy Equation	59
6.2	Numerical Modeling of Heat Pipe	60
6.2.1	Geometry	60
6.2.2	Mesh	60
6.2.3	Setup	61
6.2.4	Solution	65
6.3	CFD Result and Discussion	66
6.3.1	Result Analysis	66
6.3.2	Transient analysis of TPCHP	82
7	CONCLUSION AND FUTURE RECOMMENDATIONS	89
7.1	Conclusion	89
7.2	Recommendations and Future Work	92
	Bibliography	93
	Appendix	99
A	Physical Property of Matter	99
B	Data collection sheet	102
C	Drawing sheet	105

List of Tables

3.1	Components material and parameters.	18
3.2	Metallic powder material properties.	29
5.1	Total Cost of Solar Water Heating System.	56
5.2	Wet bagasse fuel composition.	57
6.1	Mesh information for TPCTHP.	61
6.2	Thermo physical properties of HP working fluids.	64
6.3	Boundary condition for TPCTHP at different section.	64
6.4	Comparative average temperature contour for 3 various working fluid at different time (K).	69
6.5	Comparative Volume fraction of vapor for three different working fluid at selected simulation time (t).	72
6.6	Pressure contour for all working fluids at different simulation time with respective average value.	75
6.7	Mass flow contour for all cases at different simulation time at condenser interior.	80
6.8	Mass flow contour for all cases at different simulation time at evaporator interior.	81

List of Figures

1.1	Ethiopia solar radiation distribution in 5kwh/m2/day	3
3.1	General research methodology procedure.	16
3.2	Components of heat pipe based evacuated tube solar water heater.	17
3.3	Heat pipe based evacuated tube solar water heater.	17
3.4	Location and topographic map of the research site.	20
3.5	Monthly average global solar radiation variation from 2013 to 2017 (kWh/m^2day).	21
3.6	Monthly average global extraterrestrial solar radiation (W/m^2).	21
3.7	Monthly average diffusive solar radiation (W/m^2).	22
3.8	Monthly average beam radiation (W/m^2).	23
3.9	Monthly average daily sunshine hour (hr).	23
3.10	Average declination angle at deferent months of the year ($^{\circ}$).	24
3.11	Monthly average daily Sunset and Sunrise angle ($^{\circ}$).	25
3.12	Monthly average daily maximum and minimum temperature ($^{\circ}C$).	25
3.13	Monthly average daily relative humidity (%).	26
3.14	Two step preparation process of nanofluids.	28
4.1	Single tube component of HPETSc ?.	36
4.2	General heat taransfer and component model in radial section.	37
4.3	EES iterative solution procedure	40
4.4	Concentric tube heat transfer network.	42
4.5	Heat pipe heat transfer network.	43

4.6	Proposed solar system diagram.	47
4.7	Solar collector configuration ?.	51
6.1	Geometry view (a). 3D model (b). Separate phase.	60
6.2	Mesh view at full model, evaporator and condenser section.	61
6.3	CFD package computer simulation graph	66
6.4	Temperature contour for different working fluid at steady state a. H_2O b. $Cu - H_2O$ c. $Al - H_2O$	68
6.5	Volume fraction contour for different working fluid at steady state a. H_2O b. $Cu - H_2O$ c. $Al - H_2O$	71
6.6	Pressure contour for different working fluid at steady state a. H_2O b. $Cu - H_2O$ c. $Al - H_2O$	74
6.7	Velocity vector for evaporation and condensation a. Full model view b. condenser c. evaporator zoom view c. $Al - H_2O$	76
6.8	Velocity contour for different working fluid at steady state a. H_2O b. $Cu - H_2O$ c. $Al - H_2O$	77
6.9	Mass flow contour for different working fluid at steady state a. H_2O b. $Cu - H_2O$ c. $Al - H_2O$	78
6.10	Selected plane for visualize evaporation-condensation process	79
6.11	Average mixture temperature with time at different section of HP a. Evaporator b. Condenser.	82
6.12	Average transient mixture density for entire fluid domain.	83
6.13	Time dependent mixture velocity for entire fluid domain of HP.	84
6.14	Average heat transfer coefficient with comparative time a. Evaporator section b. Condenser section c. Overall coefficient.	86
6.15	Average thermal resistance for different working fluids with time a. Overall coefficient b. Evaporator section c. Condenser section	87
6.16	Average wall heat flux a. Evaporator b. Condenser section.	88

Nomenclature

<i>CI</i>	<i>initial investment cost(Birr)</i>
<i>G</i>	<i>radiation (W/m²)</i>
<i>h</i>	<i>heat transfer coefficient(W/m²k)</i>
<i>i</i>	<i>market discount rate(%)</i>
<i>K</i>	<i>thermal conductivity(W/mk)</i>
<i>LCC</i>	<i>Life Cycle Cost(Birr)</i>
<i>LCS</i>	<i>Life Cycle Saving (Birr)</i>
<i>M</i>	<i>Mass(Kg)</i>
<i>m</i>	<i>mass flow rate(Kg/s)</i>
<i>Mw</i>	<i>Molecular weight(Kg/Kg mol)</i>
<i>Q</i>	<i>Heat energy(W,J)</i>
<i>V</i>	<i>Volume(m³)</i>
<i>v</i>	<i>volume flow rate(L/s)</i>

Abbreviations

<i>3D</i>	<i>Three Dimension</i>
<i>CFD</i>	<i>Computational Fluid Dynamics</i>
<i>ETSc</i>	<i>Evacuated Tube Solar collector</i>
<i>HP</i>	<i>Heat Pipe</i>
<i>NPI</i>	<i>National Pollutant Inventory</i>
<i>STP</i>	<i>Standard Presure and Temperature</i>
<i>SWHS</i>	<i>Solar Water Heating System</i>
<i>TES</i>	<i>Thermal Energy Storage</i>
<i>TPCT</i>	<i>Two Phase Closed Thermosyphon</i>
<i>TSWH</i>	<i>Thermosyphon Solar Water Heaters</i>
<i>VOF</i>	<i>Volume Of Fluid</i>
<i>Vol</i>	<i>volume</i>

Greek letters

α	<i>Absorptivity (%)</i>
β	<i>Collector slope (°)</i>
δ	<i>Declination angle (°)</i>
ω	<i>Sunrise/Sunset angle (°)</i>
Φ	<i>Latitude (°)</i>
τ	<i>Transmittance (%)</i>
Φ	<i>Volume concentration (%)</i>
Ψ	<i>Weight percentage (%)</i>
ρ	<i>Ground reflectivity (%)</i>

Subscript

<i>B</i>	<i>Beam</i>
<i>bf</i>	<i>base fluid</i>
<i>D</i>	<i>Diffusive</i>
<i>e</i>	<i>element</i>
<i>f</i>	<i>fuel</i>
<i>P</i>	<i>period</i>
<i>pr</i>	<i>product</i>
<i>pt</i>	<i>particle</i>
<i>pol</i>	<i>pollutant</i>
<i>sr,ss</i>	<i>sunrise,sunset</i>
<i>t</i>	<i>tilt</i>
<i>tot</i>	<i>total</i>

Symbols

<i>Al</i>	<i>aluminum</i>
<i>Cu</i>	<i>copper</i>
<i>CO₂</i>	<i>Carbon dioxide</i>

INTRODUCTION

Recently, the world population increases from time to time also the demand of energy increase due to that the price of fossil fuel products and resources will be exhausted in a relatively short period of time. The current high prices of fossil fuel resources are affecting economic and social development worldwide. The impact of energy crises is particularly felt in developing countries where a high percentage of national budgets for development must be diverted to the purchase of fossil fuel products. To reduce the dependency on imported fuels with high price, most countries have initiated programs to develop alternative energy sources based on domestic renewable resources ?.

Energy plays great role in an execution of one country development and global climate change. As one achieving greatly human being welfare and improve quality of lives of community. As one of the key requirements for fulfilling human needs, it helps in achieving greater productivity, prosperity, and comfort. Lack of access to modern energy sources means use of polluting kerosene lamps for lighting, cooking with inferior fuels and therefore, extended exposure to harmful smoke and fumes, and in most cases, ending the productive day at sundown. Expanding access to energy for citizens would lead to multi-dimensional solutions for various urgent and interconnected challenges ?.Energy is related with environmental problems are currently dominant issue in our globe; pollutant is release from different energy excavation and implementation of sources. In recent years, the wide concerns about global warming and harmful emissions from carbon fuels have resulted in an emerging interest in the development of renewable energy applications ?.

All sources of energy may be grouped into two general categories; incoming energy, which is

the energy reaching the earth from outer space, and capital energy, which is the energy that already, exists on or within the earth. Income energy includes solar energy. The utilization of income energy sources is very attractive because they are non-depletable sources of energy and they are relatively pollution free, which is a very important consideration ?. Renewable energy sources are expected to become economically competitive as their costs already have fallen significantly compared with conventional energy sources in the medium term, especially if the massive subsidies to nuclear and fossil forms of energy are phased out. Finally, new renewable energy sources offer huge benefits to developing countries, especially in the provision of energy services to the people who currently lack them. Up to now, the renewable sources have been completely discriminated against for economic reasons. However, the trend in recent years favors the renewable sources in many cases over conventional sources ?.

Solar energy is the world's most abundant and permanent source, with a reputation for being inexhaustible and environmentally benign, is one of the most important parts of renewable energies and has been widely used in residential, industrial, remote, and transportation areas. Almost all the renewable energy sources originate entirely from the sun. The sun's rays that reach the outer atmosphere are subjected to absorption, reflection, and transmission processes through the atmosphere before reaching the earth's surface. On the other hand, depending on the earth's surface topography, the solar radiation shows different appearances ?. The amount of solar radiation received by the surface of earth per minute is greater than the energy utilization by the entire population in one year. For the time being, solar energy, being available everywhere, is attractive for stand-alone systems particularly in the rural parts of developing nations ??.

Solar energy can be utilized by two routes namely solar thermal and solar photo voltaic. Solar thermal energy devices convert radiant energy of the sun into thermal energy for different productive works. It is a promising way of utilizing solar energy by converting it into thermal energy which is largely required by industrial and domestic consumers. Solar thermal energy devices convert radiant energy of the sun into thermal for different productive works. The conversion of sunlight into thermal energy is easily or conveniently achieved by means of a metallic or plastic cover painted black with ordinary black board paint or having selected coating over it and covered with one or double glazing cover for transmitting solar radiation inside it. In the terms of the amount of energy available for utilization the solar energy option is the largest

energy resource with the added advantage of being environment friendly and renewable ?. However, solar energy collectors highly affected by collector inclination, shadow, dust accumulation, heat loss in different aspects, heat removal factors, system design and storage system are common in all. Thus the performance evaluation evacuated tube solar thermal collector to increase efficiency, reduce system loss and cost effective energy supply ??.

1.1 Background

Ethiopia's location gives it strategic dominance as a jumping off point in the Horn of Africa, close to the Middle East and its markets. Landlocked, it borders Eritrea, Somalia, Kenya, South Sudan, and Sudan its tiny neighbor Djibouti. Ethiopia's huge population of about 102 million (2016) makes it the second most populous nation in Africa, after Nigeria ?.

Ethiopia has enormous energy potentials of hydro power, wind, solar and geothermal energies. Its hydro power potential, for instance, is rated as the second largest potential in Africa next to Congo ?. The energy potential estimated to between 30GW - 45GW ????. Approximated the gross hydro power potential of the country to be over 74GW and economically feasible potential to be from 16GW to 18.3GW; considering an average plant utilization factor of 0.6 however, only about 2% of this huge potential is developed so far ??.

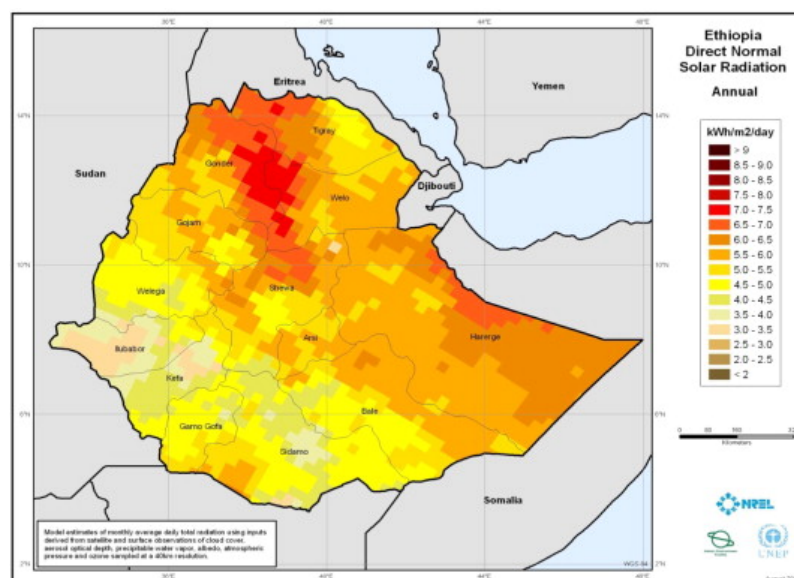


Figure 1.1: Ethiopia solar radiation distribution in 5kwh/m2/day

Solar energy in most parts of Ethiopia have approximately over 3000 hours of sunshine annually receiving 5.0 kWh/m² with the northern part of the country having an estimated annual solar energy of over 6.0 kWh/m² per day ? Also estimated the annual solar irradiation of Ethiopia to be between 5.0 and 7.5 kWh/m² depending on the region ?. Total exploitable solar energy potential of the country to be about 106GW having an average isolation of 5kwh/m²/day ?. Insolation distribution of solar energy over the country shown in Figure ??.

The developing country like Ethiopia is need large amount of energy for the accomplishment industrial aid development. Many industries in the country use fuel and electricity for water heating process. However, energy costs for water heater is increasing at considerable rate by increase operating costs and reducing profitability due to continuous escalating of fuel price. Hence, this research explores solar energy as a sustainable alternative for large scale water heating and it is a step forward to reduce dependency on imported oils ?.

1.2 Statement of the Problem

In Ethiopia industries hot water demand greatly depend on biomass and electrical water heater this application is currently replace with other alternative energy sources due to the environmental pollution and economic feasibility.

The hot water demand of the Wonji-Shoa sugar factory depend on industrial by product. Bagasse is uses for cattle feeding food, fiber production, briquetting, pulp, paper, fibour body and other applications. In other way the use hot water extracting from boiler that use for steam turbine electric generator this greatly influenced full capacity of turbine; current output capacity it reduced by 50% from full performance. Other problem is water content of bagasse; during combustion it leads to air pollution by realizing SO_2 , NO_X , CO_2 and CO from boilers and furnaces. Due to this solar water heating with storage system is feasible, environmentally friend and has a capacity can operate standalone energy source.

The study deals with hot water demand of Wonji-Shoa sugar factory from solar energy based supply. Concurrently, the study also deals with an efficient heat pipe based evacuated solar water heater need for further research.

1.3 Objectives

1.3.1 Main objective

Investigate and optimize possible Characteristics of heat pipe based evacuated tube solar water heater for the case of Wonji-Shoa sugar factory that increase efficiency, reduce heat loss, minimizing energy cost and environmental impact.

1.3.2 Specific objectives

- Analyses of solar radiation, environmental temperature, wind speed data from case study site and collector geometry specification from manufacturer.
- Analyse the tilted angle, material and geometric effect of wick-less heat pipe for improved evacuated tube solar water heater performance.

- Optimizes the effect of working fluid in Two Phase Closed Thermosyphon (TPCT) heat pipe for yielding high performance evacuated tube solar water heater.
- Determine heat transfer network and total heat transfer rate for evacuated tube and heat pipe respectively.
- Design solar water heater system for milling plant section hot water demand.
- Investigate the improvement of TPCT heat pipe using ANSYS Fluent Volume of Fluid (VOF) for CFD simulation.
- Create 3D model of heat pipe-evacuated tube solar collector by using SOLIDWORKS.
- Investigate techno-economic feasibility.
- Study the reduction of emission attributable to evacuated tube collector with thermal storage.

1.4 Delimitation

This research was intended to find effective, efficient and assessed implication of solar thermal energy collector in Wonji-Shoa sugar factory on the standalone water heating system for milling plant. Also clarify the parametric effect on solar collector efficiency and attribute heat loss. The study also compare the previous efficiency, design and analysis of vacuum tube solar water heater using CFD package and SOLIDWORKS modeling. The prototyping and direct solar insolation measurement is not included in this research.

LITERATURE REVIEW

2.1 Solar Water Heater

Solar water heating is a combination of solar collector array, an energy transfers system and storage tank. The main parts of solar water are the solar collector array, which absorbs solar radiation and converts it to heat. This heat absorbed by a heat transfer fluid (water, non-freezing liquid, or air) that pass through collector. This heat can then be stored or used directly. Because it is understood that portion of the solar energy system are exposed to by high insolation level during period of low energy demand?.

Two types of solar heating system: -

- a. Active system (forced circulation)
 - Direct circulation (open loop) system
 - Indirect circulation (closed loop) system
- b. Passive system (natural circulation)
 - Thermosiphon (direct and indirect)
 - Integrated collector storage

The Performance of solar water heaters varies depending on how much energy is available and how cold the water is coming into the system. The amount of hot water a solar water heater produces depends on type,size, installation of the system and available solar insolation.

2.2 Evacuated tube Collector Modeling

Lacour *et al.*? present analysis of the thermal performance solar water heating system with heat pipe evacuated tube collector using data obtained from a field trial over the year. An automated subsystem was developed and incorporated to control the hot water draw offs and electric immersion heater to mimic the operation of SWHs in domestic dwellings. Result get 70.3°C outlet temperature with average energy daily collected is $20.4\text{MJ}/\text{d}$ and $3.6\text{MJ}/\text{d}$ pipe loss for 33.8% solar fraction. Finally, set HP-ETCs are more efficient than their flat plate counterparts when operating as components of a SWHs, the solar circuit supply pipes should be kept as short as possible in order to reduce energy loss and a better pump control strategy for heavily overcast and intermittent cloud covered days could result in an improvement of the HP-ETC SWHs.

S. Siva Kumar *et al.*? designed and investigate evacuated tube with heat pipe solar thermal collector by taking geometrical consideration and building material for evacuated tube and heat pipe calculation. The net heat transfer network optical efficiency of tube, thermal loss and heat flow rate are determined on this study. The effect of solar intensity, heat flowrate and number of tube has great effect on the performance of collector.

Martín *et al.*? study design of evacuated tube solar collector network works for a hot water supply dairy factory in Guanajuato, Mexico. By taking a target temperature 85°C , 300 working days in year, and $4401.01\text{KWh}/\text{day}$ total energy consumption data. As a conclusion, the thermal and hydraulic length, the selected network and starting time for the design of evacuated tube collector without heat pipe; determination of the optimal inlet temperature through optimization is the necessary next step and this must be followed by an operating strategy linked to a control system.

Michel Hayek *et al.*? prepare experimental set-up, involving full scale collectors made of a row of 20 evacuated tubes and their tank, and a circulation system with measurement tools, was constructed and used. The experiments were carried out during the period of November to January, i.e. under winter-like conditions, at days where the sky was almost clear with some clouds scattered here and there. The results show that the heat-pipe-based collectors are better than the water-in-glass designs and their efficiency is almost 15 to 20% higher. Their payback periods are much higher owing to their larger initial cost in the local market.

Avadhesh Yadav *et al.*? conduct an experimental study on natural circulation evacuated tube

solar collector for steam generation in winter season. Prepare an apparatus for experiment 40 evacuated tube with a dimension of 1500mm length, 37 and 47 internal and outer diameters respectively, inclined header and steam collector cylinder. Finally, attain for the maximum radiation time 620ml of steam collect, with 43.6% maximum collector efficiency.

M.A. Sabiha *et al.*? this paper review the latest studies on evacuated tube solar collector. Determining what is the reason to prefer evacuated tube collector over the other solar collector technologies, type, application, structure and challenge of evacuated tube solar collector. ETSCs can collect both direct and diffuse radiations, excellent thermal performances, have convenient installation and easy transportability is the dominance character. ETSCs cost and maintenance, Fragility, snow removal and overheating regulation are listed as a challenge. ETSCs structure, heat pipe internal surface groove, use Nano fluids working fluid, adding solar tracker, reduction of CO_2 , and large industrial application recommended as future works.

Roonak Daghigh *et al.*? study a heat pipe solar water heater was designed and constructed, tested theoretical and proved experimentally. Developed mathematical model based on theoretical analysis of the system and evaluate effect of mass flow rates of working fluid, number of heat pipe on the efficiency. They concluded that, the distribution of temperature is directly related with number of pipes and solar insulation and setting up auxiliary heating for smallest insolation.

Raghurajsinh *et al.*? study evacuated tube solar water heater for horticultural product refrigeration system use, using thermodynamic equation to find out efficiency of HP-ETCs. Also review design parameter, theoretical model and experimental result. Finally, HP-ETCs is has best performance among all and improvements need to increase performance.

Evacuated tube solar collector is efficient than flat plate with a capacity of less heat loss; also can collect direct and diffusive solar radiation. Heat pipe based evacuated tube solar collector higher in efficiency than conventional type;also preserve global warming in a proposed system. HP-ETSWH system performance dependent on pumping, piping, number of tubes, flow rate and inlet temperature of demand water. Theoretical analysis is compatible and concurrent with experimentally proved result. Due to indeterminacy of solar radiation, performance of heat pipe based evacuated tube solar water heater still need improvement on absorption energy and rate of heat transfer. In this study, to ensure that maximum useful energy collection and efficient system by considering the following points.

- Absorber material and size.
- Heat pipe surface polishing black.
- Use high heat transfer capacity of working fluid HP.
- Use locally available high insulation materials and size for cost effective energy system

2.3 Thermal Storage Modeling

Behnaz Rezaei *et al.*? Works on transient behavior during charging and discharging of a fully mixed, open TES is modeled and analyzed. Included are developments and analyses of the charging temperature function and the maximum charging temperature of the TES, the charging energy flow function and the maximum heat flow capacity of the TES, the discharging temperature function and the minimum charging temperature of the TES, the discharging energy flow function and the maximum heat flow capacity of the TES, and the expression for one cycle of the TES. The impact of various factors on charging and discharging are investigated. The results show that, by increasing the input energy flow rate, the charging temperature of the TES is raised, and that an increase in the input energy flow rate raises the discharging temperature of the TES in the early stage of discharging, while a decrease in the outlet energy flow rate increases the discharging temperature of the TES in the late stage of discharging.

S.A.Vijay P. *et al.*? An experimental study done for a comparative analysis thermal energy storage (TES) and thermal behavior of the LHS system is investigated for various operating conditions. The effects of flow rates on charging times and energy storage of the TES systems are studied. Concurrently, similar studies for charging of SHS systems are also performed. The charging characteristics of the SHS and LHS systems are compared. Finally, It is concluded that LHS systems are a viable option for solar heat energy storage. Possessing considerable advantages over SHS systems, it can be used as an alternative to current domestic sensible solar water heating technologies.

Hoshi *et al.*? A study compared the charging cycle times of a thermal storage with use of two PCMs with different thermal conductivities. First, they used KNO_3 with thermal conductivity of $0.5W/K.m$ as a phase change material and second Pb with thermal conductivity of $31W/K.m$. They assumed the heat storage was charged to $100MJ/m^3$ and their numerical

model results indicated that the time required for Pb and KNO_3 to charge the heat storage are 250min and 2000 min, respectively. Although KNO_3 is one of the most promising PCMs for CSPP application, its low thermal conductivity makes it an unsuitable candidate, unless thermal conductivity enhancement techniques are used to reduce the charging and discharging cycle times.

Lane et al.? identified several potential phase-change, heat storage materials suitable for encapsulation. He also assessed the technical and economic feasibility of using encapsulated PCMs for thermal energy storage in solar driven residential heating applications. His studies showed micro-encapsulation of $CaCl_2 \cdot 6H_2O$ in polyester resin was particularly successful for development of wall and floor panels with heat storage abilities. Also, micro-encapsulation of $CaCl_2 \cdot 6H_2O$ in plastic film containers reported to be another promising method for heat transfer enhancement in heating systems using air as the heat transfer medium.

Thermal energy storage has basically higher capability in different system, size and form; heat storage forms are PCM and SH. The solar energy absorption storage applicability is dependent on collecting, delivering mechanism and system need due to intermittent character of sun. Heat storage performance can be calculated analytically by using thermodynamic and heat transfer principle. In this study, the storage performance, capacity, type, and size determined by proposed system in efficient and cost effective ways.

2.4 Heat pipe modeling

Bandar Fadh et al.? a comprehensive CFD modelling was built to simulate the details of the two-phase flow and heat transfer phenomena during the operation of a wickless heat pipe or thermosiphon. Water was used as the working fluid. The volume of the fluid (VOF) model in ANSYS FLUENT was used for the simulation. The evaporation, condensation and phase change processes in a thermosiphon were dealt with by adding a user-defined function (UDF) to the FLUENT code. Good agreement was observed between CFD predicted temperature profiles and experimental temperature data.

Alizadehdakhel et al.? provided a two dimensional model and experimental studies in which they investigated the effect of input heat flow and fill ratio of the working fluid on the performance of a two-phase closed thermosiphon. They validated their study using experimental re-

sults. Three input heat flow rates of 700, 500, and 350W and three fill ratios of 0.3, 0.5, and 0.8 were considered. Under these operating conditions, they found the performance of the thermosiphon improved when the input heat flow was increased from 350 to 500W. Further, they discovered the best performance was at a fill ratio of 0.5.

Patil Aniket et al. review a prepare investigate the experimental and computational study of thermosiphon is essential to find out the factor affecting performance of thermosiphon. State material, heat load, filling ratio aspect ratio, mass flow rate of coolant and inclination of heat pipe are the main parameter affect thermal performance. He concluded that using a copper as heat pipe material, condenser section greater than evaporator section, filling ratio 45% – 65%, and inclination $50^{\circ} \sim 80^{\circ}$ use for high performance efficient heat pipe.

Bandar Fadhl et al. examines the application of CFD modeling to simulate the two-phase heat transfer mechanisms in a wick less heat pipe, also called a thermosiphon. Two refrigerants, R134a and R404a, were selected as the working fluids of the investigated thermosiphon. CFD simulation results were compared with experimental measurements, with good agreement obtained between predicted temperature profiles and experimental temperature data, thus confirming that the CFD model was successful in reproducing the heat and mass transfer processes in the R134a and R404a charged thermosiphon, including the pool boiling in the evaporator and the liquid film in the condenser section.

Ahmed A. Alammari et al. carried out experimental work at two initial sub-atmosphere pressure (3 and 30kPa), heat input value (90 – 160W) and a filling ratio 50% using water as working fluid. The results of the new thermosiphon have been compared with a plain copper TPCT to consider the enhancement in thermal performance resulting from resurfacing of the thermosiphon wall. The results revealed that using internal wall roughness in TPCT can enhance its thermal performance by reducing the evaporator temperature, thereby the total thermal resistance decreasing by about 42% and 13% at initial pressures of 3kPa and 30kPa, respectively. On the other hand, the evaporator thermal resistance decreases and the evaporator heat transfer coefficient increases by about 115% and 68% at initial pressures of 3kPa and 30kPa, respectively. However, the condenser thermal performance decreases using the resurfaced TPCT compared with plain thermosiphon. And recommend for energy conversion and heat removal application.

Ambrosini et al. perform numerical fluid dynamic stability analysis of single phase natural

convection thermosyphone loop by using finite difference method. Setting up three single-phase loop configuration (rectangular, toroidal, symmetric toroidal loop) and boundary condition (flow variable and heat source). The obtained results clearly show the effect of truncation error on stability prediction: greater stability than in reality is generally predicted when a coarse nodalization is used. Moreover, explicit numerical methods must be also preferred since they show smaller diffusion than implicit ones. The effect of loop configuration and boundary great on the stability criterion.

Heat pipe categorized in to two types wick-less and wicked. Type is selected based on application of systems; the heat transfer capacity is dependent working fluid type, filling ratio, input heat, configuration and orientation. The 50% filling ratio and using a variety of working fluid is more effective way of Hp heat transfer enhancement by reducing thermal resistance. The complex mechanism of HP, evaporation-condensation phenomena can visualize and analyze in numerical simulation by using ANSYS/Fluent volume of fluid CFD package. The study aims enhancing heat transfer in HP-ETSWc using following points.

- Using efficient and stable heat transfer fluid.
- At collector orientation and heat pipe configuration.

2.5 Nanofluid

Naseemaa, S. et al.? study design of compact heat exchanger devices that possible only for a fluid with high heat transfer characteristics for improved performance. In order to come up with realistic analytic design done experiment design using Al_2O_3 and Cuo nano-particle with water base nanofluid at 0.1%, 0.25% and 0.4% volume concentration; tested under turbulent condition. The result is shown higher convective heat transfer coefficient at three and for smallest volume concentration in aluminum and copper oxide respectively.

Ravikanth et al.? present their paper on specific heat and density of Al_2O_3 nano-particle suspended in 60:40 mass concentration of ethylene glycol-water mixture. Experimental result was discussed; an increasing of volume concentration nano-solid and specific heat of nanofluid decreases adding lower property of specific heat is compatible; also density is increased proportional to concentration and compatible when add to base fluid.

Adnan M. et al.? study therm physical property of Al_2O_3 , SiO_2 and TiO_2 suspend in titillated water; measured experimentally with 1, 1.5, 2, and 2.5% volume concentration of solid. The compared result shows the highest thermal conductivity Al_2O_3 flowed by SiO_2 , TiO_2 and water; viscosity is higher in SiO_2 , Al_2O_3 , TiO_2 and water respectively as descending order. The materials generally behave higher density and lower viscosity in comparison with base fluid.

Amarinder Singh et al.? experimental conducted study is determine the change overall heat transfer coefficient and thermo-hydraulic property for single pass multi cross flow heat exchanger using Al_2O_3 nanofluid. The synthesized fluid contain 0.05% and 0.5% volume concentration nano-particle; bases of 60 : 40% by volume in fluid mixture of ethylene glycol-water. Rectangular horizontal fin surface model tested experimentally at two different temperature, presented discussion is, the fluid behavior enhance when increasing of temperature is great; overall heat transfer coefficient is increased in the fin side; slight higher density of fluid decreases when temperature increased.

Shijo Thomas et al.? investigate the rectangular thermosyphone loop steady state time and stability character sics by using Al_2O_3 -water nanofluid. Analysis have been done at different combination of heat input and sink temperature; higher temperature gradient shown loop with nanofluid than base fluid which shows the higher heat removal capacity of nanofluid.

Jawad Raza et al.? analyses the effect of copper nano-particle shape in the synthesis of water based nanofluid numerically. Final result shows heat transfer rate increased with concentration of nano-particle volume fraction, Reynolds number decreases near the wall of control volume and thermal boundary thickness increased for both cylindrical and spherical shape and concluded that spherical is better in performance.

Wisut Chamsard et al.? paper reviewed research in to nanofluid property use for enhancement of solar thermal collector performance. Presented discussion was thermo-physical property of nanofluid, synthesis techniques, base fluid property, types of solid and concentration; finally marked further research need in this field incorporate with fluid in direct solar thermal collector adsorption.

Nanofluid prepare from nanometer sized particle mixing in the higher concentration of base fluid. A nanotechnology heat transfer fluids used in different heating and cooling application device. The synthesis methods are one-step and two-step; two-step extensively used in metallic

nanofluid preparation. The particle size from 0 – 100nm, spherical shape and 0.5 – 5vol% efficient in heat transfer for different nanoparticles. The study aim to prepare nanofluids in a consideration of consider the following points for improved system component.

- Use high thermal conductive, latent heat and less heat capacity nanoparticle
- Prepare slighter dens nanofluids
- Use efficient and cost effective synthesis of nanofluid.

The Performance of solar water heaters varies depending on how much energy is available and how cold the water is coming into the system. The amount of hot water a solar water heater produces depends on: The type and size of the system, The amount of sun available at the site, proper installation, heat transfer fluid, Working fluid (in case of indirect thermosyphone), internal space pressure of evacuated tube, tilt angle, geometry, and orientation of the collectors. Performance of heat pipe based evacuated tube solar water heater still under studies; modeling on solar collector recommend efficient geometrical improvement and heat pipe modeling deals with standalone loop. Heat pipe application for improved solar collector performance is main concern here in this study.

METHODOLOGY

An optimized design of HPETSc used for water heating system which includes system sizing, collector geometric optimization and build stand alone water heating system. The research conducted by using both analytic and computer simulation. It meant that methodology use the software package and compatible equation previously exist and new adapted formulas on the basis of collected data from actual study area. On this chapter discusses the specif techniques, tools and procedures applied to achieve a given objectives. Generally, research design procedure for this study is shown in figure ??.

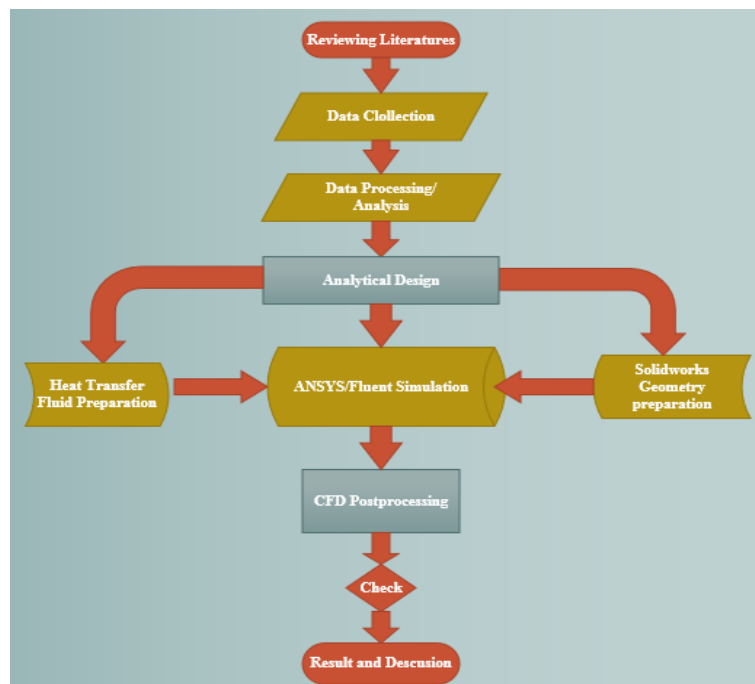


Figure 3.1: General research methodology procedure.

3.1 Working principle of HPETSc Solar Water Heater

Evacuated tube collector receiver consists of a copper heat pipe inside a glass vacuumed tube. The tube is surrounded by a cylindrical thin black copper absorber; which is transfer radiation that pass through concentric tubes and heat transfer to pipe fluid. The tap water or cold storage tank was supplied to the **HP-ETC** solar water heater and run for a day to reach a steady state condition; working fluid enters the collector inlet pipe at the header, then it is evenly distributed to the header tubes, absorbs heat and, at the end, it is returned to the outlet header pipe.

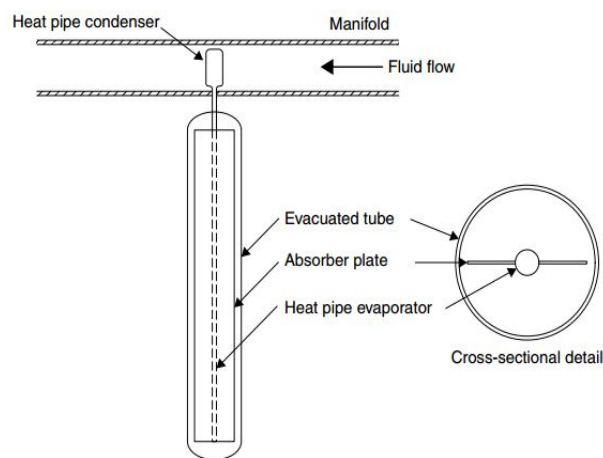


Figure 3.2: Components of heat pipe based evacuated tube solar water heater.

3.2 Component's and Material's HPETSc

Concentric tube

Concentric tube is a double layer borosilicate glass tubes evacuated for providing insulation. The

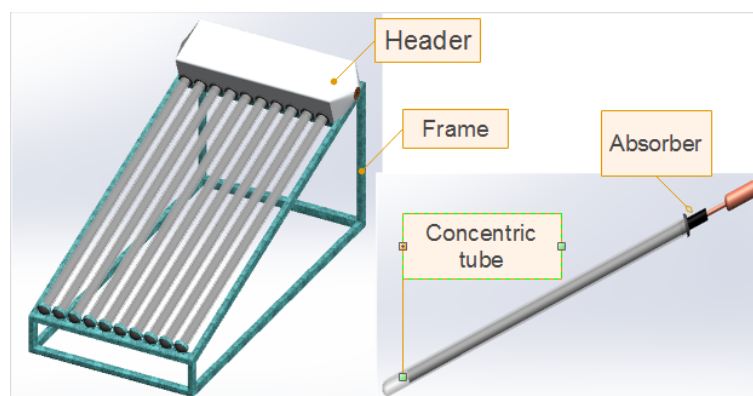


Figure 3.3: Heat pipe based evacuated tube solar water heater.

Table 3.1: Components material and parameters.

Component	Material	Parameter	Value
Concentric tube	Borosilicate glass	D_o	50mm
		D_i	40mm
		t	1.5mm
		L	1500mm
		α	0.07
		τ	0.92
		γ	0.01
Heat pipe	Black polished copper	$D_{o,e} = D_{o,ad}$	16mm
		$D_{c,o}$	50mm
		$D_{i,e} = D_{i,adb}$	14mm
		t_{HP}	1mm
		L_e	1484mm
		α	0.78
		L_{ad}	100mm
		L_c	160mm
Absorber	Black painted thin copper	$D_{o,ab}$	37mm
		t_{ab}	1mm
		L_{ab}	1500mm
Header	Copper	$D_{o,hd}$	160mm
		t_{hd}	1mm
		L_{hd}	720mm
Thermal insulation	Bagasse	t_{ins}	25mm
Casing	aluminum	t_{ins}	1mm
Working fluid	Water		
Heat transfer fluid	Water, nanofluids		

outer tube has very low reflectivity and very high transmissivity that radiation can pass through.

Absorber

The absorber surface is often coated to maximize this energy collection. The inner wall of the concentric tube is coat with selective absorbing material. This helps absorption of solar radiation and transfers the heat to pipe. The function of absorber is to effectively convert solar radiation into heat. The coating is this designed with a high absorption coefficient for the sun's radiation spectrum. Absorptivity is the fraction of incident sunlight captured by it.

Heat pipe

A heat pipe is a device that combines the high efficiency of boiling and condensation. Literally pipes transfer heat from a hot region to cold one. Heat pipe consisting of evaporator adiabatic and condenser section. A heat transfer fluid which limited amount is to be field after evacuating

HP tube.

Heat transfer fluid

As the solar collector heats up, the fluid in TPCHP increases in temperature. This fluid is then moved out of the evaporator section so the heat can be extracted for some useful purpose by condenser section in collector header.

Header

Header is the upper part that has passage for transferring working fluid and well insulated aluminum cover embed into its part. Also use as heat exchanger part of the collector.

Working fluid

Water quality plays an important role in selection of the technology as well as heat exchange mechanism. Taking a comparative analysis, cost effectiveness and available site water is taken.

Casing

Header and system casing contains all components of the collector and protects them from environmental impact. Casing shall also make the collector sturdy and stable. Material used for casing must be resistant to corrosion.

Thermal insulation

Thermal insulation reduces undesirable heat loss from the back and sides of the collector area. Insulation must also be able to withstand the maximum temperature of the absorber plate.

3.3 Site Assessment

The study area located in south-East part of Ethiopia which is called **Wonji-Shoa**; specific location of the factory is **Dodota** near to **Nazareth**. Commencing production in 1954 it is the oldest and pioneer in history of Ethiopia's sugar industry. The company located in $8^{\circ}, 24', 25.82''$ latitudinal and $39^{\circ}, 16', 18.12''$ longitudinal. Global location is northern hemisphere from equator. The site is clear from shadow and dust; the cloud cover sky clearness index is determined in the data analysis. Understanding the motion of the Sun is essential for proper solar systems design and the choice of location for solar collectors configuration is captured by directly from the site.

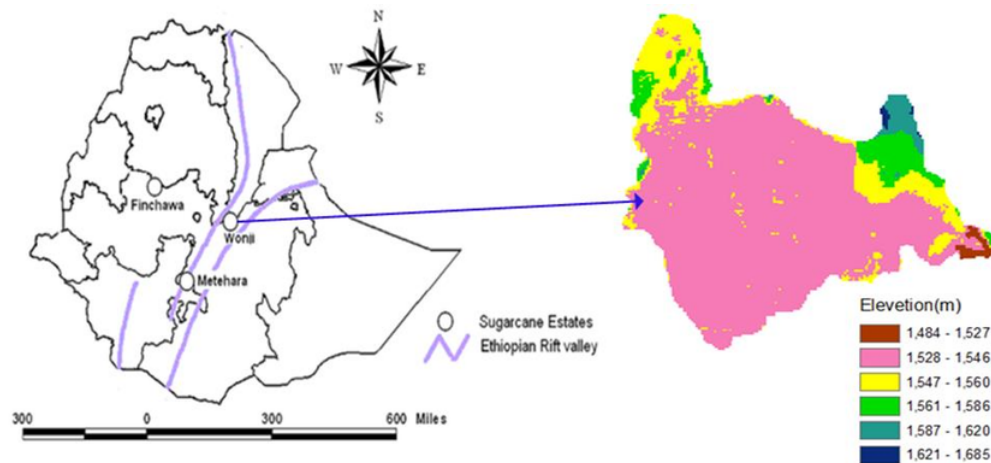


Figure 3.4: Location and topographic map of the research site.

3.4 Data Collection and Analysis

The required meteorological data for the selected site were taken from the Typical Meteorological Year data. Relevant information assessed from National **Meteorological Service Agency (NMSA)** like wind speed, direction of sunshine, duration of sun, relative humidity and ambient temperature of research site which is influential on collector performance. The other is from Wonji-Shoa sugar factory energy demand, water mass flow rate, alternative source and temperature for milling plant. Also used Organized literature review of different previous published and unpublished research, researchers view and future recommendations on the development of solar thermal energy application. The study used both primary and secondary source data. The efficiency and performance of solar water heating systems depend on a site's solar energy resource, environmental condition and demand of the selected system and site.

3.4.1 Solar Data

I. Global solar radiation

Global radiation is a measurable total irradiation of sun reach in our atmosphere; which is sum of diffusive and beam radiation. First step of for data analysis of global solar radiation from Oct, 2013 to Dec, 2017. The meteorological data is taken every fifty minute time gap and convert into average calculation for daily solar radiation by equation ???. The annually total global solar radiation decrease by 9.79% from 2013 graphical representation shown in figure ???.

$$1kW/m^2 \times 24h/day = 365day/yr \times 24kWh/m^2day \quad (3.1)$$

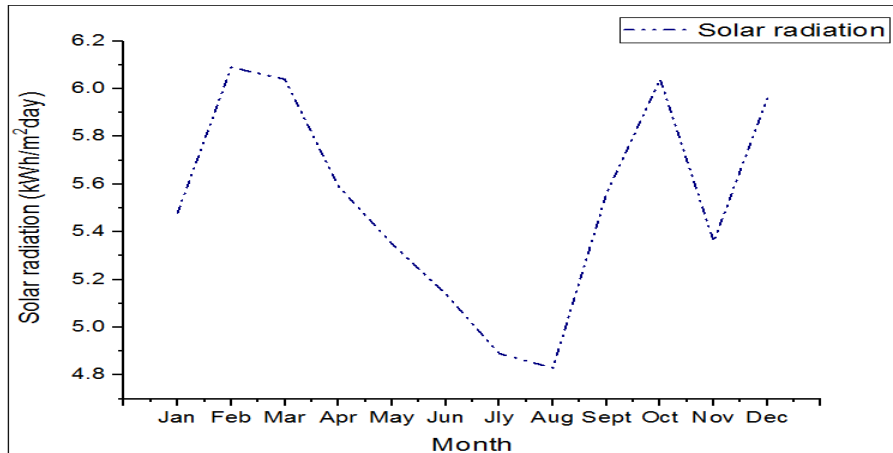


Figure 3.5: Monthly average global solar radiation variation from 2013 to 2017 (kWh/m^2day).

II. Global extraterrestrial radiation

Radiation would be received in the surface of atmosphere is called extraterrestrial. The approximate estimated values can get in equation ??.

$$G_{on} = G_{sc}(1 + 0.033 \cos(\frac{360n}{365})) \quad (3.2)$$

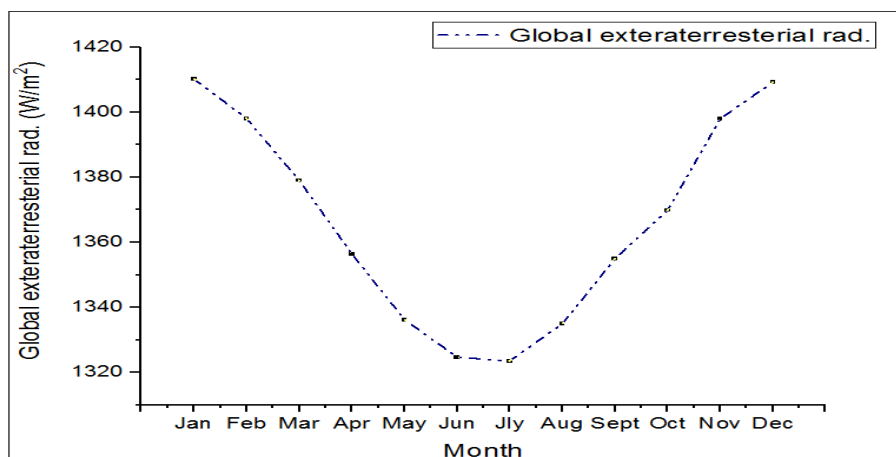


Figure 3.6: Monthly average global extraterrestrial solar radiation (W/m^2).

III. Diffusive solar radiation

The solar incident ray scattered because of atmospheric attenuation is called diffusive radiation. The solar heat at any point on earth depends ozone layer thickness, distance traveled through the atmosphere to reach that point, amount of haze in the air (dust particles, water vapor, etc.) and extent of the cloud cover. The value is estimated from global and extraterrestrial insolation in the basis of sky clearness index. it is used to determine percent of atmospheric attenuation ?.

$$k_T = \frac{G}{G_{on}} = \frac{614.78}{1366.3} = 0.449 \quad (3.3)$$

For $0.1 < k_T < 0.75$

$$\frac{G_D}{G} = 1.188 - 2.272k_T + 9.4373k_T^2 - 21.865k_T^3 + 14.648k_T^4 \quad (3.4)$$

$$G_D = 0.685G$$

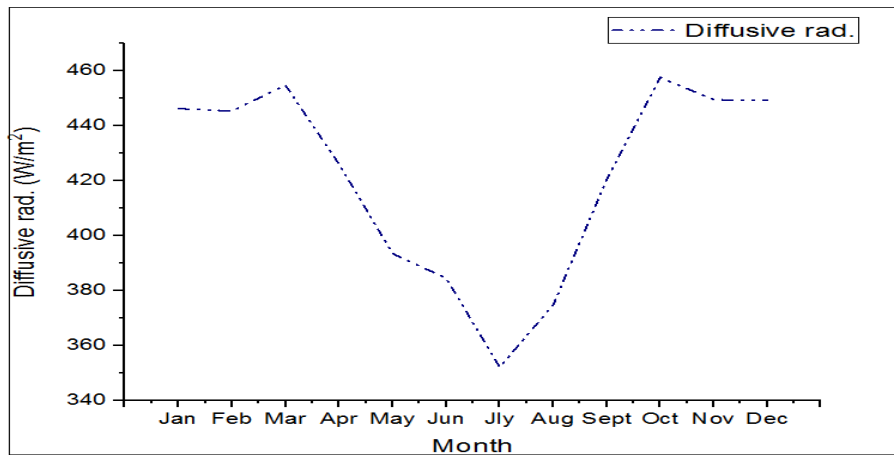


Figure 3.7: Monthly average diffusive solar radiation (W/m^2).

IV. Beam radiation

Solar radiation received from the sun without having been scattered by the atmosphere is called beam. The estimation of beam radiation is from equation ?? in consideration of negligible ground reflective insolation ?.

$$G = G_D + G_B \Rightarrow G_B = G - G_D \quad (3.5)$$

V. Sunshine hour

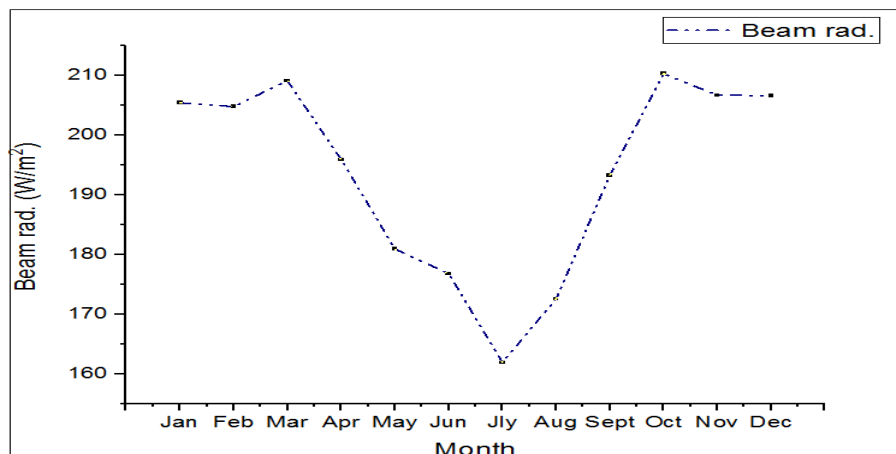


Figure 3.8: Monthly average beam radiation (W/m^2).

The time based on apparent angular motion of sun across the sky with solar noon and meridian of site. The sun hour data for selected station analyses from January 2010 to December 2017. The average solar daily insolation time is $8.5hr$. The average monthly data is modified to respective sun hour for reliable and more accurate source; also help to determine collector performance for specific working hours.

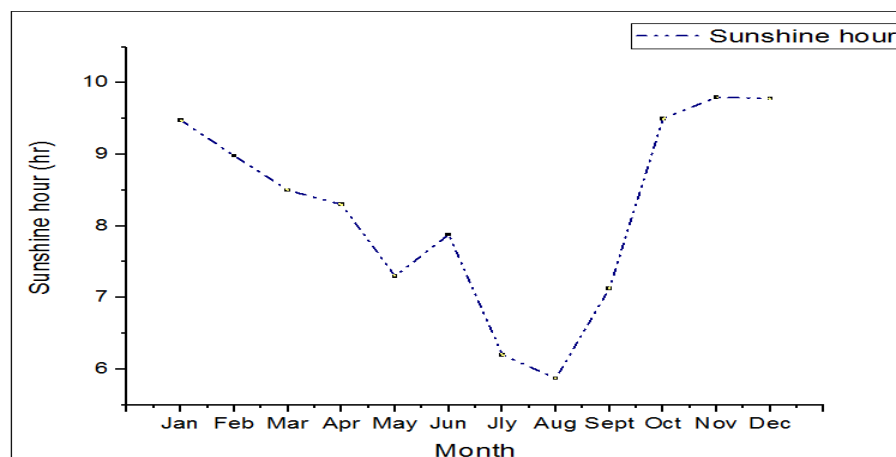


Figure 3.9: Monthly average daily sunshine hour (hr).

3.4.2 Solar Angles

The earth makes one rotation about its axis every 24hr and completes a revolution about the sun in a period of approximately 365.25 days. This revolution is not circular but follows an ellipse

with the sun at one of the foci's. Sun's position in the sky changes from day to day and from hour to hour. It is common knowledge that the sun is higher in the sky in summer than winter.

I. Declination

Declination is angular position of the sun at solar noon; corresponding to the moment when sun is at the highest point of the sky. The solar declination is the angular distance of the sun's rays north or south of the equator, north(site hemisphere) declination designated as positive. The angle calculation for yearly average monthly recommended number of day with the latitude < 66.5 is shown Equation ?? ?.

$$\delta = 23.45 \sin(2 \times \Pi \times 284 + n/365) \quad (3.6)$$

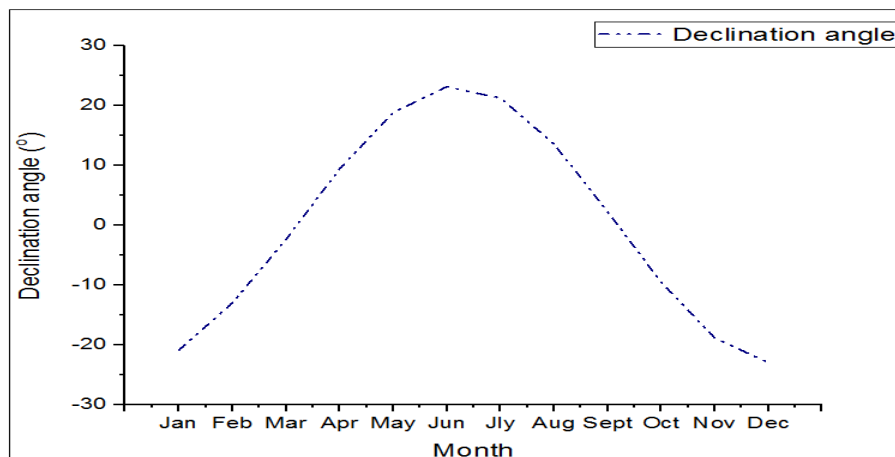


Figure 3.10: Average declination angle at different months of the year (°).

II. Sunset and Sunrise angle

Sunset and Sunrise angle is a point on the earth's surface is defined as the angle through which the earth would turn to bring and leave the meridian of the point directly under the sun. For the selected station (site) for a latitude of 8.45° an estimated result calculated in Equation ?? ?. Finally, the result for each months of the year is represented graphically in figure ??.

$$\omega_{ss} = -\omega_{sr} = -\tan(\Phi) \times \tan(\delta) \quad (3.7)$$

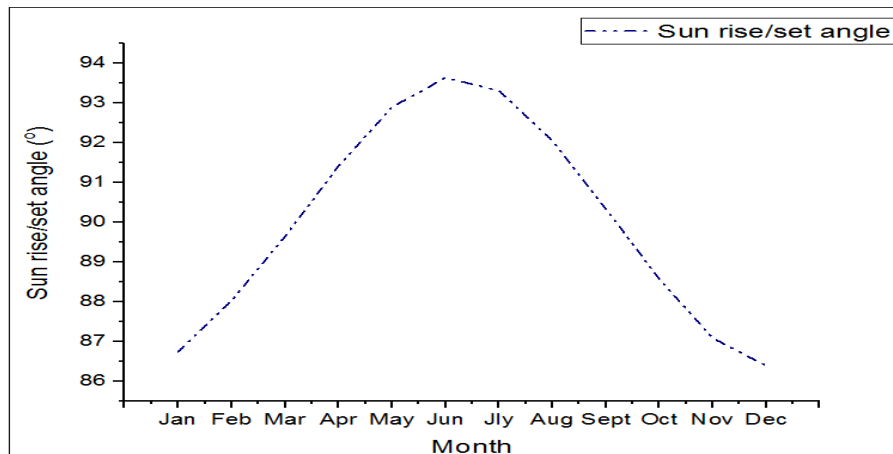


Figure 3.11: Monthly average daily Sunset and Sunrise angle ($^{\circ}$).

3.4.3 Environmental Data

The selected site of study environmental data is analyze cause of the lowering collector performance. For this case ambient temperature and relative humidity is analyzed.

I. Ambient temperature

Ambient temperature for selected station is used NMSA data for the time range of from Jan,2007 to Dec,2017. The average daily maximum and minimum temperature data for 12 month is displayed in Table ??.

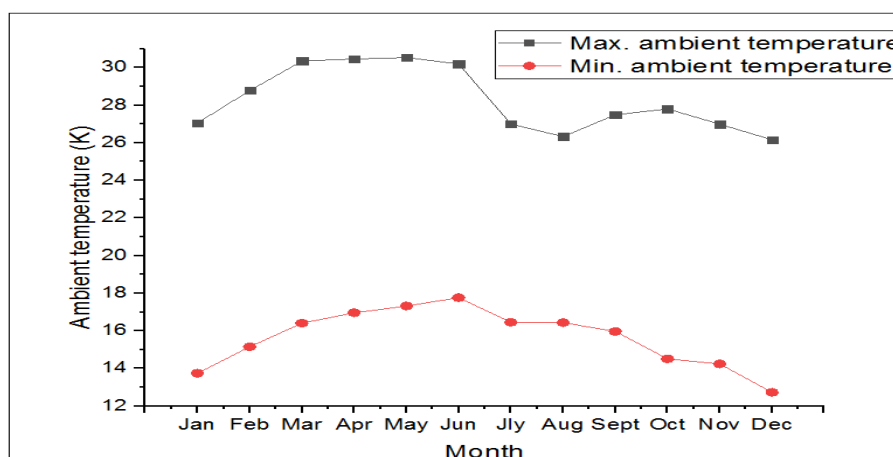


Figure 3.12: Monthly average daily maximum and minimum temperature ($^{\circ}C$).

II. Relative humidity

Relative humidity for selected site daily averaged is analyzed graphically.

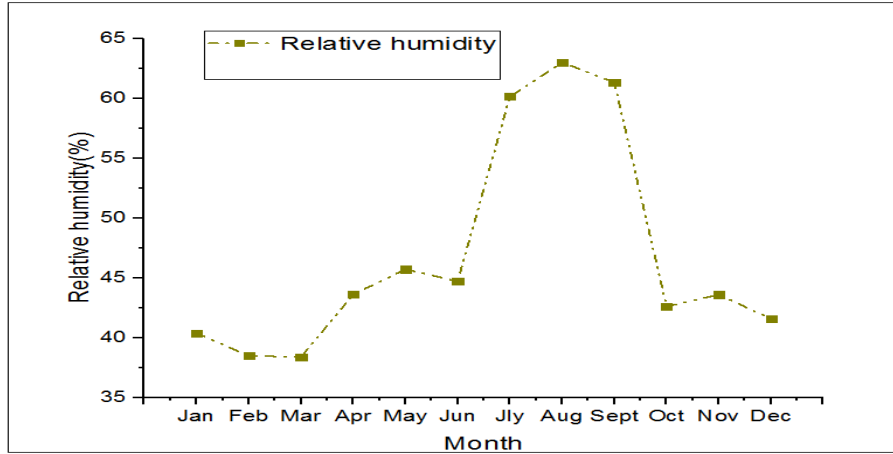


Figure 3.13: Monthly average daily relative humidity (%).

III. Wind speed

For the random data from NMSA for 2007 to 2017 time duration and take the average is selected for last two previous years full data is analyzed. The average wind speed is 2.5 m/sec.

3.4.4 Estimation of Load

The most important parameter that needs to be considered in the design of a solar water heating system is the hot water demand over a certain period of time. The selected plant demand is set with 34% from total mass crushed sugarcane juice. The section last 3 years maximum crushing capacity is 3244Kg juices for 24hr working duration. Hot water demand flow rate is going through out the crushing duration with a constant pattern. Daily hot water demand is calculate in the following ways.

$$M_w = m_j \times 0.34 = 3244 \times 0.34 = 1102.96 \text{kg of water/day} \Rightarrow V_w 1.1 \text{m}^3/\text{day} \quad (3.8)$$

Mass and volume flow rate is...

$$\dot{m}_w = \frac{M_w}{\text{day} \times \left(\frac{24 \text{hr}}{\text{day}}\right) \times \left(\frac{3600 \text{sec}}{\text{hr}}\right)} = 0.013 \text{kg/sec} \quad (3.9)$$

$$\dot{v}_w = \frac{\frac{M_w}{\rho_w}}{\left(\frac{24hr}{day}\right) \times \left(\frac{3600sec}{hr}\right)} = 1,276 \times 10^{-5} m^3/sec = 0.013L/sec \quad (3.10)$$

for solar collector flow rate is calculate using working hour.

$$\dot{m}_c = \frac{33088.12Kg/month}{30day/month \times 8hr/day \times 3600sec/hr} = 0.0383Kg/sec = 0.0383 \times 10^{-3} m^3/sec$$

Total daily hot water demand for a maximum temperature of $80^\circ C$ and process water initial temperature is $27^\circ C$.

$$Q_{load} = c_p \times \rho_w \times V_w \times (T_h - T_c) = \dot{v}_w \times c_p \times (T_h - T_c) \quad (3.11)$$

for 8 month working time per year demand will be

$$Q_{load} = 243.69MJ/day \times 240day/yr = 58485.6MJ/yr = 16.6MWhr$$

3.5 Synthesis of Nanofluids

Design consideration for matching heat pipe to a given application demand on working fluid, tube material, inclination and operating limit. Selection of the right liquid for heat is highly influential and dependent on its properties. Recommended is high latent heat, high surface tension (for wicked HP), low liquid viscosity and high thermal conductivity ?.

Nanofluids are nanotechnology-based heat transfer fluids that are derived by stably suspending nanometer-sized particles (with typical length scales of 1 to 100 nm) in conventional heat transfer fluids, usually liquids. Nanoparticles have photo-thermal properties that can be exploited for localized heating resulting in drug release. Many industrial processes involve the transfer of heat by means of a flowing fluid in either the laminar or turbulent regime as well as flowing or stagnant boiling fluids. The processes cover a large range of temperatures and pressures. Many of these applications would benefit from a decrease in the thermal resistance of the heat transfer fluid. This situation would lead to smaller heat transfer systems with lower capital costs and improved energy efficiencies. Nanofluids have the potential to reduce such thermal resistances, and the industrial groups that would benefit from such improved heat transfer fluids are quite varied ?.

3.5.1 Preparation Methods

There are two main techniques for preparation of nanofluid; one-step and two-step method. **One-step** method combines the production of nanoparticles and dispersion of nanoparticles in the base fluid into a single step. The single-step direct evaporation approach was developed by Vacuum Evaporation Running Oil Substrate (VEROS) technique. **Two-step** preparation process is extensively used in the synthesis of nanofluids by mixing base fluids with commercially available nanopowders. An ultrasonic vibrator or higher shear mixing device is generally used to stir nanopowders with host fluids. Two-step process is very suitable to prepare nanofluids containing metallic nanoparticles and most advisable in economic process for nanofluids production. For effective application and economical consideration nanoparticles volume concentration $< 5\%$ is recommended due to an increasing of thermal boundary layer for higher concentration. ????. Two-step method use for theoretical preparation in this study and process flow diagram shown in figure ???. Steps include changing the pH value of suspension, using surface activators and/or surfactant, using ultrasonic vibration at STP. NaHO use for Al and Cu nanofluid respectively with a small amount from 0.05g to 6.0g of nanoparticle weight from 1.0 to 12mg/ml ???.

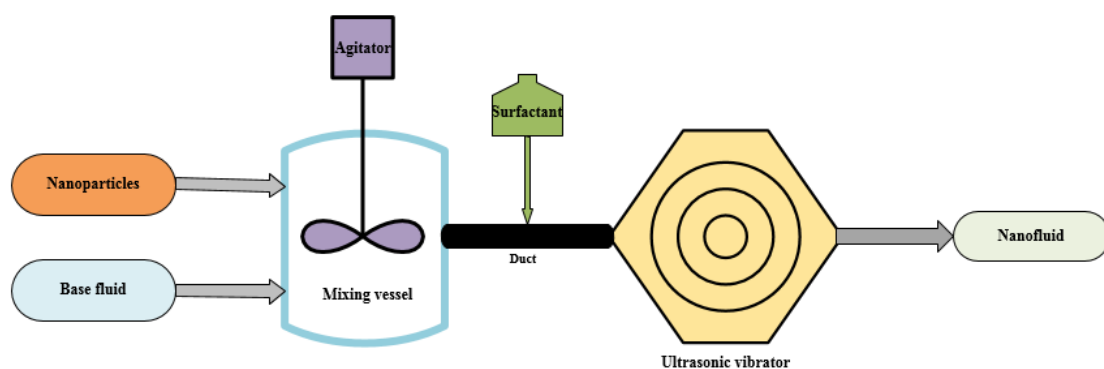


Figure 3.14: Two step preparation process of nanofluids.

Copper and Aluminum nanoparticle

Materials selected on the basis physical property expressed at starting of this section; also Particle size and shape is considered. The smallest concentration $< 1\%$ is are effective in use of copper ?? and aluminum nanoparticle is concentration in the range 2.5 – 5% is experimentally proven research enhance heat transfer 0.5-60% ?. Selected metallic powder available in

market and suit for specific application their material property is tabulated in table ?? at room temperature.

Table 3.2: Metallic powder material properties.

Property	Copper-nanoparticle	Aluminum-nanoparticle
Purity	99.9%	99%
Molecular Weight	63.55Kg/Kmol	26.98Kg/Kmol
Appearance	Black-Brown	Grey
Melting point	1083°C	660.37°C
Boiling point	2567°C	2467°C
Bulk density	0.15 – 0.35g/cm ³	008 – 0.20g/cm ³
True density	8.933g/cm ³	2.700g/cm ³
Size range	2 – 6nm	2 – 50nm
Average particle size	25nm	18nm
Specific surface area	30 – 50m ² /g	40 – 60m ² /g
Morphology	Spherical	Spherical
Poisons ratio	0.34	0.35
Thermal expansion	16.5µm/m · k	23.1µm/m · k
Vickers hardness	369Mpa	167Mpa
Young's Modulus	110 – 128Gpa	70Gpa

3.5.2 Estimation of Nanofluids Physical Property

The physical properties of nanofluids are quite different from the base fluid. Density, specific heat and viscosity are also changed which enhance the heat transfer coefficient exceeding the thermal conductivity enhancement results as reported in some experimental studies. For estimating concentration of nanoparticle in base fluid; the mass of particle is 0.001g for both materials Copper and Aluminum; base fluid proportional mass is 0.02 and 0.008 respectively ??.

Estimation of **weight percentage** use equation ?? ??.

$$\Psi_p = \frac{m_p}{m_{bf}} \quad (3.12)$$

Estimated **volume concentration** calculation depend on mass and density of mixing material by using equation ?? ??.

$$\Phi_p = \frac{\frac{m_p}{\rho_p}}{\frac{m_p}{\rho_p} + \frac{m_{bf}}{\rho_{bf}}} \quad (3.13)$$

Thermo physical properties is determine in regression equation that used in experimental and theoretical study of different nanofluid synthesis research. Specific heat and density of solid particle dispersed in a liquid for two phase mixture will be a function of concentration. **Density** and **specific heat** is determined by equation ?? and ?? respectively ??.

$$\rho_{nf} = \left(\frac{\Phi_p}{100}\right)\rho_p + \left(1 - \frac{\Phi_p}{100}\right)\rho_{bf} \quad (3.14)$$

$$Cp_{nf} = \frac{\frac{\Phi_p}{100}(\rho Cp)_p + \left(1 - \frac{\Phi_p}{100}\right)(\rho Cp)_{bf}}{\rho_{nf}} \quad (3.15)$$

Thermal conductivity of prepared nanofluid is estimated in equation ?? ?.

$$k_{nf} = (1 + 3\Phi_p)k_{bf} \quad (3.16)$$

The **viscosity** of nanofluid estimate with the well known Einstein equation ?? for volume concentration < 5% ?.

$$\mu_{nf} = (1 + 2.5\Phi_p)\mu_{bf} \quad (3.17)$$

In a mixing of liquid-solid is create change in molecular weight which is dependent volume concentration; and calculated by using equation ?? ??.

$$M_{nf} = \Phi \times M_p + (1 - \Phi) \times M_{bf} \quad (3.18)$$

Mixture **enthalpy** is dependent on concentration of material determined by the following equation ??.

$$h_{nf} = \Phi \times h_p + (1 - \Phi) \times h_{bf} \quad (3.19)$$

Taking homogeneous mixture and stable nanofluid liquid prepared under consideration and the property not part of one component its determine in volume concentration of base fluid; the

properties at different phase use same equation as liquid for two phase mixture and determined for gas phase property; the particle material properties is determine at saturation state of base fluid in vapor phase of solid-liquid mixture. ??.

I. Copper-nanofluid

For Copper-nanofluid *weight percentage* at liquid state is

$$\Psi_{c,p} = \frac{0.001}{0.02} = 0.005 = 5\%$$

Estimated *volume concentration* for copper-nanofluid

$$\Phi_{c,p} = \frac{\frac{0.001}{8933}}{\frac{0.001}{8993} + \frac{0.02}{997}} = 0.005 = 0.5\%$$

Density is determine here

$$\rho_{cu,nf} = \left(\frac{0.5}{100}\right) \times 8933 + \left(1 - \frac{0.5}{100}\right)997 = 1036.68kg/m^3$$

Specific heat

$$Cp_{cu,nf} = \frac{\frac{0.5}{100}(993 \times 385) + \left(1 - \frac{0.5}{100}\right)(997 \times 4180)}{1036.68} = 4016.49J/kg \cdot K$$

Thermal conductivity

$$k_{cu,nf} = (1 + 3(0.005)0.607) = 0.616W/m.K$$

The kinematic viscosity

$$\mu_{cu,nf} = (1 + 2.5(0.005) \times 0.891 \times 10^{-3}) = 0.9 \times 10^{-3}kg/m \cdot s$$

Molecular weight

$$M_{cu,nf} = 0.005 \times 63.546 + (1 - 0.005)18 = 18.228kg/Kmol$$

liquid state *enthalpy of vaporization* equal value and opposite in sign with vapor state.

$$h_{cu,nf} = 0.005 \times 304.6Kj/mol + (1 - 0.005) \times 40.65kj/mol = 41.97kJ/mol$$

Generally copper-nanofluid properties at vapor phase calculated below.

Density

$$\rho_{cu-v,nf} = 0.005 \times 8933 + (1 - 0.005) \times 0.231 = 44.89 \text{ kg/m}_3$$

Specific heat

$$C_{p_{cu-v,nf}} = \frac{(0.005)(8933 \times 384.2) + (1 - 0.005)(1870 \times 0.231)}{44.89} = 391.85 \text{ J/kg.K}$$

Thermal Conductivity

$$k_{cu-v,nf} = (1 + 3(0.005))0.0186 = 0.018879 \text{ W/m} \cdot \text{K}$$

Kinematic viscosity

$$\mu_{cu-v,nf} = (1 + 2.5(0.005)) \times 0.98 \times 10^{-5} = 0.992 \times 10^{-5} \text{ kg/m} \cdot \text{s}$$

II. Aluminum-nanofluid

Weight percentage at liquid state in a preparation standard is...

$$\Psi_{al,p} = \frac{0.001}{0.008} = 0.111 = 11.1\%$$

Estimated volume concentration calculation...

$$\Phi_{al,p} = \frac{\frac{0.001}{2700}}{\frac{0.001}{2700} + \frac{0.008}{997}} = 4.41\%$$

Density is

$$\rho_{al,nf} = \left(\frac{4.41}{100}\right) \times 2700 + \left(1 - \frac{4.41}{100}\right) \times 997 = 1071.932 \text{ kg/m}^3$$

Specific heat is

$$C_{p_{al,nf}} = \frac{\frac{4.41}{100}(2700 \times 903) + \left(1 - \frac{4.41}{100}\right)(997 \times 4180)}{1071.932} = 3818.82 \text{ J/kg} \cdot \text{K}$$

Thermal conductivity is

$$k_{al,nf} = (1 + 3(0.0441))0.607 = 0.687 \text{ W/m.K}$$

The kinematic viscosity is

$$\mu_{al,nf} = (1 + 2.5(0.0441)) \times 0.891 \times 10^{-3} = 0.989 \times 10^{-3} \text{ kg/m} \cdot \text{s}$$

Molecular weight is calculated

$$M_{al,nf} = 0.0441 \times 26.982 + (1 - 0.0441) \times 18 = 18.396 \text{ kg/Kmol}$$

aluminum nanofluid enthalpy of vaporization $h_{al,nf} = 0.0441 \times 293 \text{ KJ/mol} + (1 - 0.0441) \times 40.65 \text{ KJ/mol} = 51.78 \text{ kJ/mol}$ Aluminum-nanofluid at vapor phase physical properties is determine the same as correlation used for liquid; particle thermo-physical properties is calculated use in interpolation at base fluid saturation temperature variation listed in Appendix A.

Density of vapor nanofluid

$$\rho_{al-v,nf} = (0.0441) \times 2700 + (1 - 0.0441) \times 0.231 = 119 \text{ kg/m}^3$$

Specific heat vapor nanofluid

$$C_{p_{al-v,nf}} = \frac{0.0441(2700 \times 893.7) + (1 - 0.0441)(0.231 \times 1870)}{119} = 895.68 \text{ kJ/kg} \cdot \text{K}$$

Thermal conductivity vapor nanofluid

$$k_{al-v,nf} = (1 + 3(0.0441)0.017) = 0.0192 \text{ W/m.K}$$

Vapor phase kinematic viscosity is

$$\mu_{al-v,nf} = (1 + 2.5(0.0441) \times 0.89 \times 10^{-5}) = 1.08 \times 10^{-5} \text{ kg/m} \cdot \text{s}$$

3.6 Software Programs

In recent years, the technology innovations makes our life and profession simple, attractive and effective. The developmental prototyping making is changed and takeout the engineers from workshop. **SOLIDWORKS** is one of software development use in mechanical engineering design discipline for component geometry and modeling used on this study.

ACFD background coded software called **ANSYS**; it's one special element Fluent with an embedded multiphase **VOF** is chosen for this study. The development of computational model which used for detail simulation and unseen reality operation approached visualization using computational fluid dynamics to predict the performance of actual Heat pipe, and obtain the model equation that's related design and performance parameters that would be useful in carrying out design optimization of stated solar thermal system (HPETSc) for a given section, geometry and working fluid for heat transfer through the component would be analyzed using the CFD software. Development of computational model analysis involves the simple user interface and validation of sub-models such as buoyancy induced fluid flow and heat transfer.

SOLAR THERMAL SYSTEM DESIGN

From the basis of analyzed data, thermal analysis of heat pipe based evacuated tube solar water heater and total system design for wanji-shoa sugure factory milling plant section will discuss.

4.1 Thermal Analysis of HPETSc

4.1.1 Absorbed Solar Radiation

The solar radiation is collected by evacuated tube collectors is collect global insolation both beam and diffusive like flat plate collector. Increasing the absorption capacity tilt angle has effect; depending on the site location cause of higher solar energy is at equator of our Globe. On tilted surface iso-tropic model developed by Hottel and Woertz and refined by Liu and Jordan. According to this model radiation is calculated by equation ??.

$$G_t = R_B \times G_B + G_D \times \left[\frac{1 + \cos \beta}{2} \right] + (R_B + G_D) \times \rho_G \left[\frac{1 - \cos \beta}{2} \right] \quad (4.1)$$

Absorbed energy on tilted surface is dependent on radiation absorbency, transmittance of collector material and sunshine hour.

$$Q_{ab} = (\tau\alpha)G_t(t) \quad (4.2)$$

Beam radiation tilt factor is calculated by using equation ??.

$$R_B = \frac{\sin(\Phi - \beta) \sin \delta + \cos(\Phi - \beta) \cos \delta \cos \omega}{\sin \Phi \sin \delta + \cos \Phi \cos \omega} \quad (4.3)$$

The value of collector slope is equal with latitude and latitude $+10^\circ$ which is usual experimentally proved collector inclination for solar water heating ?. By considering inclination effect in heat pipe performance use addition of 10° .

$$\beta = \Phi + 10^\circ = 8.45^\circ + 10^\circ = 18.45^\circ$$

In the basis of above result of collector slop, latitude of location, average declination and sunrise/sunset angle is calculated??.

$$R_B = \frac{\sin(-10) \sin(-7.45) + \cos(-10) \cos -7.45 \cos(88.84)}{\sin(8.45) \sin -7.45 + \cos(8.45) \cos(88.84) \cos(-7.45)} = \frac{0.023 + 0.01976}{-0.019 + 0.0198}$$

$$R_B = 5.345$$

Total radiation on tilted collector is calculated, taking reflectivity for ordinary ground is 0.2

$$G_t = 5.345 \times 177.35 + 421.1 \times \left[\frac{1 + \cos 18.45}{2} \right] + (614.78) \times \rho_G \left[\frac{1 - \cos 18.45}{2} \right]$$

$$= 947.94 + 410.277 + 3.159$$

$$= 1361.38W/m^2$$

The absorbed energy for 8hr collector working hour is determined to find the total utilization of energy without accounting heat losses.

$$Q_{ab} = 0.892 \times 0.98 \times 1361.38W/m^2 \times 8hr = 95205.5Whr/m^2day$$

$$Q_{ab} = 5KWhr/m^2day$$

4.1.2 Energy Balance for the Collector components

the energy fall on the surface collector is not delivered the absorbed to working fluid; there is loss in different transfer mechanism and material property. For designing heat transfer the following assumption is taken.

1. Heat transfer analysis is for complete single tube of collector.

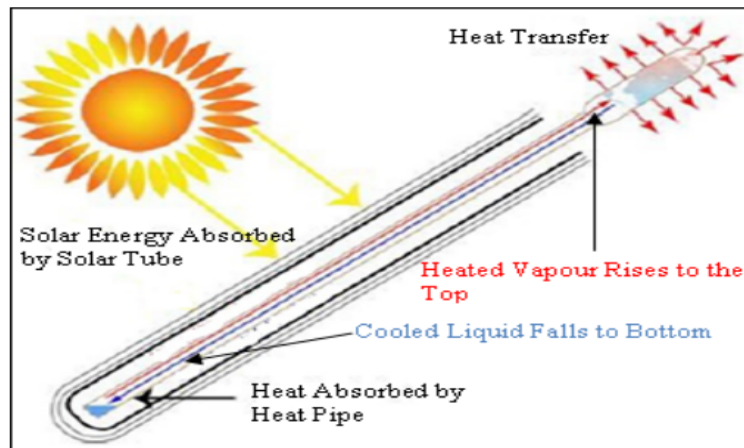


Figure 4.1: Single tube component of HPETSc ?.

2. Due to vacuum space the effect of temperature gradient around the tube is neglected.
3. Sky temperature is considering radiation analysis.
4. There is no convective heat transfer in concentric tube and space between absorber-inner glass.
5. due to smallest thickness and material properties conduction resistant is neglected.
6. The collector flow is steady.
7. Evaporation provide uniform flow to heat pipe tube.
8. Assume the internal air is closed and the gap is small due to this neglect heat loss by convective and radiative.
9. Heat loss for well insulated header is neglected.

Concentric Tube and Absorber Analysis

The heat transfer and surface temperature variation for concentric tube and heat pipe is calculated separately. All forms of transfer mechanism is discussed.

1. Evacuated tube

Borosilicate made of concentric tube heat is absorbed heat in to inside. The analysis is in one dimensional in radial section of tube.

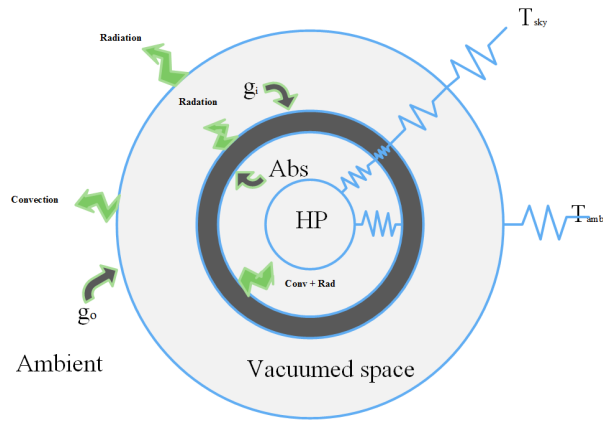


Figure 4.2: General heat transfer and component model in radial section.

Outer surface analysis:- half area of outer surface imposed to the incoming radiation and heat for outer glass face is calculated using basic radiation equation ?? with sky/ambient temperature.

$$Q_{rad-g_o} = \varepsilon_{g_o} \sigma A_o (T_{g_o}^4 - T_{sky}^4) = G_t A_o \quad (4.4)$$

Imposed surface area for cylindrical geometry is calculating. the interaction outer glass and ambient.

$$A_o = \Pi r L = \Pi \times 0.025 \times 1.5 = 0.12m^2$$

$$Q_{rad-g_o} = 1361.38 \times 0.12 = 163.366W$$

For determining outer glass surface temperature modify equation ?. The effective sky temperature simple empirical relation expressed below in kelvin unit ?. $T_{sky} = T_{amb} - 6 = 300 - 6 = 294K$

$$A_i = \Pi * 0.02 \times 1.5 = 0.09m^2$$

Inner glass heat and temperature distribution is in a consideration of absorptivity, transmittivity, emissivity, and very small reflectivity of outer glass; interaction between outer and inner glass ?.

$$\alpha = 1 - \tau - \rho = 1 - 0.92 - 0.01 = 0.07$$

$$Q_{rad-g_i} = \tau \alpha G_t A_i = 0.92 \times 0.07 \times 1361.38 \times 0.09 = 7.89W$$

Solar faced absorber surface area calculated

$$A_{abs} = \Pi rL = \Pi \times 0.0175 \times 1.5 = 0.0825m^2$$

Heat transfer in inner glass to absorber surface??.

$$Q_{rad-abs} = \tau^2 \alpha G_t A_{abs} = (0.92)^2 \times 0.98 \times 1361.38 \times 0.0825 = 93.2W$$

Heat transfer coefficient

Radiative heat transfer between outer glass and ambient determined by the following equation ???.

$$h_{rad,g0-amb} = \varepsilon_{g0} \sigma (T_{g0}^2 + T_{sky}^2) (T_{g0} + T_{sky}) \quad (4.5)$$

Radiative heat transfer coefficient Between outer and inner glass surfaces determined by equation ??.

$$h_{rad,g0-gi} = \frac{\sigma (T_{gi}^2 + T_{g0}^2) (T_{gi} + T_{g0})}{\frac{1}{\varepsilon_{gi}} + \frac{A_{gi}}{A_{g0}} \left(\frac{1}{\varepsilon_{g0}} - 1 \right)} \quad (4.6)$$

Radiation between inner glass and absorber surfaces is

$$h_{rad,gi-abs} = \frac{\sigma (T_{abs}^2 + T_{gi}^2) (T_{abs} + T_{gi})}{\frac{1}{\varepsilon_{abs}} + \frac{A_{abs}}{A_{gi}} \left(\frac{1}{\varepsilon_{gi}} - 1 \right)} \quad (4.7)$$

The heat transfer from absorber internal surface to heat pipe outer surface is

$$h_{rad,hp-abs} = \frac{\sigma (T_{hp}^2 + T_{abs}^2) (T_{hp} + T_{abs})}{\frac{1}{\varepsilon_{hp}} + \frac{A_{hp}}{A_{abs}} \left(\frac{1}{\varepsilon_{abs}} - 1 \right)} \quad (4.8)$$

Convective transfer coefficient

Forced convection by wind cause of heat transfer outer glass and ambient average wind speed for selected site is 2.56m/sec.

$$h_{conv,g0-amb} = 5.7 + 3.8V = 5.7 + 3.8 \times 2.56 = 15.428W/m^2 \cdot K \quad (4.9)$$

An empirical correlation for predicting the heat transfer coefficient for a cylinder under free convection, inclined at any arbitrary angle with horizontal Nusselt, Prandtl and Grashof number. Characteristics length expressed equation ??; for initial time the air temperature interior of single tube 27°C and wall of absorber inner face is known from above calculations. Determining

the specific properties at film temperature ??.

$$T_f = \frac{T_{abs} + T_{amb}}{2} \quad (4.10)$$

Properties of air determine at film temperature and characteristic length fo a given inclined cylinder is

$$L_c = \left[\frac{Ld}{(L/d) \cos \beta + (d/L) \sin \beta} \right]^{\frac{1}{2}} \quad (4.11)$$

Grashof number for free convection is defined as

$$Gr = \frac{gBL_c^3(T_{ab} - T_{\infty})}{\nu^2} \quad (4.12)$$

Also non-dimensional Nusselt number is

$$Nu^{1/2} = 0.54 + a \left[\frac{Pr \times Gr}{[1 + (0.559/Pr)^{9/16}]^{16/9}} \right]^b \quad (4.13)$$

$$Nu = \frac{d_{cyl}h}{k} \Rightarrow h_{conv,abs-hp} = \frac{k}{d} Nu \quad (4.14)$$

Heat losses

Heat loss from outer surface can determined by product of summation of heat transfer coefficient with temperature difference at outer glass surface area.

$$Q_{l,go-amb} = A_{go}(h_{rad,go-amb} + h_{conv,go-amb})(T_{go} - T_{amb}) = \frac{T_{go} - T_{amb}}{R_{go-amb}} \quad (4.15)$$

Similarly, heat loss from inner glass to outer glass inside concentric tube.

$$Q_{l,gi-go} = A_{gi} \times h_{rad,gi-go} \times (T_{gi} - T_{go}) = \frac{T_{gi} - T_{go}}{R_{gi-go}} \quad (4.16)$$

the heat loss from absorber surface to glass is given by

$$Q_{l,abs-gi} = A_{abs} \times h_{rad,abs-gi} \times (T_{abs} - T_{gi}) = \frac{T_{abs} - T_{gi}}{R_{abs-gi}} \quad (4.17)$$

finally the loss from heat pipe surface to absorber is determined by the heat transfer coefficients and absolute temperature difference from heat pipe surface area.

$$Q_{l, hp-abs} = A_{hp}(h_{rad, hp-abs} + h_{conv, hp-abs})(T_{hp} - T_{abs}) = \frac{T_{hp} - T_{abs}}{R_{hp-abs}} \quad (4.18)$$

To solve the problem, the two glass cover, absorber and heat pipe surface temperatures are guessed and then by iteration are corrected until a satisfactory solution is reached by satisfying the following equations, obtained by combining Eqs. ??, ??, ?? and ??:

$$A_{go}(h_{rad, go-amb} + h_{conv, go-amb})(T_{go} - T_{amb}) = A_{gi} \times h_{rad, gi-go} \times (T_{gi} - T_{go}) = A_{abs} \times h_{rad, abs-gi} \times (T_{abs} - T_{gi}) = A_{hp}(h_{rad, hp-abs} + h_{conv, hp-abs})(T_{hp} - T_{abs})$$

Numerical result of surface temperature is get using Engineering Equation Solver powerful tool that contain material physical properties with respect to its calculation activity the process of solving surface temperature is determine progressively as shown in fig ??.

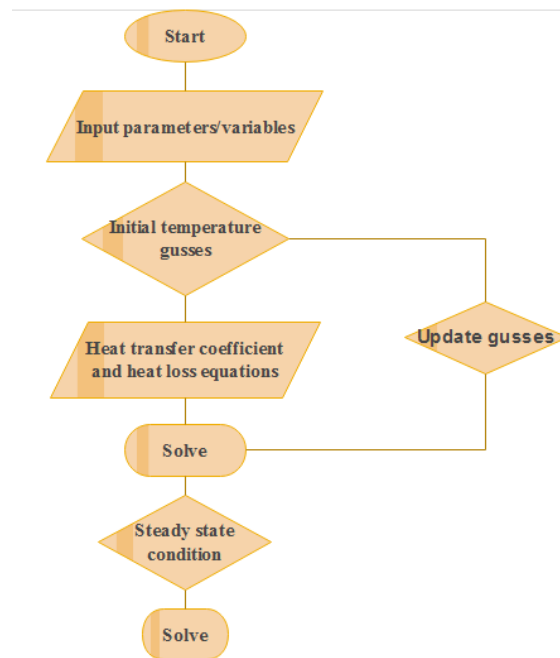


Figure 4.3: EES iterative solution procedure

The iterative value of surface temperature is T_{go} , T_{gi} , T_{abs} and T_{hp} is 315.7K, 374.5K, 444.03K, and 489.2K. from this we can determine the allover heat transfer parameters by placing the value in mentioned equation on the above.

Radiative heat transfer coefficient between outer glass to ambient is

$$h_{rad,g_0-sky} = 0.88 \times 5.67 \times 10^{-8} \times (315.7^2 + 294^2)(315.7K + 294) = 5.827W/m^2 \cdot K$$

similarly, for concentric glass surfaces

$$h_{rad,g_o-g_i} = \frac{5.67 \times 10^{-8} \times (374.5^2 + 315.7^2)(374.5 + 315.7)}{\frac{1}{0.88} + \frac{0.09}{0.12} \left(\frac{1}{0.88} - 1 \right)} = 7.58W/m^2 \cdot K$$

radiative heat transfer between inner glass and absorber

$$h_{rad,g_i-abs} = \frac{5.67 \times 10^{-8} \times (444.03K^2 + 374.5^2)(444.03K + 374.5)}{\frac{1}{0.9} + \frac{0.0825}{0.09} \left(\frac{1}{0.88} - 1 \right)} = 11.41W/m^2 \cdot K$$

radiative heat transfer between absorber to heat pipe surface

$$h_{rad,hp-abs} = \frac{5.67 \times 10^{-8} \times (444.03K^2 + 489.2^2)(444.03K + 489.2)}{\frac{1}{0.9} + \frac{0.0746}{0.0825} \left(\frac{1}{0.9} - 1 \right)} = 13.71W/m^2 \cdot K$$

finally, the natural convection between absorber and heat pipe is determined bellow

$$T_f = \frac{444.03K + 300}{2} = 372.02K$$

properties of air at film temperature is

$$\nu = 2.155 \times 10^{-5} m^2/s \quad k = 0.02994W/m.K$$

$$pr = 0.741 \quad B = \frac{1}{372.02}$$

and characteristic length is

$$L_c = \left[\frac{1485 \times 35}{(1485/35) \cos 18.45 + (35/1485) \sin 18.45} \right]^{\frac{1}{2}} = [1288.8]^{\frac{1}{2}} \\ = 35.0mm = 0.035m$$

Grashof number is

$$Gr = \frac{9.81 \times (0.0359m)^3 (492.1 - 300)}{444.03 \times (2.155 \times 10^{-5})^2} = 4.69 \times 10^5$$

for the constant coefficient stated for the range Prandtl and Grashof in 0.68 – 0.77 and $1.4 \times 10^4 - 1.2 \times 10^{10}$ respectively; the value of a is 0.390 and b is 0.168 ?.

$$Nu^{1/2} = 0.54 + 0.390 \left[\frac{0.741 \times 4.69 \times 10^5}{[1 + (0.559/0.741)^{9/16}]^{16/9}} \right]^{0.168}$$

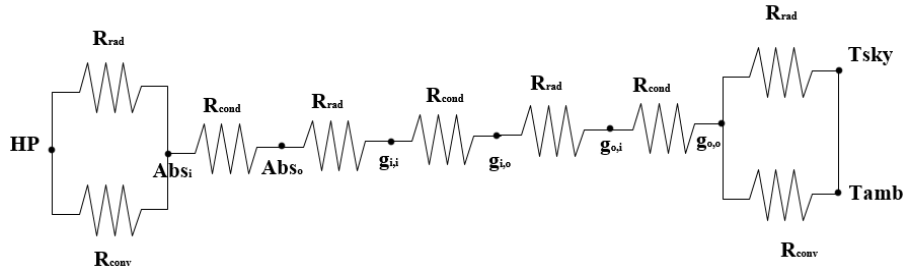


Figure 4.4: Concentric tube heat transfer network.

$$Nu = \sqrt{3.316} = 1.82$$

then

$$Nu = \frac{d_{cyl}h}{k} \Rightarrow h_{conv,abs-hp} = \frac{k}{d}Nu = 1.313W/m^2 \cdot K$$

The overall heat resistance and heat transfer coefficient related in equation ??.

$$R = \frac{1}{h \times A} \quad (4.19)$$

Resistance between outer glass to sky

$$R_{rad,g_0-sky} = \frac{1}{h_{rad,g_0-sky} \times A_o} = \frac{1}{5.827 \times 0.12} = 1.43K/W$$

between concentric tube

$$R_{rad,g_0-g_i} = \frac{1}{h_{rad,g_0-g_i} \times A_i} = \frac{1}{7.58 \times 0.09} = 1.465K/W$$

outer tube to absorber

$$R_{rad,g_0-abs} = \frac{1}{h_{rad,g_0-abs} \times A_{abs}} = \frac{1}{11.4 \times 0.083} = 1.06K/W$$

absorber to heat pipe

$$R_{rad,abs_{hp}} = \frac{1}{h_{rad,abs_{hp}} \times A_{hp}} = \frac{1}{11.4 \times 0.0746} = 1.17K/W$$

Total resistance for radiative is

$$R_{rad,tot} = R_{rad,g_0-sky} + R_{rad,g_0-g_i} + R_{rad,g_0-abs} = 1.43 + 1.465 + 1.06 + 1.17 = 5.125K/W$$

forced convective heat transfer resistance

$$R_{conv,go-amb} = \frac{1}{h_{conv,go-amb} \times A_o} = \frac{1}{15.428 \times 0.24} = 0.27K/W$$

convective resistant between absorber and heat pipe

$$R_{conv,abs-hp} = \frac{1}{1.33 \times 0.0746} = 8.3K/W$$

total convective resistance

$$R_{conv,tot} = R_{conv,go-amb} + R_{conv,abs-hp} = 0.27 + 8.3 = 10.07K/W$$

Heat Pipe Analysis

Analysis is in radial and internally in longitudinal direction. A heat transfer fluid pass through evaporation and condensation process in order to achieve mechanism. Film boiling created inside heat pipe and the specific properties is determined at film temperature. The film boiling heat flux is determined by equation ??.

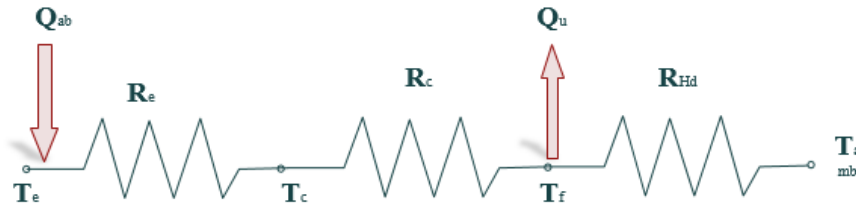


Figure 4.5: Heat pipe heat transfer network.

$$\dot{q}_{film} = 0.62 \left[\frac{g k_v^3 \rho_v (\rho_l - \rho_v) [h_{fg} + 0.4 C_p (T_{hp} - T_{sat})]}{\mu_v D (T_{hp} - T_{sat})} \right]^{1/4} (T_{hp} - T_{sat}) \quad (4.20)$$

Property of water at saturation temperature

$$\rho_l = 924.4 \quad h_{fg} = 2257 \times 10^3 \times J/Kg$$

$$T_f = \frac{T_{hp} + T_{sat}}{2} = \frac{489.2 + 373}{2} = 431.1K$$

interpolating properties water vapor at T_f is

$$\mu_v = 1.375 \times 10^{-5} kg/m \cdot s \quad k_v = 0.02994W/m.K$$

$$\rho_v = 1.8665 \text{ Kg/m}^3 \quad h_{fg} = 2151.1 \times 10^3 \quad C_{p_v} = 2229.9 \text{ J/kg} \cdot \text{K}$$

film flux is

$$\dot{q}_{film} = 0.62 \left[\frac{9.81 * (0.02994)^3 * 1.8665 * (924.4 - 1.8665) [2151.1 \times 10^3 + 0.4 * 2229.9 * (489.2 - 373)]}{(1.375 \times 10^{-5}) * 0.016 * (489.2 - 373)} \right]^{1/4} (489.2 - 373)$$

$$\dot{q}_{film} = 16.24 \text{ KW/m}^2$$

First law of thermodynamics requires that the rate of heat transfer from the hot fluid ne equal to rate of heat transfer to cold one. Rate of heat transfer for evaporator film boiling is

$$\dot{Q}_{boil} = \dot{q}_{film} * A_e = 16.24 \text{ KW/m}^2 * 0.0746 \text{ m}^2 = 1211 \text{ W}$$

mass flow rate of evaporation

$$\dot{m} = \frac{\dot{Q}_{boil}}{h_{fg}} = \frac{1211}{2151.1 \times 10^3} = 0.56 \times 10^{-3} \text{ Kg/sec}$$

the heat transfer coefficient for film condensation

$$h_{cond} = 0.729 \left[\frac{g \rho_l (\rho_l - \rho_v) h_{fg}^* k_l^3}{\mu_l (T_{sat} - T_{con}) D} \right]^{1/4} \quad (4.21)$$

the modified latent heat of vaporization determined by using equation ??.

$$h_{fg}^* = h_{fg} + 0.68 C_{p_l} (T_{sat} - T_{con}) \quad (4.22)$$

$$h_{fg}^* = 2151 \times 10^3 + 0.68 \times 4597.2 \times (373 - 300) = 2388.1 \times 10^3$$

then coefficient is

$$h_{cond} = 0.729 \left[\frac{9.81 \times 922.5 \times (922.5) \times 2388.1 \times 10^3 \times 0.319}{(0.2 \times 10^{-3}) (373 - 300) \times 0.05} \right]^{1/4}$$

$$h_{cond} = 69.8 \times 10^2 \text{ W/m}^2$$

for inclined surface

$$h_{cond,t} = h_{cond} \times (\cos \beta)^{1/4} = 69.8 \times 10^2 \times (\cos 18.45)^{1/4} = 68.89 \times 10^2 = 6889 \text{ W/m}^2$$

condensing process resistance

$$R_{c,ii} = \frac{1}{h_{cond}} \Pi d_i L_c = \frac{1}{6889} \Pi \times 49 \times a0^{-3} \times 0.16 = 5.89 \times 10^{-3} \text{ K/W}$$

total heat pipe resistance is

$$R_{tot, hp} = R_{c, ii} = 5.89 \times 10^{-3} K/W$$

Due to the well insulated header the heat transfer not barrier by outside temperature. Total resistance in the tube is summation of all resistant.

$$R_{tot} = 10.07 + 3.695 + 5.89 \times 10^{-3} = 13.73 K/W$$

4.1.3 Useful Energy

Gaining of solar energy pass through different heat transfer mechanism and loss will happen in the process due to material resistance property, environmental condition and efficiency mechanism. heat loss for a single tube calculate by equation ??.

$$Q_{loss} = \frac{T_{hp} - T_{abs}}{R_{tot, gi-Hp}} \quad (4.23)$$

for the evacuated tube heat loss to the ambient is zero due to the vacuum space in concentric glass. The loss analyzed with inner glass to header.

$$Q_{loss} = \frac{419.2 - 444.03}{13.73} = 3.29 W$$

Heat pipe absorbed energy is

$$Q_U = Q_{abs} - Q_{loss} = 93.2 - 3.29 = 89.9 W$$

useful energy for 10 tubes standard single collector incorporate with heat pipe is determined.

$$Q_{u,c} = 8 * Q_U = 10 * 89.9 = 899 W$$

for 8 hr sunlight duration

$$Q_{u,c} = 899 J/sec \times 8 hr \times 3600 sec/hr = 25.891 MJ/day = 7.192 KWhr$$

4.1.4 Collector Efficiency

Area of collector with 1760mm length 720mm width and 20mm tube space.

$$A_c = 1.76 \times 0.720 = 1.27 m^2$$

collector absorber area

$$A_{ab} = 0.12 \times 10 = 1.2m^2$$

single collector thermal efficiency

$$\eta_c = \frac{Q_{u,c}}{G_t \times A_{ab}} = \frac{899}{1361.38 \times 1.2} = 0.55 = 55\%$$

4.2 Water Heating System Design

A solar water heater is a combination of solar collector, energy transport and storage tank. The main part of solar water heater is the solar collector array, which absorbs solar radiation and convert to liquid. Selection of heating system is the base of following criteria.

1. Simplicity in design
2. Effectiveness
3. Easy/tilt maintenance requirement
4. Quite performance requirement
5. cost

4.2.1 System and Component Descriptions

Selected system is designed in the basis application and economical feasibility. Direct-Passive thermosyphone system selected for using potable water or when it is not available use cold storage tank water is heat directly in the collector and heat transfer fluid use natural convection to flowing fluid in the collector header. Thermosyphoning effect occurs because of the water density with increasing of temperature and flow of heat transfer fluid continuous until driving force is getting small. The system is use large pipe sizes to minimize pipe friction. The advantage of system are they don't relay on pumps and controllers, more reliable and have a longer life than forced circulation system. Both pressurized and unpressurized thermosyphoning system is used for makeup water from potable and cold storage tank respectively.

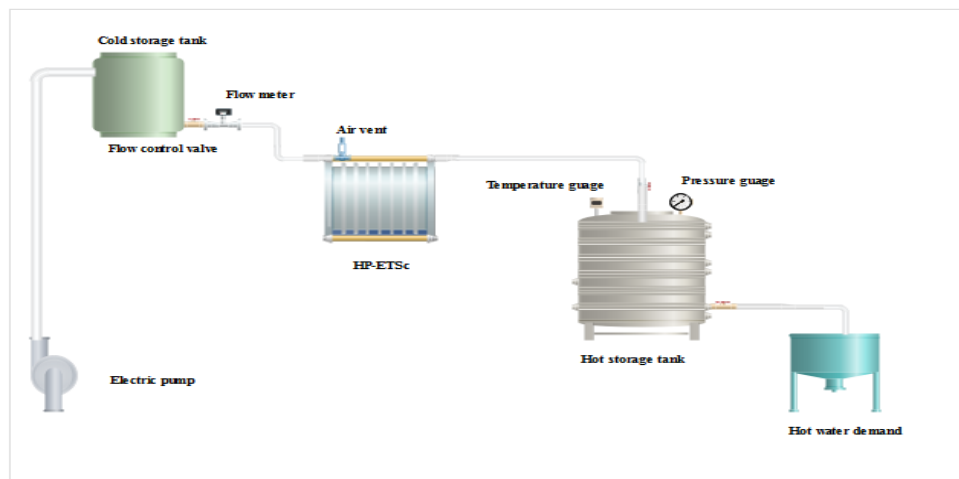


Figure 4.6: Proposed solar system diagram.

System component description

1. **Evacuated tube solar collector:-** Borosilicate glass tube embed heat pipe in concentric part for heat transfer with a single collector area $1.08m^2$.
2. **Cold and Hot water storage:-** the cold tank is stored collector fluid place at top of roof higher than installed collector, it use for avoiding shortage of cold water demand. The well insulated hot storage has capacity with a fully demand of milling plant for 24hr working hour.
3. **Pipe:-** the designed tube diameter, it made of copper and externally insulated. transporting hot fluid to storage and cold storage to collector.
4. **Auxiliary heating unit:-** heating capacity of unit is equal with the loss and placed inside hot storage tank. it is electrical driving heat source.
5. **Air vent:-** is used as escaping air from system until the flow is fully develop and it is placed at collector header.
6. **Pressure relief valve:-** is reduce higher pressure from the system.
7. **Balancing valve:-** it is a flow regulating or balancing valve in the collector array.
8. **Differential temperature controller:-** is use control poor performance of the system and over temperature bay taking three different value from cold, hot and storage of the system.

9. **Pump**:-the selected pump uses flow from tap to storage tank.
10. **Shutoff valve**:- is stopping flow in the system it may be system is stop or over temperature is caused.
11. **Pressure reduce valve**:- reduce make up water pressure from cold storage and potable water.

4.2.2 Collector Orientation

Capturing solar radiation is greatly depend on sun to collector viewing for higher performance of the system. This need specific collector orientation for selected research site.

Azimuth angle:-fixed surface of collector in the north hemisphere is due south.

Tilt angle:- many literature is give different correlation; most reliable and common collector slope for water heating is equal to latitude of the location or add 10° the second coloration is for this research.

4.2.3 System Sizing

It is extremely important to select the correct size of the solar water heater system. The solar water heater sizing needs to be done based on the hot water requirements. The basic idea of having a solar water heater is to reduce electricity consumption for water heating and hazardous gases for environment from burning of oil aid biomass/agricultural west. An under-sized system is insufficient to meet the hot water requirement, an over sized system will result in overheating of the water.

System Collector Area

Determining solar collector area is one in the designing of system and it uses. Number of collector is ratio of demand load to useful energy.

$$N_c = \frac{Q_l}{Q_{u,c}} = \frac{243.69MJ/day}{25.891MJ/day} = 9.41 \approx 10collectors$$

total useful energy from collector is summation of their individuals output.

$$Q_U = Q_{u,c} \times N_c = 899W \times 10 = 8.99KW$$

for a system collector area

$$A_{sys,c} = A_c \times N_c = 1.27 \times 10 = 12.7m^2$$

Sizing of Storage Tank

The energy storage has an enormous influence on overall system cost, performance and reliability. Design of cylindrical shape storage tank is volume of 1100 liter. Let length of storage is $2 * D$.

$$V_{cyl} = A \times L_{st} = \frac{\Pi}{4} D_{st}^2 \times L_{st}$$

then

$$D_{st} = \sqrt[3]{\frac{2 \times V_{cyl}}{\Pi}} = \sqrt[3]{\frac{2 \times 1.1}{\Pi}} = 0.888m$$

$$L_{st} = 2 \times D_{st} = 1.776m$$

Collector Arrangement

connecting collector is highly affect the system performance and life time because of higher pressure drop. The choice of series or parallel arrangement depends on the temperature required from the system and available roof top. For determining arrangement determine the collector output temperature.

$$T_o = \frac{Q_U \times N_c}{\dot{m}_c \times C_p} + T_i = \frac{899 \times 10}{0.0383 \times 4,180} + 27 = 77.57^\circ C$$

The demand temperature is get at Out put of all collector when in serious connection; cause of this the collector use internal manifolds.

Piping Arrangement

Collector Piping:- collector piping seizing account the condenser length and filling ratio in header part.

$$L_{con} = D_{c,p}$$

System Piping:- piping design in economical way is greater advantage. Assume collector water speed is $0.3m/sec$; hence, thermosyphon system effective at lower speed..

$$\dot{V} = \frac{G_t \times \eta_c}{C_{pw} \times \Delta T} = \frac{1361.38W/m^2 \times 0.548}{4.8KJ/kg \cdot k(\frac{hr}{sec}) \times (70 - 27)} = 14.96Kg/m^2hr = 15L/m^2hr$$

pipe diameter

$$D_{sys,p} = \sqrt{\frac{4(\frac{A_c \times \dot{V}}{v})}{\Pi}} = \sqrt{\frac{4(\frac{9.72 \times 15}{0.3})}{\Pi}} = 13mm$$

4.2.4 Thermal Performance of the System

Piping Loss

Heat loss in the system is never deny; it may minimize using different mechanism. The pipe must be small segment and output temperature of one is entering to the next collector. Loss from system piping with 25mm insulation thickness and average collector fluid temperature.

$$q_{p,loss} = \frac{2 \times \Pi \times k \times \Delta T}{\ln(\frac{D_o}{D_i})} = \frac{2 \times \Pi \times 0.046 \times (36 - 27)}{\ln(\frac{63}{13})} = 1.65W/m$$

for total 12.6m connection pipe total loss is 0.02KW

Storage Loss

Heat loss from collector storage is in radial side by conduction from ambient temperature with 50cm cellulose insulation wall.

$$Q_{st,l} = UA_{st} \times (T_{st} - T_{amb})$$

storage tank conduction heat loss coefficient is

$$(UA)_{st} = \frac{1}{R_{st.con}} = \frac{2 \times \Pi \times k_{ins}L_{st}}{\ln(\frac{D_o}{D_i})} = \frac{2 \times \Pi * 0.046 \times 1.776}{\ln(\frac{1.888}{0.888})} = 0.68W/K$$

energy is store at demand temperature

$$Q_{st,l} = 0.68(353 - 300) = 36.1W$$

Energy stored in tank

$$Q_{st} = Q_u - Q_{load} - Q_{st,l} - Q_{p,l} = 8.8KW - 2.88kW - 0.0361kW - 0.02kW = 5.86kW$$

system performance is 99.2% by determined all loss.

4.2.5 Collector Installation

Performance of solar water heater will depend largely on the proper installation of the system. In consideration of different economical and performance analyzed.

Site Placement

Selection of appropriate installation site is with criteria of

- Shadowing
- Environmental hazard like animal, wind
- Distance from demand plant
- Less economical site

Structural Support

Support structure should be stable, resistive to corrosion and angle of tilt must be proper. Support structure must be anchored to the roof by bolt with available rooftop. The anchoring must be sufficient to ensure that strong winds are not able to topple the structure and solar collectors.

Collector Spacing

Collector spacing in the installation configuration affect the collector performance by preventing solar insolation because of shadowing one in to other. On this design collector length is in

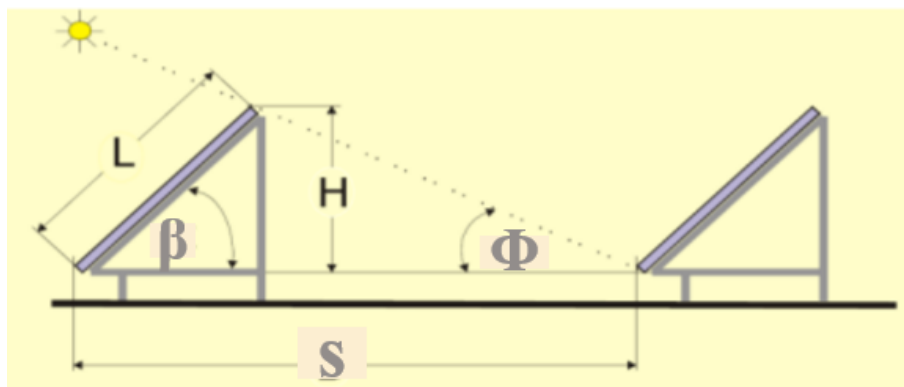


Figure 4.7: Solar collector configuration ?.

including header length.

$$L_c = L_T + L_{ad} + L_{cond} + t_{ins} = 1500 + 100 + 160 + 50 = 1810\text{mm} = 1.8\text{m}$$

collector height

$$H = L_c * \sin \beta = 1810 * \sin 19.45 = 572.8\text{mm} = 0.573\text{m}$$

collector spacing

$$S = L_c * \sin(180 - (\beta + \Phi)) = 1810 * \sin(180 - (18.45 + 8.45)) = 5.6\text{m}$$

Storage Tank Configuration

Thermosyphoning system depends on the stratification of water in the storage, vertical tank configuration are more effective and preferable for other integrated system. Horizontal tank influenced by conduction between the high temperature auxiliary. Finally, vertical configuration of tank selected. in order to avoid galvanization use similar material for piping and tank, placement is inside room below collector piping and transportation material cost is minimized.

4.2.6 Pressure loss

Design parameters and collected data help as to determine pressure loss at average demand water temperature which is 36°C . At this state the fluid property density, kinematic viscosity determine from appendix and collector volume flow rate is designed before estimation of load with sun hour at methodology part. The pressure drop at header, in fittings and inside connection pipe. The volume flow rate at average fluid temperature.

$$\dot{Q} = \frac{0.0383}{993} = 3.856 \times 10^{-5}\text{m}^3/\text{sec}$$

I. Pressure drop inside header

assume the uniform flow rate for each collector. Average velocity is determined by ratio of flow rate and area of header.

$$v_{ave} = \frac{\dot{Q}}{A_{hd}} = \frac{3.856 \times 10^{-5}\text{m}^3/\text{sec}}{0.36\text{m}^2} \quad (4.24)$$

since area of header is

$$A_{hd} = \Pi \times D_{hd} \times L_{hd} = \Pi \times 0.72 \times 0.16 = 0.36\text{m}^2$$

Reynolds number is

$$R_e = \frac{\rho \times v_{ave} \times D}{\mu} = 246.37 \quad (4.25)$$

since the $R_e < 2000$ flow is laminar. Pressure drop in the header $f = 64/R_e = 0.259$.

$$\nabla P_{hd} = f \frac{L_{hd} \times \rho \times v_{ave}^2}{2D_{hd}} = 1.279 \times 10^{-5} Pa \quad (4.26)$$

for total number of collectors is $1.279 \times 10^{-4} Pa$

II. Pressure drop inside fittings

for 90° bend elbow friction coefficient is $k_{fit} = 0.9$

$$\nabla P_{fit} = k_{fit} \frac{\rho \times v_{ave}^2}{2} = 4.78 \times 10^{-2} Pa \quad (4.27)$$

for 11 total number of fittings is $0.526 Pa$

III. Pressure drop inside connection pipes

total length of connection pipe is 6.2m and 0.013m between collectors and storage tank.

$$\nabla P_{conn} = f \frac{L_{conn} \times \rho \times v_{ave}^2}{2D_{conn}} = 6.79 \times 10^{-4} Pa \quad (4.28)$$

total pressure drop is summation of all.

$$\nabla P_{tot} = \nabla P_{hd} + \nabla P_{fit} + \nabla P_{conn} = 0.527 Pa$$

TECHNO ECONOMIC ANALYSIS

Cleaner energy technologies towards increasing eco-efficiency and reducing risks to both humans and the environment are becoming increasingly significant for different industrial sectors; options of solar water heating systems were identified as having both economic and environmental advantages. For each option, the most economical advantages that can be achieved in energy savings along with its simple payback periods were quantified. Based on their economic, environmental, and product quality advantages, implementing the galvanized solar water heater was favored due to its shorter payback period. The selective solar water heaters had a higher NPV than the others.

5.1 Techno Economical Indicators

Solar energy systems are generally characterized by high initial cost and low operating/maintenance costs. For decision of employing a solar energy system, the cost of collectors, system equipment, and conventional fuel required as backup must be lower than the cost of other conventional energy sources to perform the same task. solar fraction is a measure of the fractional energy savings relative to that used for a conventional energy system ?. This is expressed in percentage, given by an equation ??.

$$F = \frac{Load - Q_{Aux}}{Load} \quad (5.1)$$

The economic analysis of solar energy systems is carried out to determine the least cost of meeting the energy needs, considering both solar and non-solar alternatives. **Life cycle as-**

assessment is evaluate material flows and environmental impacts associated with production of goods provisions services over its full time extraction and processing of raw material through manufacturer, operating and final disposal ?.

Life Cycle Cost

LCC is the sum of all costs associated with an energy delivery system over its lifetime in today's money, taking into account the time value of money ??.

$$LCC = CI + C_{mp} \frac{1}{i} \left(1 - \frac{1}{(1+i)^n}\right) \quad (5.2)$$

Life Cycle Savings

LCS for a solar plus auxiliary energy system, is defined as the difference between the LCC of a conventional fuel-only system and the LCC of the solar plus auxiliary system. LCS suitable for lower collector area around $40m^2$, in same way for hirgher collector area it leads to negative.

$$LCS = C_{sys} FQ_{load} \frac{1+i_f}{1-i_f} \left[1 - \left(\frac{1+i_f}{1+i}\right)^n\right] \quad (5.3)$$

5.1.1 Total System Cost

Total system cost include the overall equipment, maintenance, installation and plumbing expense.

5.1.2 Fuel Cost

Bagasse is Preexisting fuel source in the company. Bagasse is that residuals of sugar cane remaining after the sugar cane containing juice crushed and squeezed, it is considered as fibrous and pithy material. The Net (low) Calorific Value (NCV) gives a more accurate indication of heat practically obtainable, but there is no means of determining it directly. The value is depend mainly on water content of bagasse and net value is $6526.34KJ/Kg$???. Factory sell the bagasse for different application like pulp, paper, fiber manufacturing and cattle rape by $1sack(80kg)$ in birr 120 i.e $1.50birr/Kg$.

$$Unitpriceof\ fuel = \frac{1.50birr/kg}{6526.34kJ/kg} = 2.3 \times 10^{-4}birr/kJ = 0.73birr/kWh$$

Table 5.1: Total Cost of Solar Water Heating System.

No.	Item	Specification	Quantity	Total price(birr)
1.	Collector	HP-ETSc	10	48,000
2.	Storage tank	stainless-steel 0.888m *1.776m	1	8,600
3.	Pumping	vertical pump	1	4000
4.	Elbow and Fittings	1/2'90°	11	500
5.	Fasteners	D-0.5cm, L-5cm	2 packet	300
6.	Auxiliary heater	1KW	1	1000
7.	Cold storage and support	2000lit,10*10 cm and 40mm	4	5,000
8.	Piping	1/2'	3	1,200
9.	Installation and labor cost	4		10,000
11.	Insulation cover	Galvanize steel,1m*1m	6	540
11.	Transportation	-	-	5,000
			Tot.	84,140
			Vat	12,621
			Total cost	96,761

taking boiler efficiency is 50% in the basis of current performance to determine total cost in account of age.

$$C_{tot,f} = \frac{0.83birr/KWh}{0.5} = 1.66birr/kWh = 4.6 \times 10^{-4}birr/kJ$$

then, daily bagasse cost for current boiler efficiency.

$$C_f = 4.6 \times 10^{-4}birr/KJ \times 243690KJ/day = 112.10birr/day$$

and yearly

$$C_f = 112.10birr/day \times 240day/yr = 26,904birr/yr$$

amount of bagasse per year

$$W_f = 26,904birr/yr \times 1.5Kg/birr = 40,356Kg/yr$$

5.1.3 Payback Period

Payback time is defined in many different ways, but the most common one is the time needed for the cumulative fuel savings become equal to the total initial investment, i.e. it is the time required to get back the money spent to erect the solar energy system from the fuel savings

incurred because of the use of the system. The fuel saved in a year n is given by equation ?? ?.

$$PB_P = \frac{\text{Systemcost}}{\text{fuelcostperyear}} = \frac{96,761}{26,904} = 3.6yr \quad (5.4)$$

5.2 Emission Estimation

Crashed sugarcane in sugar industry is leave its fibrous result/ bagasse contain 35 – 50% of total weight is moisture. Wet bagasse combustion would be poor and incomplete; combustion carbon present in bagasse transforms into carbon dioxide and hydrogen into water. composition of the theoretical air required for 1kg of wet bagasse combustion is 2.65kg of air ????. The composition of wet bagasse is presented in table ?? by percentage.

Table 5.2: Wet bagasse fuel composition.

Composition	symbol	Percentage (Kg/Kg)
Carbon	C	0.225
Hydrogen	H_2	0.03
Oxygen	O_2	0.23
Moisture	-	0.5
Ash	-	0.015

Source: ?

The basic equation ?? used in fuel analysis emission calculations?.

$$E = W_f \times \%_{pol} \times (Mw_p \div Mw_e) \quad (5.5)$$

CO_2 emission from carbon content of fuel is

$$E_{CO_2} = 35100Kg/yr \times 0.225\left(\frac{44}{12}\right) = 28,957.5kg/yr$$

H_2O emission in the vapor form fuel is

$$E_{H_2O} = 35100Kg/yr \times 0.03\left(\frac{18}{2}\right) = 9,477kg/yr$$

the rest of combustion emission is water, nitrogen, oxygen and ash.

MATHEMATICAL MODELING AND HEAT PIPE CFD ANALYSIS

CFD is computation method flow and related phenomena can be describing by partial differential (integrate-differential) equation which can out be solved and difficult in analytical. the approximate equation can applied to small domain in space and/or time so the numerical solution for a discrete location. In this chapter discusses the governing equation solved by ANSYS/Fluent solution approach. the multiphase, energy and turbulent models used for the simulation of two phase closed heat pipe with the different heat transfer fluid in the 50% filling ratio from volume of evaporater section.

6.1 General Governing Equation

Fluid flow is caused by externally applied force commonly gravity, shear and rotation; generally classified into two surface and body force. The fluid flow affect by other phenomena; these include temperature difference which is lead to heat transfer, the density variation which rise to buoyancy, concentration of solute greatly affect flows significantly or even be the sole case of flow. On this study flow phenomena conservation principle consider for a given quantity of matter and its extensive properties.

6.1.1 Continuity Equation

The fundamental physical principle equation works in an intensive mass is conserved. the governing flow equation the application of this physical to any models with finite control volume in fixed space, moving with fluid, infinitesimal small element fixed in space and infinitesimally small fluid moving with the flow. Equation ?? use for this study and an approach fluid element with flow for a property equal to 1.

$$\frac{\partial}{\partial t}\rho + div(\rho v) = 0 \quad (6.1)$$

6.1.2 Momentum Equation

Momentum equation is one approach to use in the control volume method, in this approach is used the intensive property is velocity for fluid containing volume of space.

$$\frac{\partial}{\partial t} \int_{\Omega} \rho v + \int_S \rho v v \cdot n dS = \sum \mathbf{f} \quad (6.2)$$

The conservation is simplify by using Gauss' divergence theorem to the convective and diffusive flux terms:

$$\frac{\partial(\rho v)}{\partial t} + \nabla \cdot (\rho v v) = \nabla \cdot (\mu \nabla v) - grad p + S_u \quad (6.3)$$

6.1.3 Energy Equation

For the governing equation derived by assume low speed flow and negligible viscous dissipation ?. The equation in terms of specific enthalpy is:

$$dh = c_p dT \quad (6.4)$$

The general equation written in the following form.

$$\frac{\partial \rho h}{\partial t} + \nabla \cdot \rho v h = \nabla \cdot \left(\frac{k}{c_p} \nabla h \right) + S_h \quad (6.5)$$

6.2 Numerical Modeling of Heat Pipe

ANSYS/Fluent 18 is selected for modeling of heat pipe. Multiphase model is useful to analyze phase change process in the volume of fluid approach.

6.2.1 Geometry

A specific geometry for TPCHP in three specified section with length of 1485mm , 100mm and 160mm for evaporative, adiabatic and condenser section respectively. The respective diameter is 16mm , 16mm and 80mm with selective material. Inclination of heat pipe investigate at collector orientation.

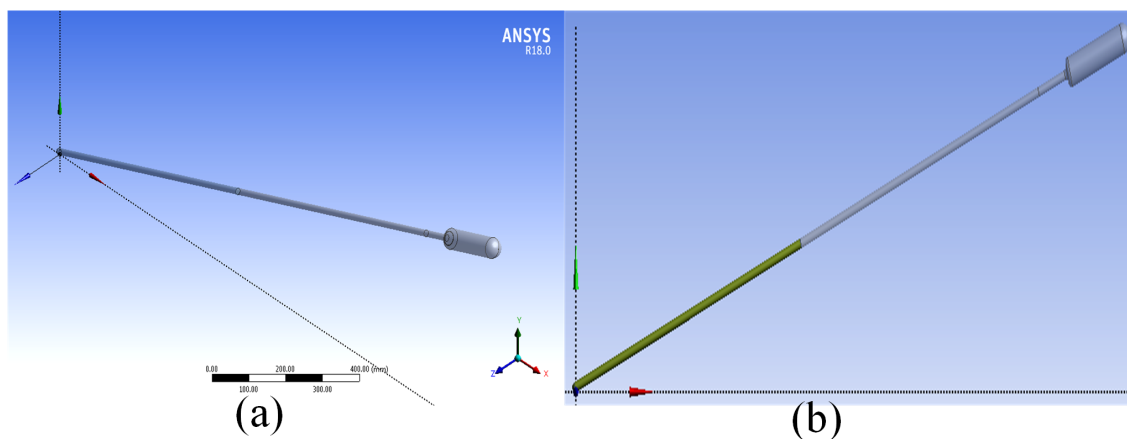


Figure 6.1: Geometry view (a). 3D model (b). Separate phase.

6.2.2 Mesh

Grid generation is a very active in research development of CFD. the large number of closely spaced grid points in those region of the flow where large gradient in the field properties exists; hence improving the numerical accuracy of a given calculation ?. CFD package workbench is provide robust, easy and automated mesh generation ?. Meshing is nothing but conversion of a model having infinite elements into finite elements. So the physics preference of meshing was mechanical and the curvature was kept on. The smoothing was medium. The meshing was deliberately made like this because otherwise the time taken to solve the model becomes very large and the courant number can limited at any time. The total griding statics is displayed in

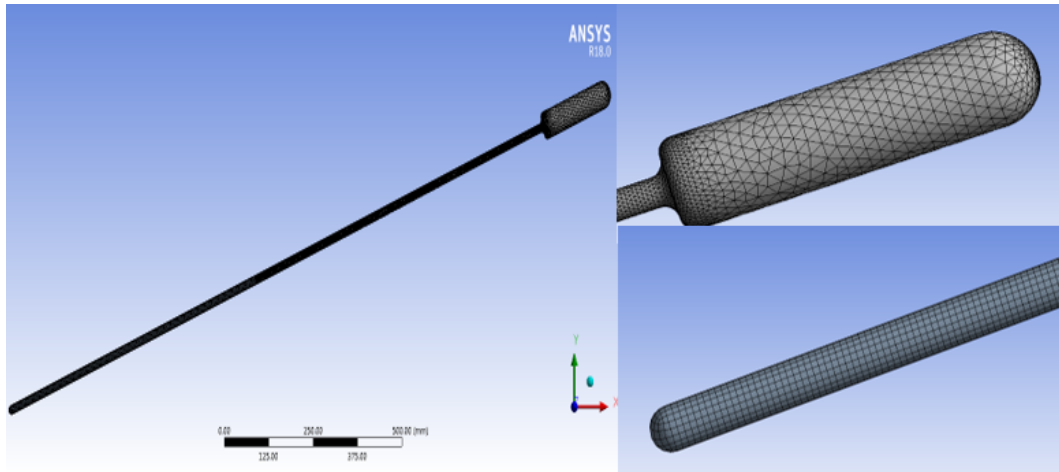


Figure 6.2: Mesh view at full model, evaporator and condenser section.

Table ?? for maximum of 5mm and minimum of 0.04mm element size.

Table 6.1: Mesh information for TPCTHP.

Domain	Nodes	Element
Gas	21695	99524
Liquid	21675	18720
All Domain	43370	118244

6.2.3 Setup

The solution models is generally starts by setting up for transient and pressure based approach with effect of gravitational force. The detail processing is discuses hear for different boundary, convergence, stability criterion, initial conditions, iteration and selective time steps.

Multiphase Model

Multiphase is large number of flows encountered in nature and technologies are a mixture phases; for selected liquid and gas phase of heat transfer fluid material with a particular properties and interaction is determined for the Bubbly flow i.e the flow of discrete gaseous fluid or bubbles in continuous fluid. Euler-Euler approach is determined here in this study; this uses in evaluating different phases in mathematically interpreting continua. Since the volume of a phase cannot be occupied by the other phases, the concept of aphasic volume fraction is intro-

duced ?.

The process can vary spatially as well as temporally. In order to accurately model multiphase flow, both higher-order spatial and time discretization schemes are used. The variables and properties in any given cell are either purely representative of one of the phases, or a mixture of the two phase, depending upon the volume fraction values. The models is determine vapor and liquid as a primary and secondary phase respectively. Phases volume fraction has three different possible conditions.

- $\alpha_l = 1$: the cell is fully occupied by secondary phase.
- $\alpha_l = 0$: the cell is vapor phase.
- $0 < \alpha_l < 1$: the cell mixture phase.

Mass transfer from liquid phase to vapor phase. By default, the source term on the right-hand side equation.

$$\frac{1}{\rho_v} \left[\frac{\partial(\alpha_v \rho_v)}{\partial t} + \nabla \cdot (\alpha_v \rho_v \mathbf{v}_v) \right] = S_{\alpha_v} + \sum_{l=1}^n (m_{lv} - m_{vl}) \quad (6.6)$$

The transient explicit formulation is applied for volume of fraction and interpret in equation for this study.

$$\frac{\alpha_v^{n+1} \rho_v^{n+1} - \alpha_v^n \rho_v^n}{\Delta t} V + \sum_f (\rho_v U_f^n \alpha_{v,f}^n) = \left[\sum_{l=1}^n (m_{lv} - m_{vl}) + S_{\alpha_v} \right] V \quad (6.7)$$

The volume fraction at the current time step is directly calculated based on known quantities at the previous time step, the explicit formulation does not require and iterative solution of the transport equation during each time step. Fluent automatically refines the time step for the integration of volume fraction equation, but you can influence this time step calculation by modifying the Courant number with the value 0.25. The Corant number dependent on element size and small time step. Gravity is act as a body force and modeled by implicitly formulation. Interface between im-miscible phases is sharp cause of their state property.

In the vapor liquid two phase system the density and viscosity in each cell is determinate by equation ?? and ??.

$$\rho = \alpha_v \rho_v + (1 - \alpha_v) \rho_l \quad (6.8)$$

$$\mu = \alpha_v \mu_v + (1 - \alpha_v) \mu_l \quad (6.9)$$

Energy Models

Energy is toggled on model setting that use for contact among the wall with phases, because of temperature difference is derive solution approach. The energy shared among the phases is used equation ??.

$$\frac{\partial}{\partial t}(\rho E) + \nabla \cdot (\vec{v}(\rho E + p)) = \nabla \cdot (k_{eff} \nabla T) + S_h \quad (6.10)$$

The VOF model treats energy and temperature as mass-averaged variables.

$$E = \frac{\sum_{p=1}^n \alpha_p \rho_p E_p}{\sum_{p=1}^n \alpha_p \rho_p} \quad (6.11)$$

Viscous Model

The fluid transportation for multiphase, methods of calculating turbulent viscosity. The features that are essentially common to all models follow, including turbulent generation due to shear buoyancy, accounting for the effects of compressibility, and modeling heat and mass transfer. The Boussinesq hypothesis is used in the Spalart-Allmaras model, the $\kappa - \varepsilon$ models. The advantage of this approach is the relatively low computational cost associated with the computation of the turbulent viscosity, μ_t ?.

The standard models for turbulence kinetic energy and the turbulence dissipation rate ε is used for this simulation.

Kinetic energy

$$\frac{\partial}{\partial t}(\rho k) + \nabla \cdot (\rho k \nabla \vartheta) = \nabla \cdot \left[\left(\mu + \frac{\mu_t}{Pr_k} \right) \right] + G_k + G_b - \rho \varepsilon - Y_M + S_k \quad (6.12)$$

Rate of dissipation

$$\frac{\partial}{\partial t}(\rho \varepsilon) + \nabla \cdot (\rho \varepsilon \nabla \vartheta) = \nabla \cdot \left[\left(\mu + \frac{\mu_t}{Pr_\varepsilon} \right) \right] + C_{1\varepsilon} \frac{\varepsilon}{k} (G_k + C_{3\varepsilon} G_b) - C_{2\varepsilon} \rho \frac{\varepsilon^2}{k} + S_k \quad (6.13)$$

The turbulent viscosity

$$\mu_t = \rho C_\mu \frac{k^2}{\varepsilon} \quad (6.14)$$

Wall treatment enhance boundary source with its thermal effects. The model constants and have default values, these have been determined from experiments for fundamental turbulent flows

including frequently encountered shear flows like boundary layers.

Materials

The properties appearing in the transport equations are determined by the presence of the component phases in each control volume. Prepared material data is input to CFD package materials endorsed by GUI.

Table 6.2: Thermo physical properties of HP working fluids.

Materials	Parameters				
	$k(W/m \cdot K)$	$C_p(j/Kg.k)$	$\mu(Kg/m \cdot s)$	$\rho(Kg/m_3)$	$h_{fg}Kj/mol$
water liquid	0.607	4180	0.891×10^{-3}	997	40.56
water vapor	0.0186	1870	0.98×10^{-5}	0.231	-40.56
Cu-nanofluid liquid	0.616	4016.49	0.9×10^{-3}	1036.68	41.97
Cu-nanofluid vapor	0.0189	391.85	0.992×10^{-5}	44.89	-41.97
Al-nanofluid liquid	0.687	3818.82	0.989×10^{-3}	1071.932	51.78
Al-nanofluid vapor	0.0192	895.68	1.08×10^{-5}	119	-51.78

Boundary and Operating Condition

The CFD model was set up with initial conditions and boundary conditions from analytical calculation. The initial temperature condition of all solid domains in the model was wall heat flux from absorbed solar. while the initial temperature of the fluid domain was $27^\circ C$ at determined material properties. The fluid and solid domains have different initial temperatures because at the beginning of simulation, before phase change began, the fluid was at a higher temperature from the wall of evaporator. Operating condition is set at lower pressure $4000pa$ for increasing evaporation rate and gravitational acceleration $9.81m/s$ in the direction of negative *yaxis*.

Table 6.3: Boundary condition for TPCTHP at different section.

	BC type	Evaporator	Adiabatic	Condenser
Wall	Temperature	$489.2K$	-	$300K$
Wall	Stationery	No-slip	No-slip	No-slip
Wall	Heat flux	-	$0W/m^2$	-
Wall	Material	Copper	Copper	Copper

6.2.4 Solution

Solution approach is used for accurate result in computational modeling. The solver methods criteria, initialization and calculation is selected based on computer performance and computational time.

Discretization Scheme

The finite volume method is applied to discretized the governing equations discussed in the above sub sections. Solution method performed by combination of pressure–velocity coupling, spatial and transient discretization. Schemes are used SIMPLE algorithm for pressure–velocity coupling; which has a robust capacity of solving shared pressure of separate phases explicit model with small CPU usage time and efficient in transient situation than other scheme, List Squares Cell-Based for gradient, PRESTO! for pressure, **First Order Upwind** for the determination of turbulent kinetic energy, dissipation rate, Geo-Reconstruct for volume fraction and **Second Order Upwind** for momentum and energy.

Solution Criteria

Solution criteria for phase change modeling is straightforward; which defines solution terminating conditions. The criterion has been done in account of solution accuracy, calculation and numerical instability; relaxation factor is uses default CFD package data. Convergence is based on the residual value of the calculated variables, pressure, mass, velocity components, volume fraction and temperature. Solver method monitored and desirably used residuals below $1e^{-3}$ for all calculation.

Solution Initialization and Run Calculation

Standard initialization is done with liquid volume fraction fully occupied for liquid domain and no gas domain at $t = 0$. The modeling considered, the time step chosen was 0.00001 seconds for achieving courant number in the specified margin. The number of iterations came out to be 400000 for solving each cases.

6.3 CFD Result and Discussion

The computational fluid dynamics analyses was done for two phase inclined heat pipe in 50% filling the volume of evaporator. The heat transfer phenomena is done by boiling and condensation process with the aid gravity for natural heat transfer has been takes placed. the simulation have been carried out till the system reached out quasi steady state which is average flow variables are time dependent this can achieved by monitoring the expanded inclined height of HP. The following sections are determined by converged computational result.

6.3.1 Result Analysis

The flow visualization is more elaborate the phenomena and mechanism; also gives the comparative analysis. The subsections shows comparative analysis on temperature, volume fraction, pressure and velocity of three different working fluid.

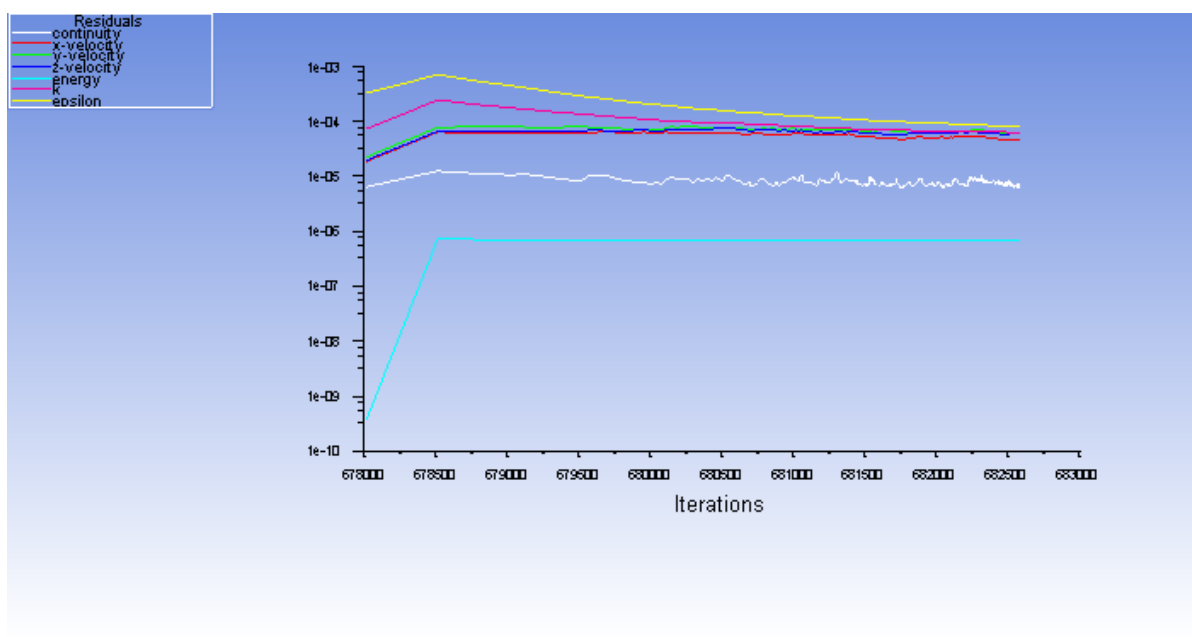
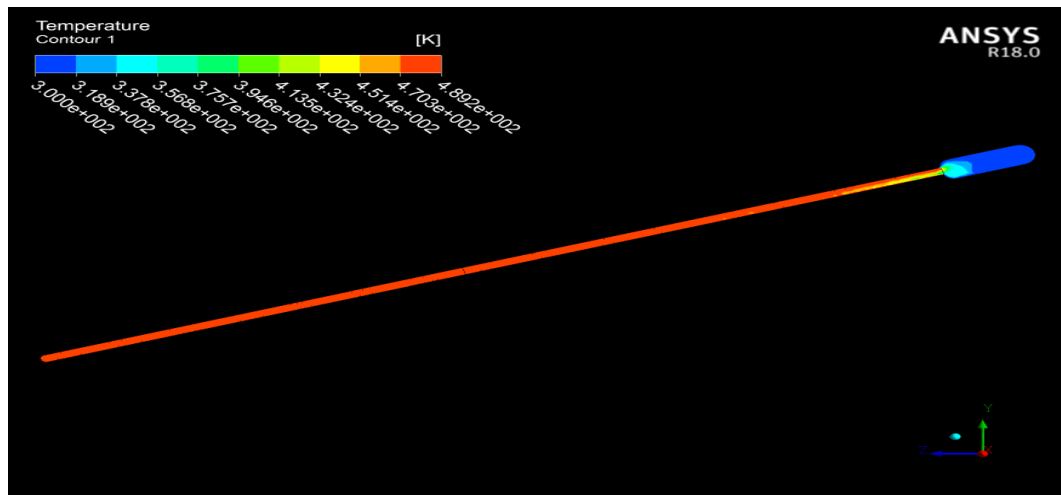


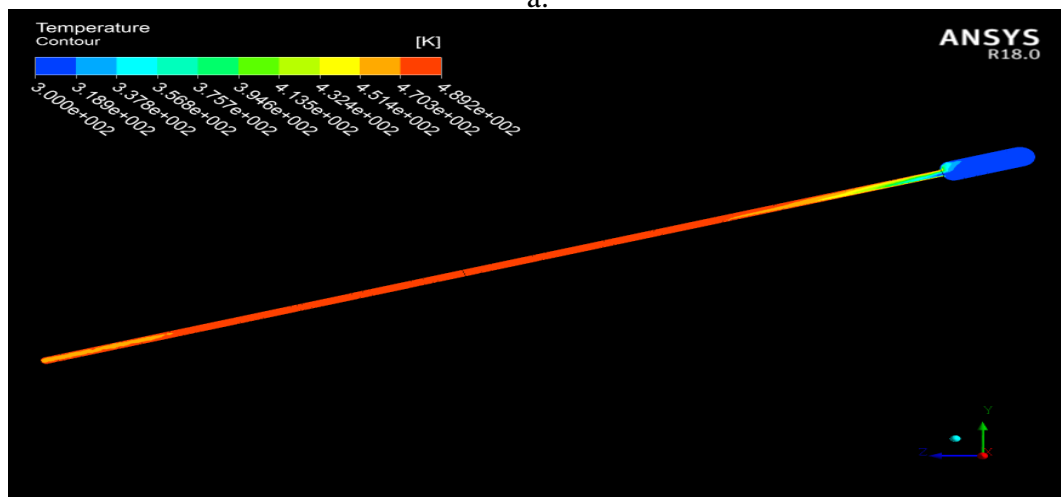
Figure 6.3: CFD package computer simulation graph

Temperature contour

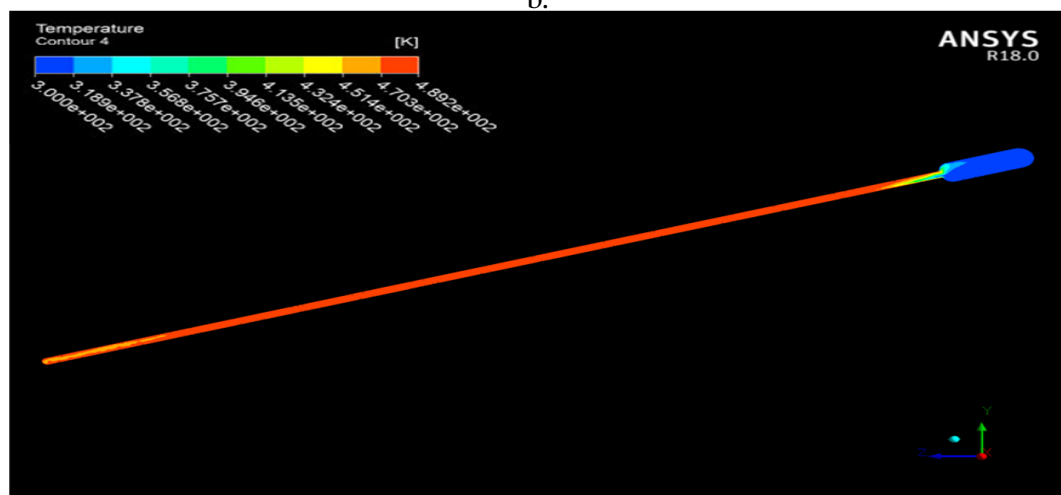
The temperature distribution along inclined HP can be seen through side view on symmetry plane of 3D model. Temperature profile along the fluid domain is shown in figure ?? for selected fluids . Temperature contour evaluation over total simulation time until it reach steady state level of different working fluid. At the starting of simulation; the vapor field crated when fluid temperature near to saturation value. The liquid was slightly lower than saturation temperature and increase gradually with time. Contours of temperature for all cases are presented in table ?? at different time till the condensation process done and it can explain performance of TPCHP clearly. The fall in temperature variation on HP sections, peak values is available on single vapor phase before it releases in the condenser sections. Maximum temperature value is registered at starting simulation half of evaporator i.e unfilled and adiabatic section cause of its free from heat loss and space occupied material air at working pressure but after the developed simulation time all are shown fluid temperature behavior. Base fluid temperature is gradually increase from low to higher and vapor form contain its temperature in the condenser section; finally, it come looks like others fluid. The higher temperature is available in Cu and Al nanofluid next to base fluid. At condenser section lower in copper particle contain fluid. The red color is show maximum and blue minimum value.



a.



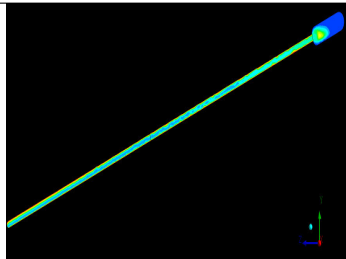
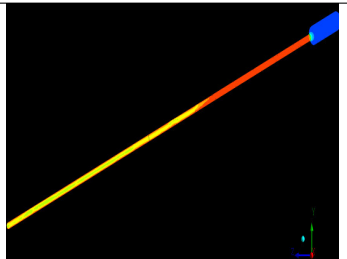
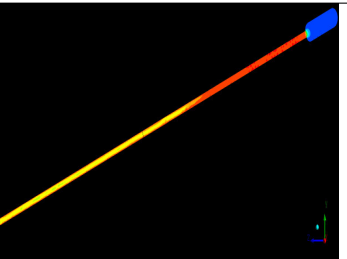
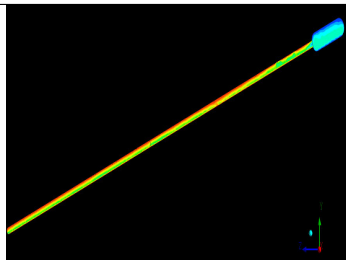
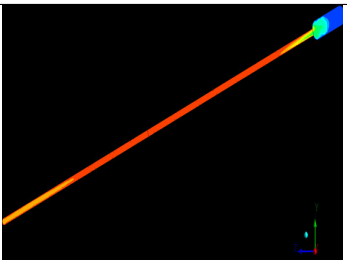
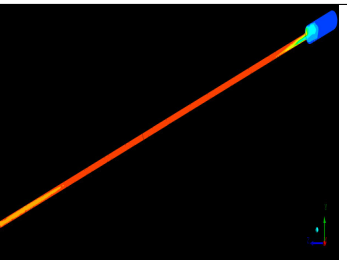
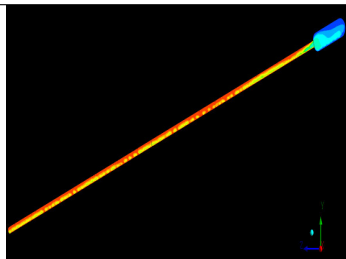
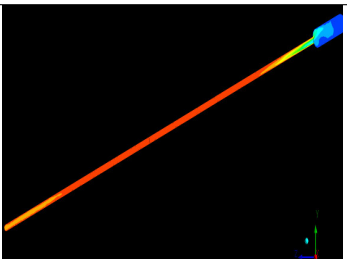
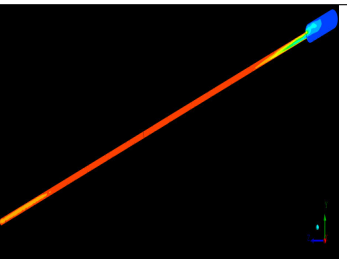
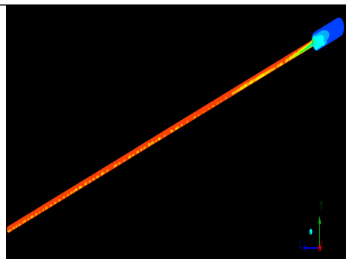
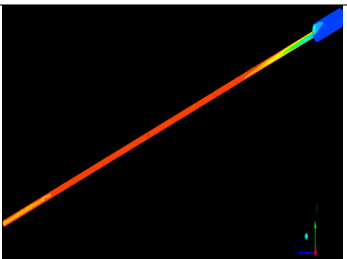
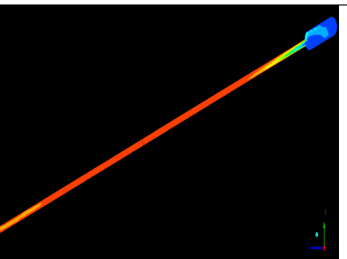
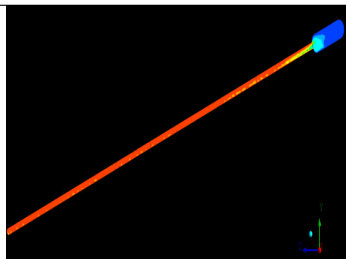
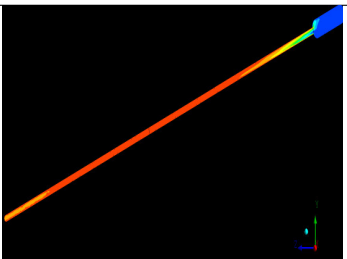
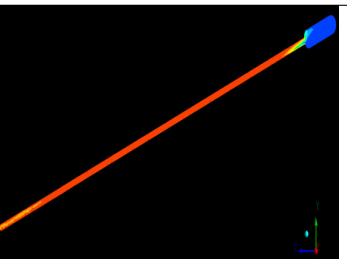
b.



c.

Figure 6.4: Temperature contour for different working fluid at steady state a. H_2O b. $Cu - H_2O$ c. $Al - H_2O$.

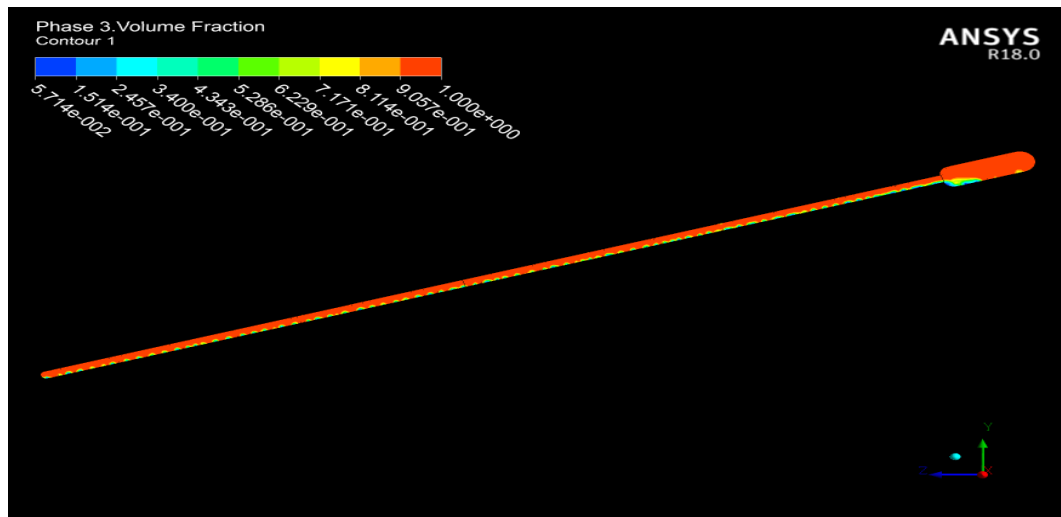
Table 6.4: Comparative average temperature contour for 3 various working fluid at different time (K).

Time	Water	Copper-nanofluid	Aluminum-nanofluid
10s	 349.300K	 437.11K	 427.58K
20	 393.98K	 452.79K	 443.47K
25s	 420.840K	 450K	 441.37K
30s	 439.7K	 447.67K	 440.57K
40s	 454.6K	 448.75K	 444K

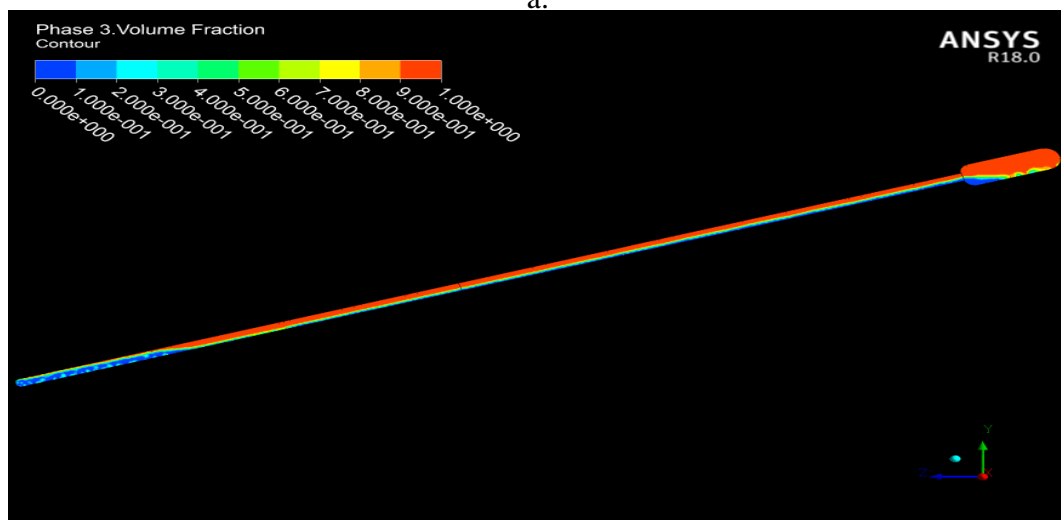
Volume Fraction

Volume fraction of pool boiling happen in the evaporator and film condensation of liquid in the condenser section. At beginning of process half of the evaporator section is filled by working fluid with volume of is occupied by liquid and vapor is zero; as the heating time increase for the boundary temperature increase and continuous evaporation rise the volume fraction of liquid and vapor is vise versa from the starting. Vapor fraction is dominate until condensation process is conducted in header part. The liquid pool of the working fluid represented by blue color and vapor is in red before film condensation happen. Contours of volume fraction of vapor with respect to full time simulation shown in figure ?? for all cases on symmetry plane of 3D model. The average value of vapor fraction 0.9, 0.73 and 0.71 for water, copper and aluminum containing nanofluid respectively; the more vapor fraction affect the heat transfer phenomena and its available in base fluid.

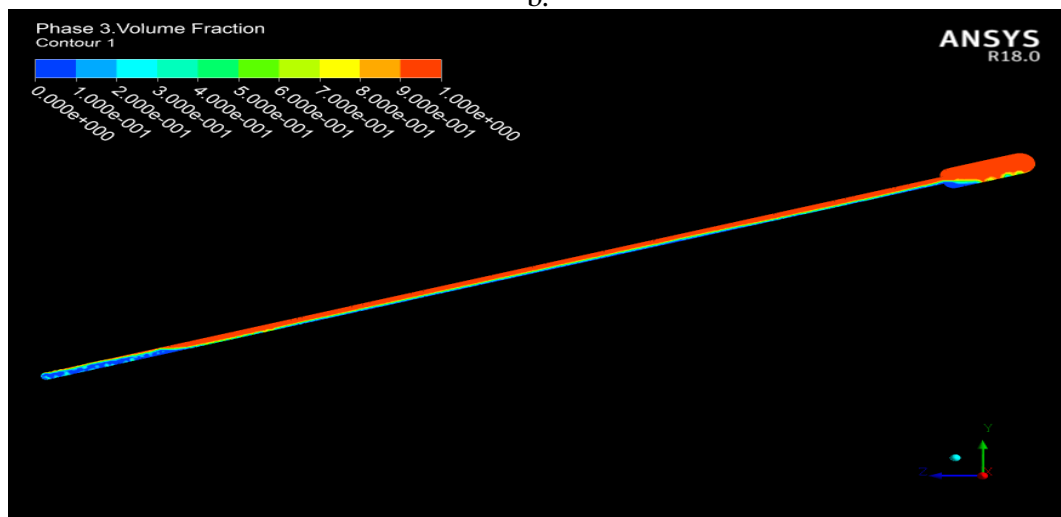
The condensed mass is more important than that provided by the inclined configuration for cyclic process. The contours taken at equal time space to provide an idea of the shape of condensed liquid and its downward momentum in inclined surface that adheres the walls of thermosyphon. The vapor production much higher in base fluid and reach condenser section fast but it has low temperature content in it than two cases. The mass concentration of vapor less than liquid at starting and finally the vapor is higher for continuous phenomena.



a.



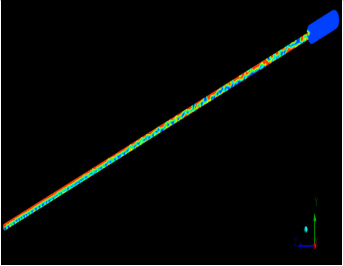
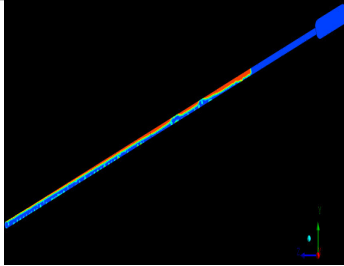
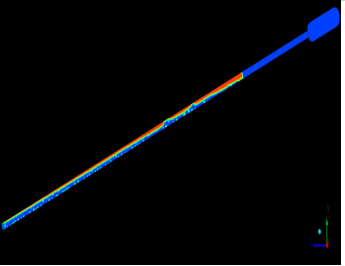
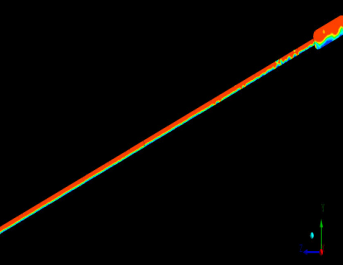

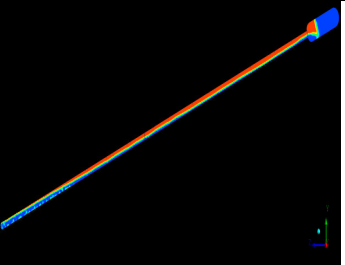
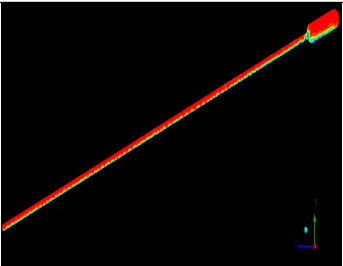
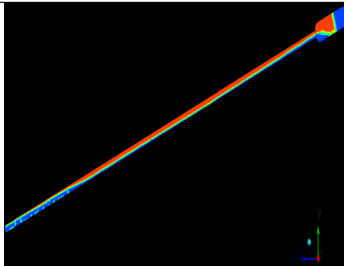
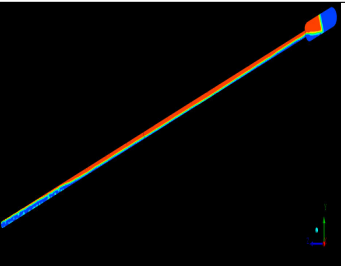
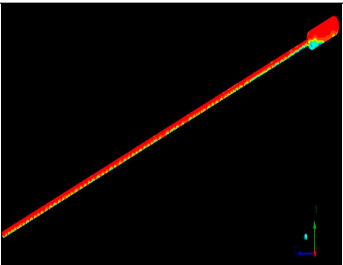
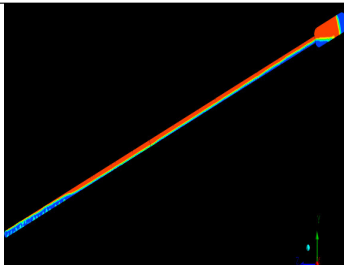
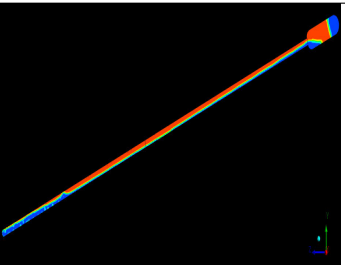
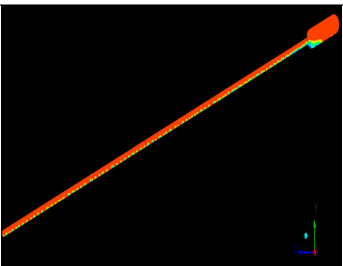
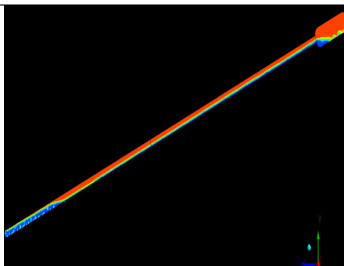
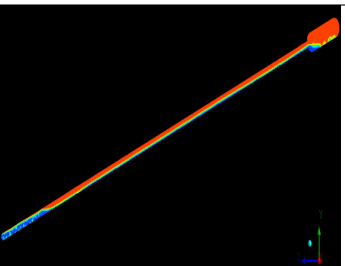
b.



c.

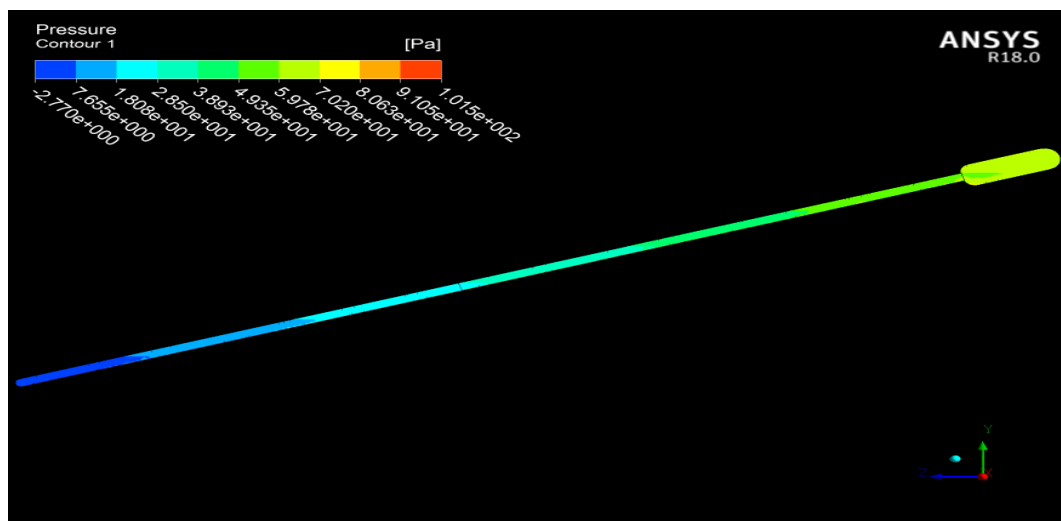
Figure 6.5: Volume fraction contour for different working fluid at steady state a. H_2O b. $Cu - H_2O$ c. $Al - H_2O$.

Table 6.5: Comparative Volume fraction of vapor for three different working fluid at selected simulation time (t).

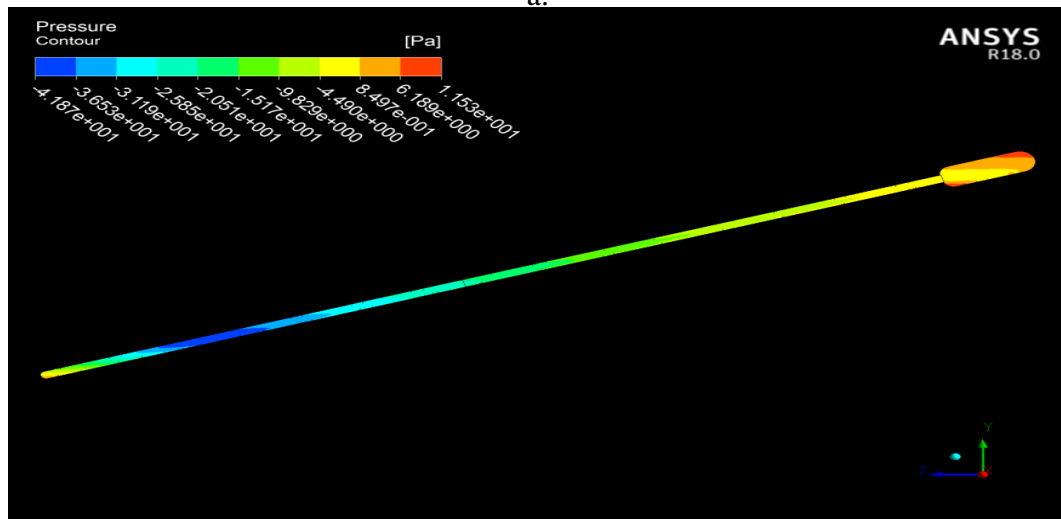
t	water	copper-nanofluid	aluminum-nanofluid
10sec	 0.492	 0.295	 0.298
20sec	 0.811	 0.519	 0.521
25sec	 0.875	 0.550	 0.550
30sec	 0.918	 0.575	 0.570
40sec	 0.990	 0.725	 0.712

Pressure Contour

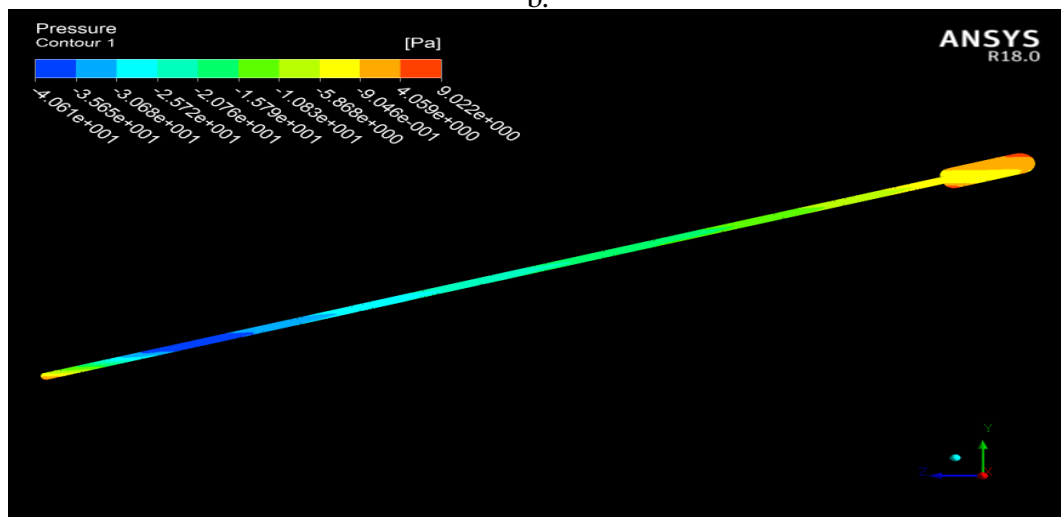
The pressure contour show in figure ?? variation inside the pipe due to phenomena and property of vapor. The pressure value maximum at the condenser section when vapor relies its energy and at evaporator section attain lower value of all over the fluid domain. The pressure increases from lower section to upper section and through it, in the progress is also has higher pressure gradient. It values higher at vapor state of working fluid. The much higher pressure attain copper-water nanofluid at steady state the negative value is shown the direction towards to bottom surface of an inclined thermosyphon heat pipe by gravity. The pressure is low starting of evaporation phenomena and its increase directly with vapor production. water working fluid attain lower pressure because of its vapor phenomena and state property, aluminum-water nanofluid is much higher vapor pressure next to copper-water nanofluid. water and aluminum-water is easily stable minimum value through the process than copper-water. the much higher vibration of molecule enhance high heat transfer in condenser. Table ?? more visualize the pressure variation through heat pipe with in a period of simulation time.



a.



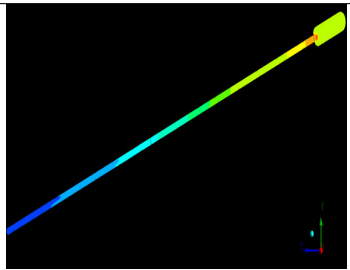
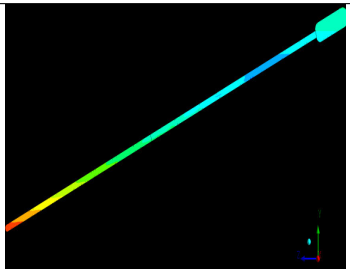
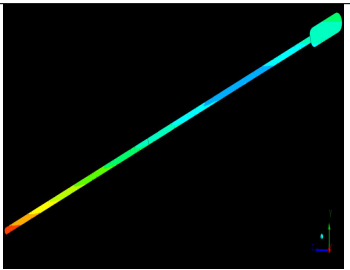
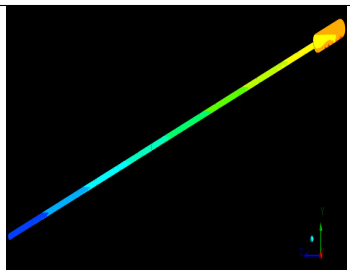
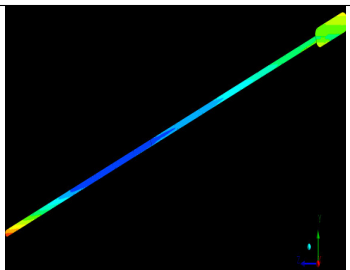
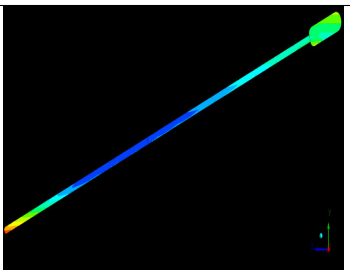
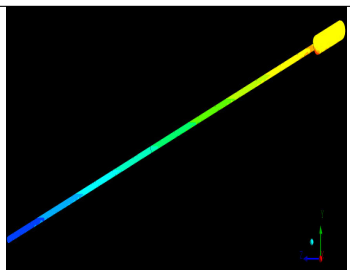
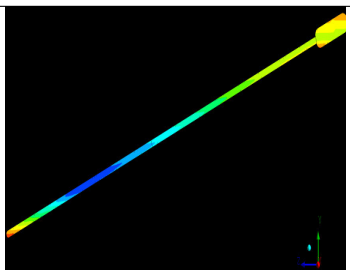
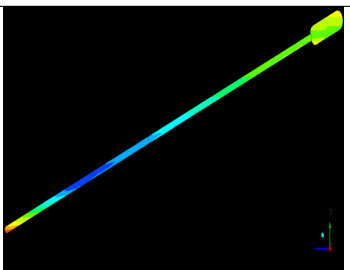
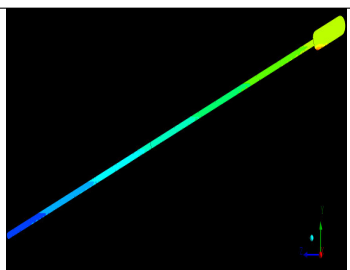
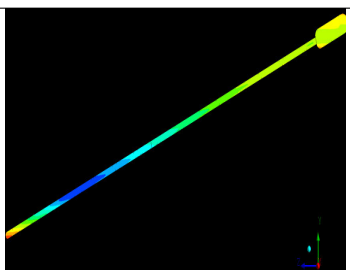
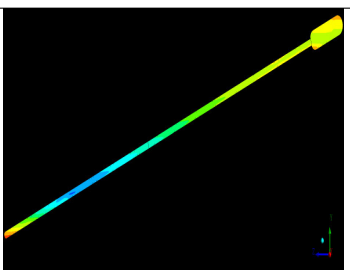
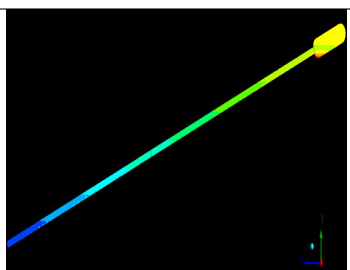
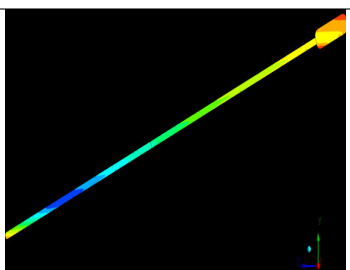
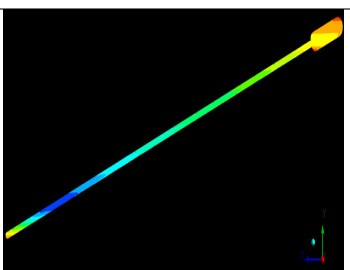
b.



c.

Figure 6.6: Pressure contour for different working fluid at steady state a. H_2O b. $Cu-H_2O$ c. $Al-H_2O$

Table 6.6: Pressure contour for all working fluids at different simulation time with respective average value.

Time	water	copper-nanofluid	aluminum-nanofluid
10sec	 134.255Pa	 -80.613Pa	 -80.905Pa
20sec	 41.408Pa	 -59.654Pa	 -39.611Pa
25sec	 24.219Pa	 -26.685	 -30.448Pa
30sec	 17.148Pa	 -24.6384Pa	 -23.686Pa
40sec	 10.603Pa	 -14.082Pa	 -17.050Pa

Velocity Contour and Vector

Velocity vector plots in figure give an idea of flow separation from one phase to another phase through closed region pipe . The recirculation of working fluid starts at rejection point of its energy contains. Velocity profile is examined to understand flow distribution at different sections of HP. The vector profile at evaporator is medium scale of velocity and half of it and adiabatic section is register higher scale of velocity; condensation section is lowered because of vapor movement is terminated by smallest temperature of condenser section and return to bottom minimal scale in the inclined side of HP to the evaporator and process is continuous till the input BC is stop. Velocity vectors clearly shows the direction to the top when it is heats or vapor form and down ward when it is condensed or at liquid state and with higher velocity return to evaporator gradually decrease near to the working fluid initial ratio. Vector on figure shows direction of fluid for two phase.

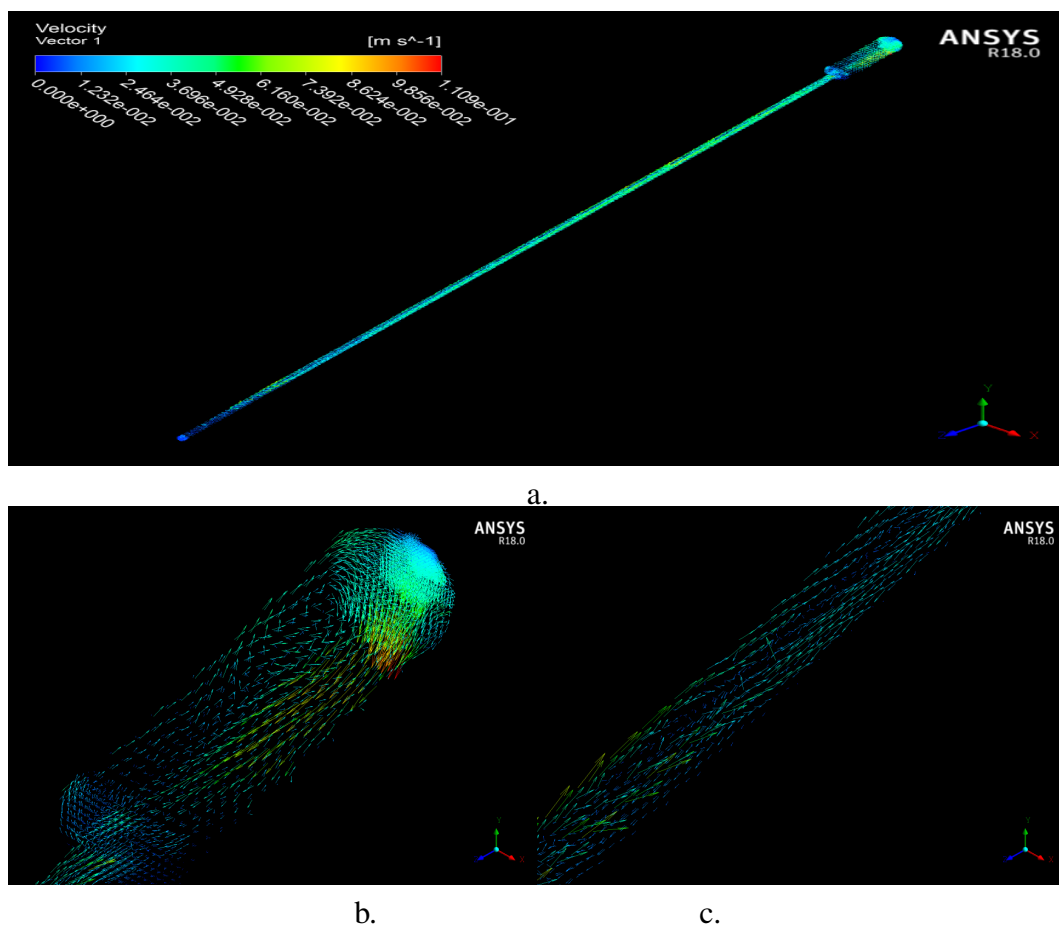
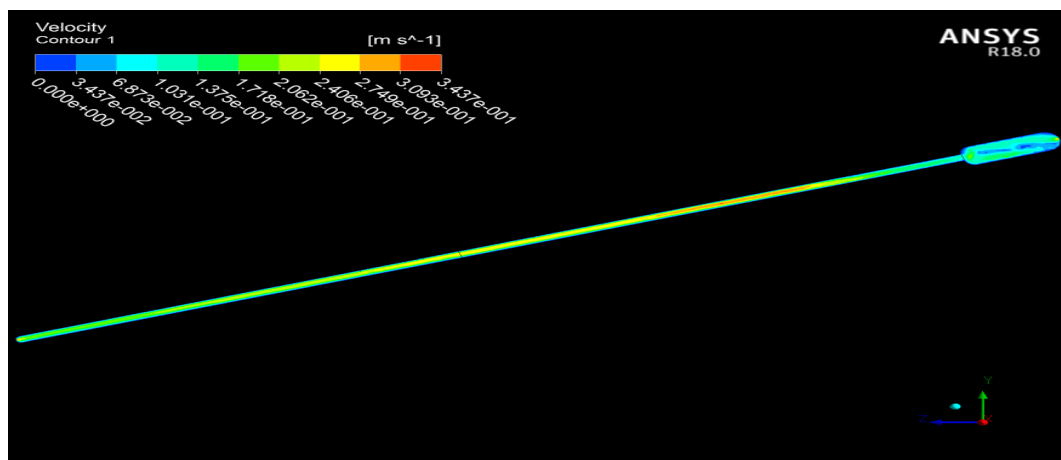
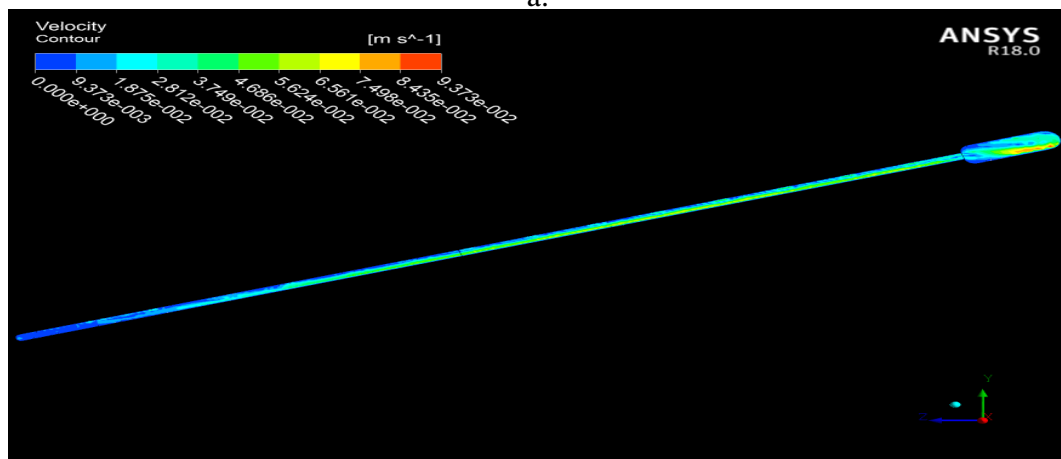


Figure 6.7: Velocity vector for evaporation and condensation a. Full model view b. condenser c. evaporator zoom view c. $Al - H_2O$.

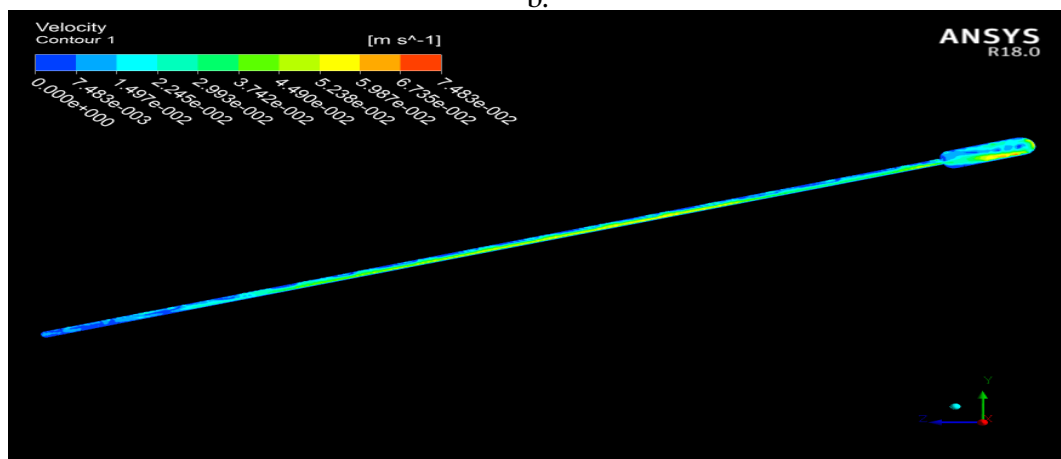
Velocity contour visualize the local distribution for different working fluid at equal time stage with an average global quantity of 0.05, 0.03 and 0.027m/s; shown in figure a, b, and c.



a.



b.

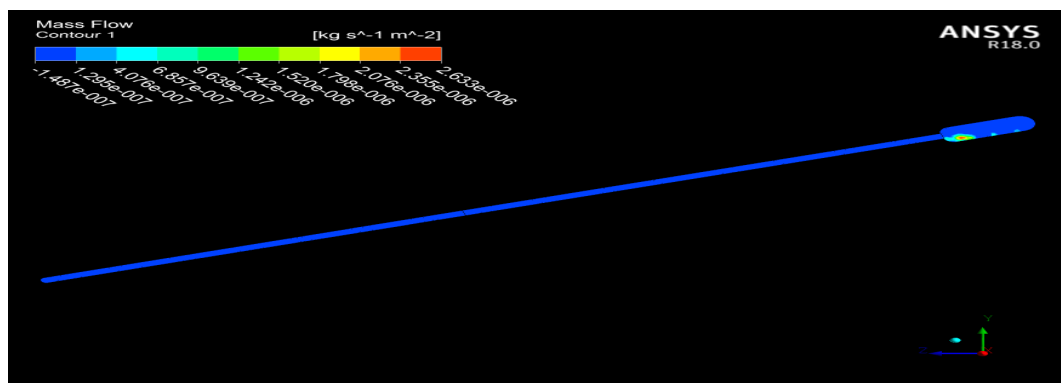


c.

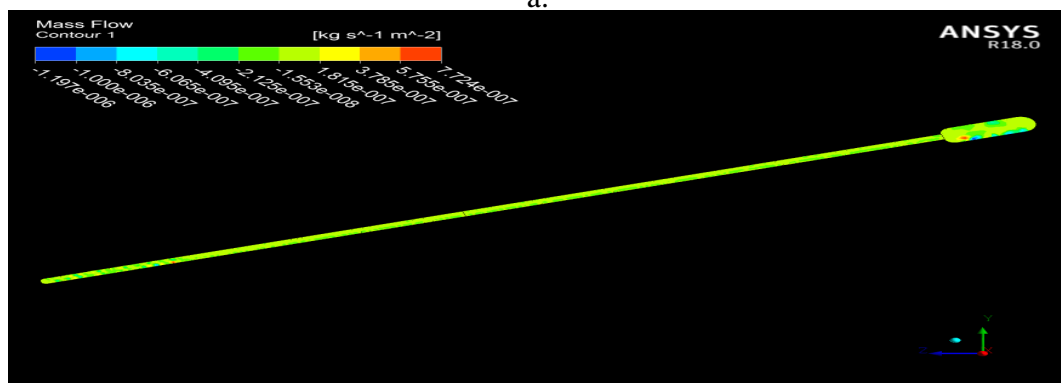
Figure 6.8: Velocity contour for different working fluid at steady state a. H_2O b. $Cu-H_2O$ c. $Al-H_2O$

Rate of mass transfer

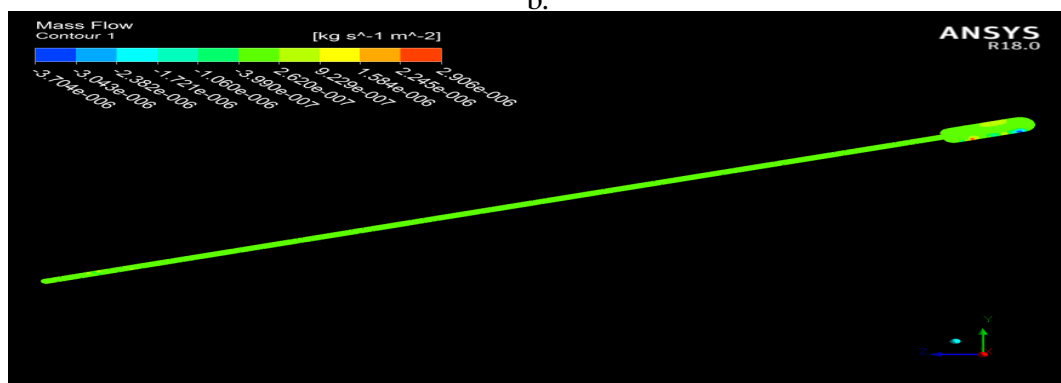
The process of mass transfer can be determined by the mass flow direction of CFD result. For all cases the amount of evaporation starts at the evaporator and condensation occurs at the condenser, which returns the liquid to its original phase. Note that the mass flow for water is negative, i.e. positive vapor mass in the evaporator and the reverse happens in the condenser with a negative value of liquid mass, showing its return to the evaporator section due to gravity.



a.



b.



c.

Figure 6.9: Mass flow contour for different working fluid at steady state a. H_2O b. $Cu - H_2O$ c. $Al - H_2O$

Local value at symmetry plane for working fluids at all phases is 4.696×10^{-5} , -4.357×10^{-5} and -4.448×10^{-5} for water, copper and aluminum particle containing fluids respectively.

From the mass flow contour results it has shown in the use base fluid more vapor flow is dominant; it means that evaporation is higher than others and less condensations is appear in the process of heat transfer.

In order to realize mass transfer through process creating five circular plane in evaporate and three in condenser section with equal spacing interior of respected sections shown in Figure ???. Need for planes, at evaporator interior is to visualize evaporation process and returning fluid mass transfer with $1488mm$ equal space size; condenser section developed film condensation visualized with $40mm$ space. Note that plane numbering is count from top to bottom with an increasing order for each separated sections.

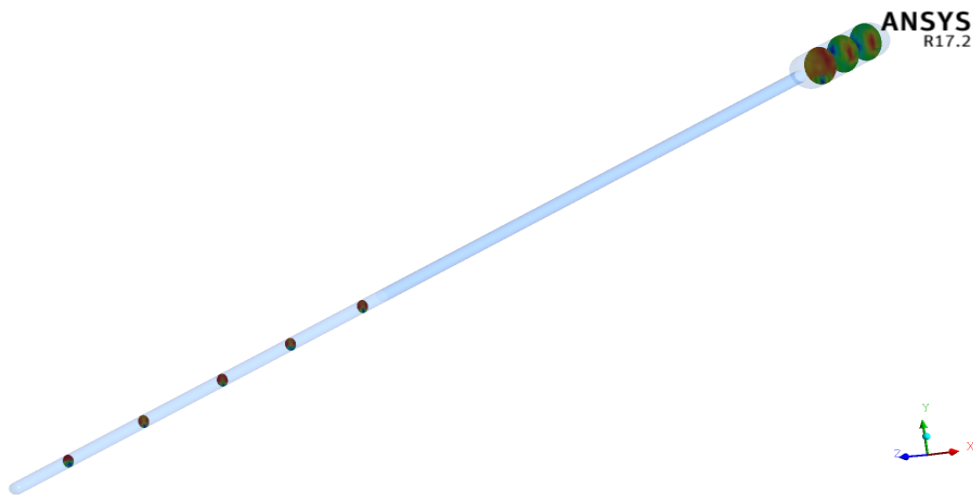
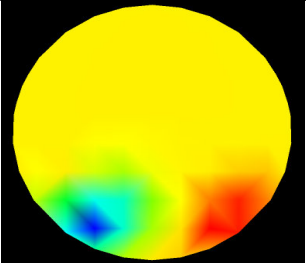
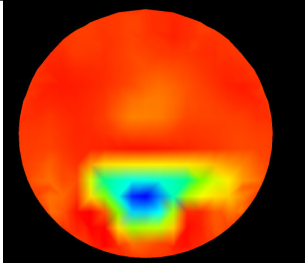
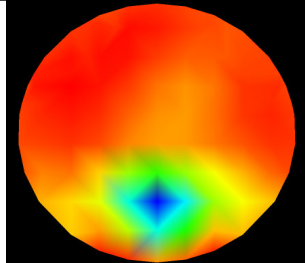
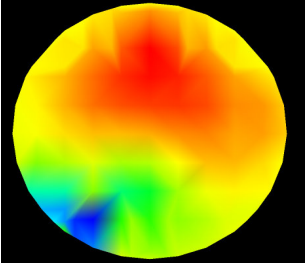
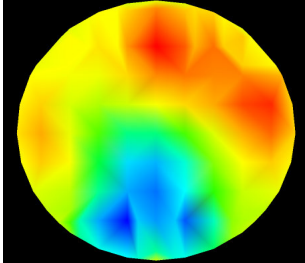
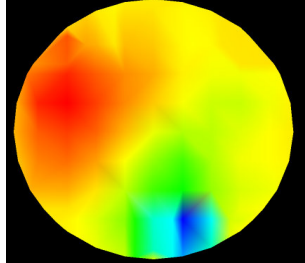
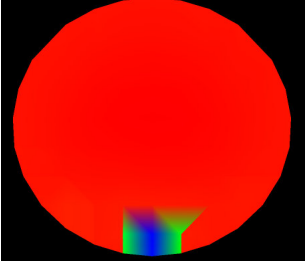
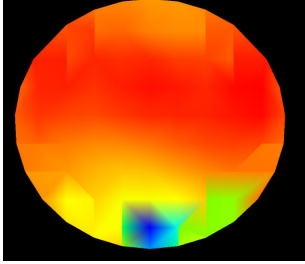
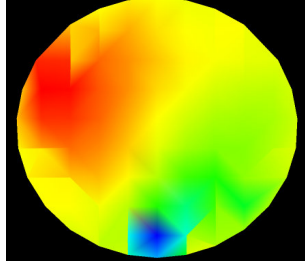


Figure 6.10: Selected plane for visualize evaporation-condensation process

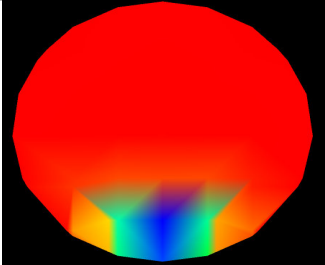
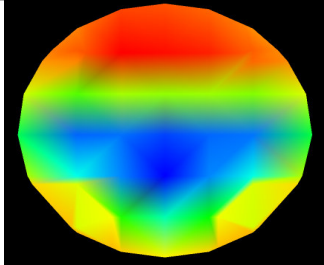
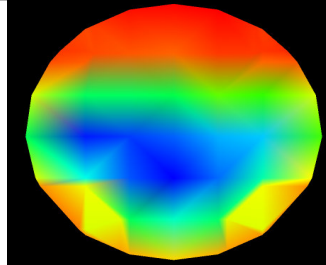
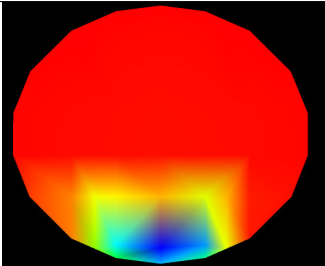
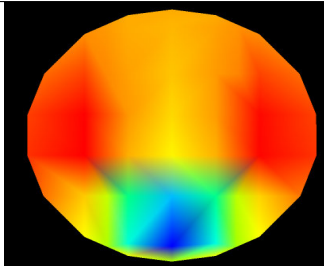
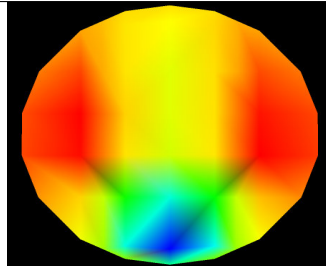
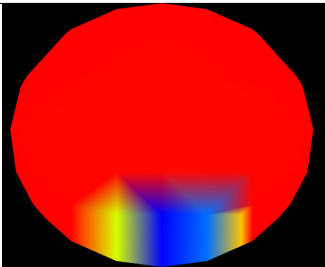
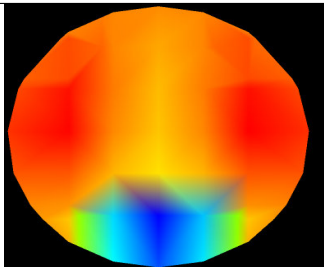
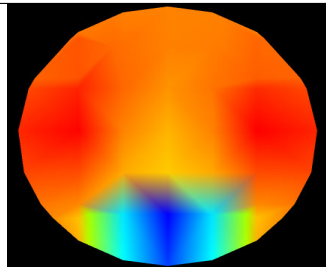
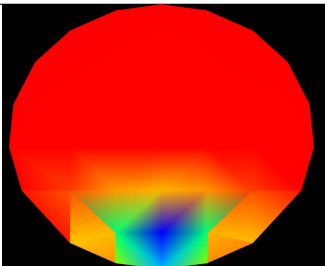
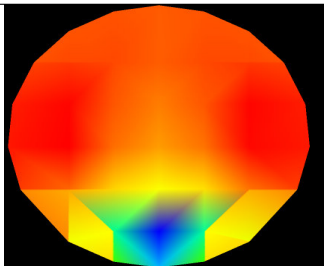
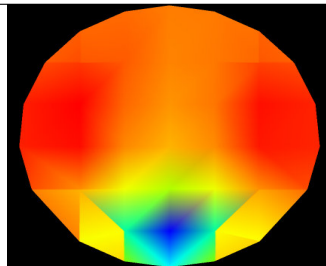
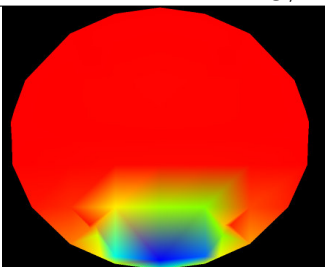
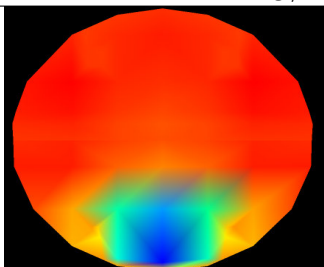
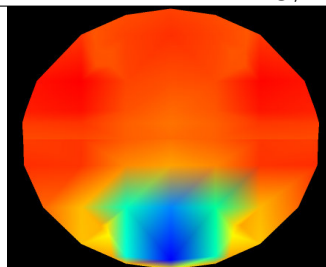
From condenser interior panes is shows the mass transfer is higher at entrance of vapor state fluid and gradually decrease length of condenser section as shown in Table ?? for plane 2 and 3. The red color visualize vapor concentration and blue one is liquid state. The water case is higher vapor; its obvious because of less film condensation process. The mass transfer is aluminum then copper particle containing fluid.

Table 6.7: Mass flow contour for all cases at different simulation time at condenser interior.

Plane	water	Cu-water nf	Al-water nf
1	 $\dot{m} = 1.723 \times 10^{-5} Kg/s$	 $\dot{m} = -4.012 \times 10^{-5} Kg/s$	 $\dot{m} = -3.917 \times 10^{-5} Kg/s$
2	 $\dot{m} = -2.291 \times 10^{-6} Kg/s$	 $\dot{m} = -3.952 \times 10^{-5} Kg/s$	 $\dot{m} = -1.597 \times 10^{-5} Kg/s$
3	 $\dot{m} = -5.127 \times 10^{-6} Kg/s$	 $\dot{m} = -3.014 \times 10^{-5} Kg/s$	 $\dot{m} = -3.971 \times 10^{-5} Kg/s$

Evaporator planes contour visualize the vapor concentration is increases from bottom to upper filled section. Mass transfer is higher in metal containing working fluid but for base fluid vapor state more dominant than liquid state and indicate the lowest value of condensed fluid is returned through out the phenomena. Contour shows in Table ?? is mas transfer in the interior elongated direction of filled evaporation section.

Table 6.8: Mass flow contour for all cases at different simulation time at evaporator interior.

Plane	water	Cu-water nf	Al-water nf
1	 $\dot{m} = 6.123 \times 10^{-8} Kg/s$	 $\dot{m} = 7.816 \times 10^{-7} Kg/s$	 $\dot{m} = 9.191 \times 10^{-7} Kg/s$
2	 $\dot{m} = 6.257 \times 10^{-8} Kg/s$	 $\dot{m} = 1.995 \times 10^{-6} Kg/s$	 $\dot{m} = 1.131 \times 10^{-6} Kg/s$
3	 $\dot{m} = 4.291 \times 10^{-8} Kg/s$	 $\dot{m} = 3.346 \times 10^{-7} Kg/s$	 $\dot{m} = 1.288 \times 10^{-6} Kg/s$
4	 $\dot{m} = 3.789 \times 10^{-8} Kg/s$	 $\dot{m} = 9.721 \times 10^{-7} Kg/s$	 $\dot{m} = 1.027 \times 10^{-6} Kg/s$
5	 $\dot{m} = 1.952 \times 10^{-8} Kg/s$	 $\dot{m} = 1.128 \times 10^{-6} Kg/s$	 $\dot{m} = 1.388 \times 10^{-6} Kg/s$

6.3.2 Transient analysis of TPCHP

Mixture Temperature

The time variation of average mixture fluid temperature along the flow path varied value with simulation time. When the pool boiling starts with constant temperature boundary; for the first 5sec increase slowly for all cases of simulation result by the time mixture temperature drop to next 5sec and rise again in continuously 10sec time duration finally goes to approach of fluids each other. Copper nanofluid average fluid temperature is easily reach a constant higher value through out total simulation time. Aluminum nanaofluid increase gradually with time and register lower value for the first 5sec.

Time variation evaporator section average fluid temperature is illustrate graphically in figure. The mixture fluid is rise with higher value for two metal nanoparticle containing fluids linearly. The base fluid temperature is low from starting and failingly attain higher in value at the end. Copper nanofluid make stable in the exchange energy with heat source boundary comparatively; average mixture temperature difference 8.2K and 11.2k from aluminium nanofluid and base fluid respectively in this section. Condenser section average fluid temperature distribution

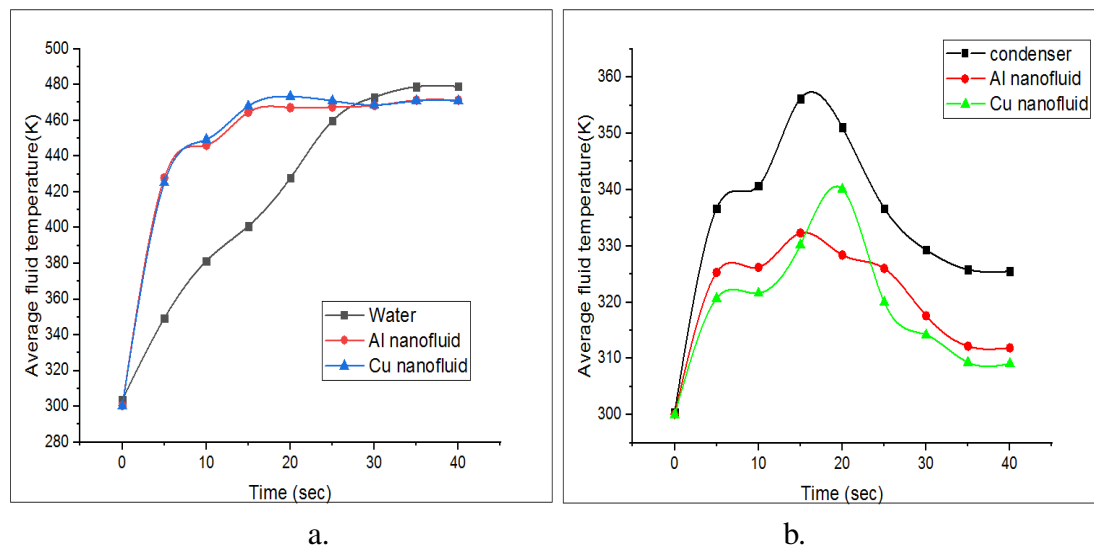


Figure 6.11: Average mixture temperature with time at different section of HP a. Evaporator b. Condenser.

is higher for the first 10sec and decrease when it comes with higher contact area with heat sink wall. The fluid with copper and aluminum nanoparticle sustain there temperature with in this section lower when it compare with base fluid. Finally, the copper nanofluid is lower value, alu-

minum and water with temperature difference 1.2k and 18.4k respectively at end of simulation; we know that from knowledge of heat and mass transfer lower average mixture temperature at heat sink enhance performance of thermal equipment.

Mixture Density

Density of working fluid is varying with in simulation time minimum attain in the vapor form and maximum liquid state. Fluid phase form at condenser and evaporator section from result of film condensation and pool boiling respectively. Transient density distribution along the inclined fluid path, which is along the upward direction vapor bubbles are increased more and more the debility become small. The average density of liquid-vapor mixture it depend on the balance of vapor bubble flow rate is the phase change heat transfer. As shown in figure the average density of liquid-vapor mixture is gradually increase for 5sec duration of simulation then decrease for nanoparticle containing fluids; Figure ?? illustrate transient value graphically. Base fluid average value is higher at starting and lower fro next simulation time finally makes itself higher at the end. Metal nanofluids attaining medium value and constant with time which indicates more stable pool boiling and film condensation. Base fluid is higher due to draying out; it means that volume fraction of vapor higher and return to evaporate section by gravity result of lower heat transfer capacity at that state; average numerical difference is $535kg/m^3$ and $534.2kg/m^3$ from aluminum and copper nanofluid when it compared at final state.

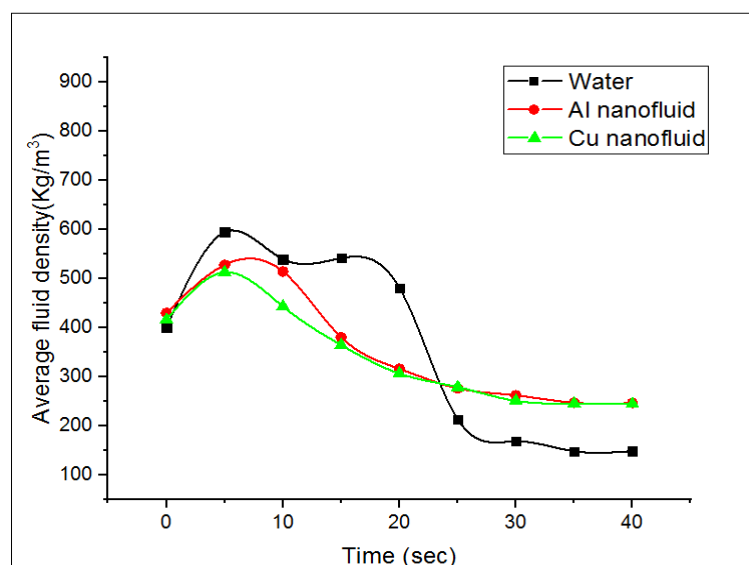


Figure 6.12: Average transient mixture density for entire fluid domain.

Velocity

The mixture fluid average velocity through thin line fluid path shown in Figure ?? illustrate the variation of three different working fluid with simulation time. Compared result velocity increase from starting proportional with vapor production; base fluid is higher with in fluctuating pattern and lower value is shown by nanoparticle containing fluids. The reason for case of base fluid is higher concentration of vaopr as shown in volume of fluid visualization. Copper nanofluid linear pattern and medium scale when compares to both working fluids.

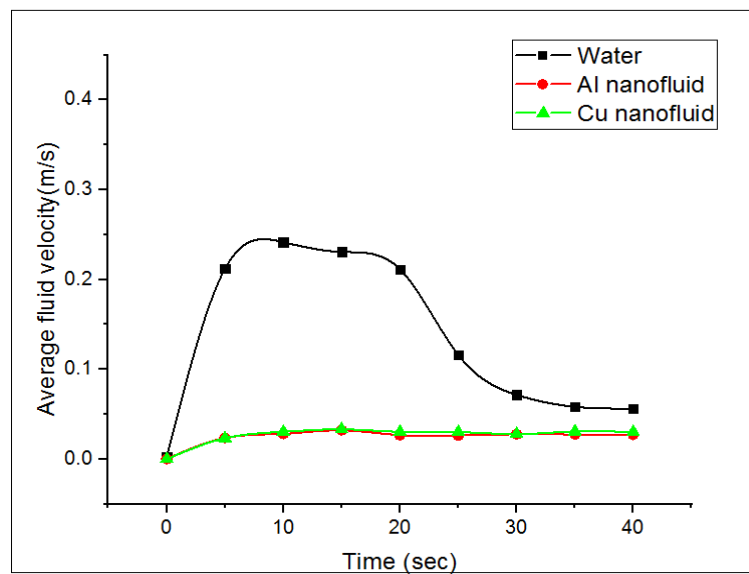


Figure 6.13: Time dependent mixture velocity for entire fluid domain of HP.

Heat transfer coefficient

Heat transfer coefficient is higher effect on the performance of thermosyphon heat pipe through wall of heat source and sink part. The heat transfer coefficient in evaporator, condenser section coefficient determine by equation ?? and ?? respectively using CFD result. Saturation temperature is at operating condition of simulation.

$$h_e = \frac{Q_e}{\Pi D_e L_e (T_{e,ave} - T_{sat})} \quad (6.15)$$

$$h_c = \frac{Q_c}{\Pi D_e L_c (T_{c,ave} - T_{\infty})} \quad (6.16)$$

The overall heat transfer coefficient with the following equation.

$$h_{ovll} = \frac{Q}{A_e(T_{e,ave} - T_{c,ave})} \quad (6.17)$$

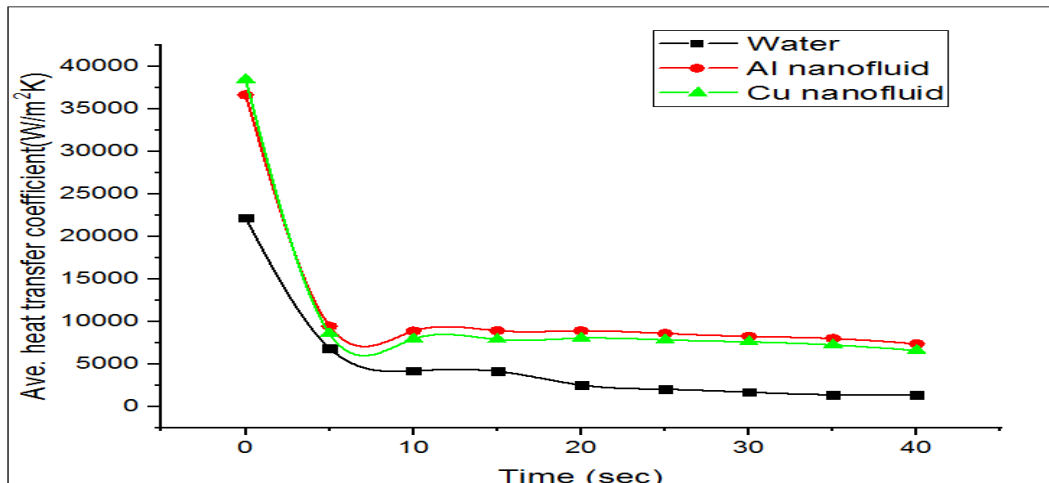
Evaporator section average heat transfer coefficient gradually decrease with respect to fluid temperature and time illustrate in Figure ??a. The reason is when the wall come up in constant with fluid state for the liquid is higher value and decreases when the vapor state is arise. The coefficient is higher for copper nanofluid and aluminum respectively; but the base fluid is lower at end of simulation cause of accumulation in vapor fraction. Copper nanofluid raise by 25.2% and aluminum nanofluid by 37.9% when it compared with base fluid at starting of pool boiling in equal time space.

Condenser section heat transfer coefficient attain high with higher fluid temperature for the case of water use as working fluid. The fluid temperature is lower higher coefficient value registered for metal particle containing fluids as shown in Figure ??b; at this section copper enhance film condensation by 78.55% and aluminum by 47.6%. Note the higher fluid temp in the section shows lower heat transfer coefficient. Finally, copper has higher heat transfer coefficient at different level of average fluid temperature. Finally, the overall heat transfer coefficient is decrease with an increaing of fluid temperature as shown in Figure ??c. The compared result indicate copper nanofluid is increase by 51.86% and aluminum nanofluid by 42.75% from base fluid heat transfer enhancement.

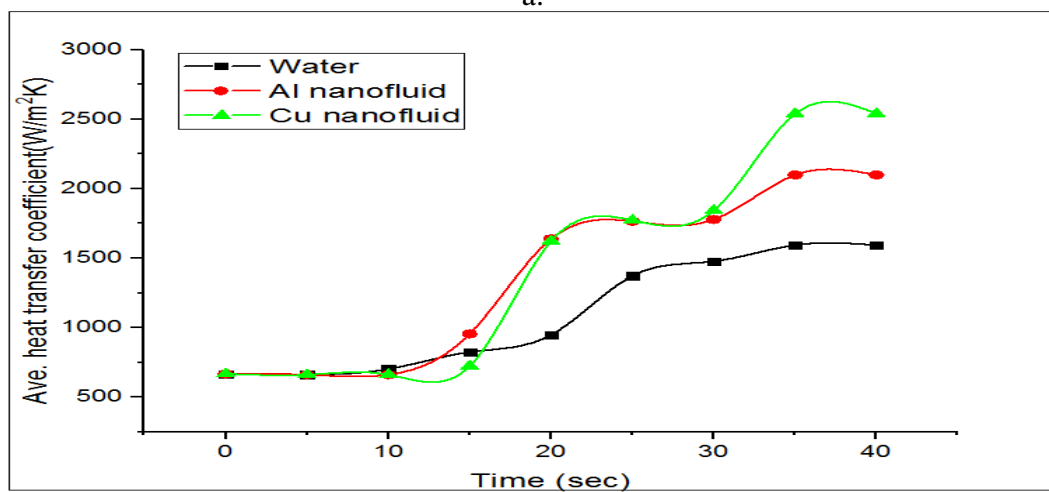
Thermal Resistance

Evaporation and condensation phenomena thermal resistance coefficient need to determine the heat transfer characteristics though out the thermpsyphon heat pipe. The resistance at condenser and evaporator section is determined by the following equations from CFD result and saturation temperature is corresponding to working fluid operating pressure; indirectly it is inverse of heat transfer coefficient. When the working fluid cannot be vaporize and recycled at higher input, the thermal resistance will be increased suddenly and situation caused drying out of working fluid inside the equipment.

$$R_c = \frac{T_{c,ave} - T_{\infty}}{Q_c} \quad (6.18)$$



a.



b.

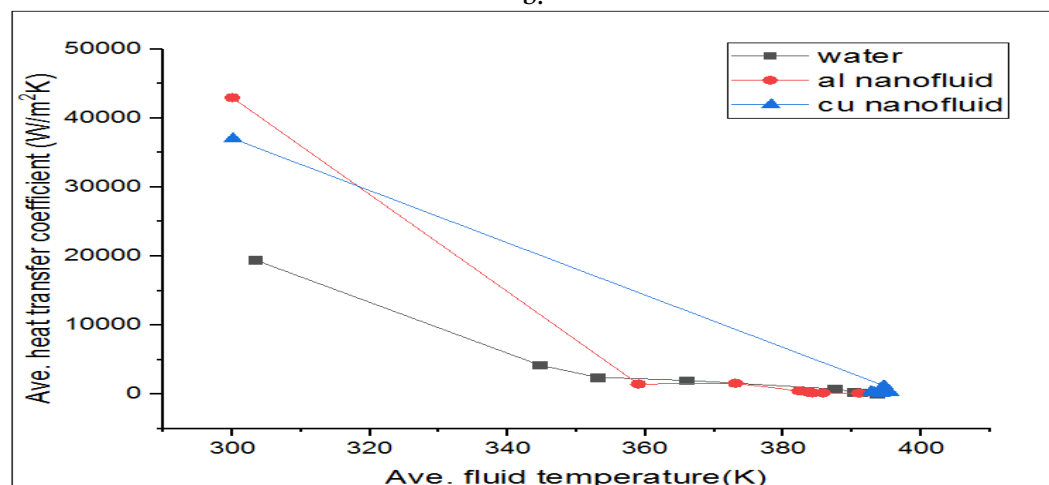
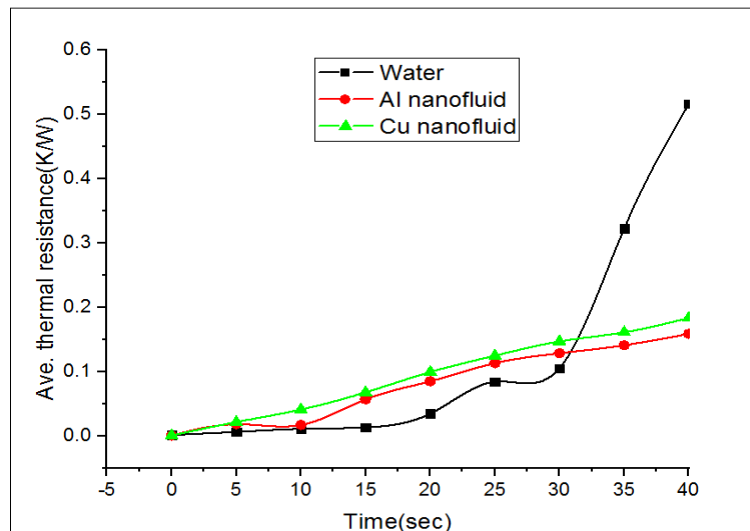


Figure 6.14: Average heat transfer coefficient with comparative time a. Evaporator section b. Condenser section c. Overall coefficient.

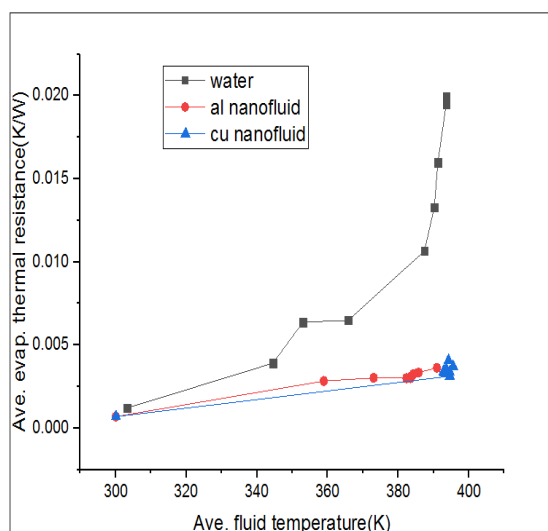
$$R_e = \frac{T_{e,ave} - T_{sat}}{Q_e} \quad (6.19)$$

Total thermal resistance of TPCHP is:

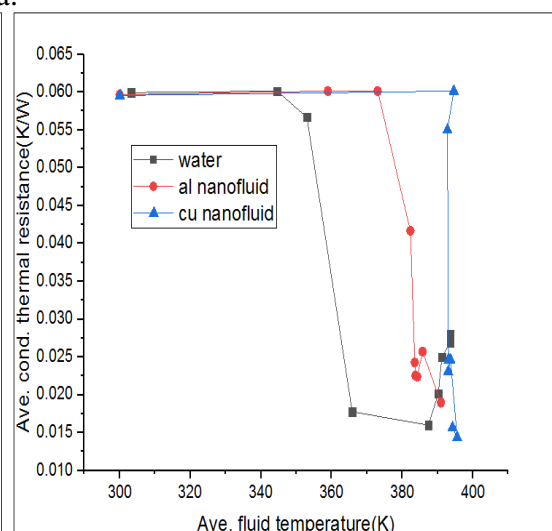
$$R_{tot} = \frac{T_{e,ave} - T_{c,ave}}{Q_{in}} \quad (6.20)$$



a.



b.



c.

Figure 6.15: Average thermal resistance for different working fluids with time a. Overall coefficient b. Evaporator section c. Condenser section

Heat transfer

The overall heat transfer proportional the effective temperature difference between evaporator and condenser and inversely proportional to the equivalent thermal resistance between two region.

$$\dot{Q} = \frac{T_{e,ave} - T_{c,ave}}{R_{tot}} \quad (6.21)$$

Average Wall heat flux numerically calculated value from result of CFD solution located named selection of boundary in grid generation of the simulation process. The new heat flux is varying with fluid temperature at constant wall temperature boundary. The result of wall heat flux at evaporator section for constant wall temperature. The wall heat flux reduces from evaporator to condenser section. The evaporator wall heat flux is higher at starting of simulation due to high thermal conductive property of wall material before transfer and propagate radially to the working fluid. As the fluid temperature is increase proportional with time; wall heat flux decreased. The higher value shown in aluminum nanoparticle, copper and water next to it when it come up in contact with liquid state phase. Condenser section heat flux is higher at high fluid temperature and decrease gradually; but higher value not initiate evaporation-condensation heat transfer mechanism. The nanofluid has lower value at the section through out the simulation time when compare with fluid temperature. Finally, copper register lower value in CFD analysis and shown great heat transfer enhancement. Result arise from higher thermal conductivity, latent heat of vaporization and lower specific heat capacity of synthesized nanofluids.

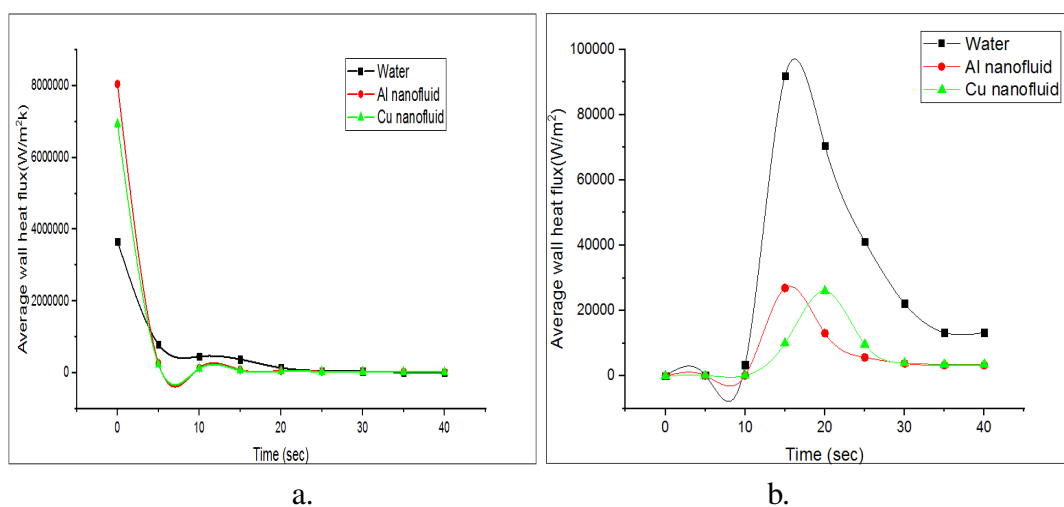


Figure 6.16: Average wall heat flux a. Evaporator b. Condenser section.

CONCLUSION AND FUTURE RECOMMENDATIONS

Using renewable energy source in Ethiopia industries not shown in presence of initiated country energy policy. Solar energy is the best alternative heating energy source. It is renewable and easily available in all parts of the world which is cheap and clean.

The main goal of this study was to develop existing model of heat pipe-evacuated tube solar collector thermal performance and design efficient SWH system. The presented report is discussed on wonji-shoa sugar factory milling plant section hot water demand and environmental benefits, in a consideration of cost. The paper also was carried out with specific objectives in connection with analytical design, developmental study and CFD evaluation of transient thermal performance of the heat pipe.

7.1 Conclusion

Research report has to be mentioned that comparing to data obtained from the quantitative, reliable survey and system costing. Evacuated tubular collector integrated solar water heating systems were designed as per standard specifications. They were selected with suitable materials as per the requirements of heat energy demand and thermal performance analysis of HP-ETSc. The theoretical analysis drawn the following conclusions.

- Proposed solar hot water heating system has 16.6MWhr annual thermal energy demand with 0.013kg/sec working flow rate for 240 days. Proposed system required 10 number

of 55% efficient collector modules with $1.1m^3$ hot storage tank, $12.7m^2$ collector area size, the annual solar fraction is 0.99 and system efficiency is 99.2 percent. The optimum collector flow rate of the present solar water heating system is 0.0383Kg/sec on the basis of average sunshine hour.

- Designed system annual solar contribution to hot water is $16.22MWhr$, energy from auxiliary heating is $0.369MWhr$, 26,904birr/yr fuel (bagasse) cost is saved and contribute to alternative uses.
- The present solar water heating system, hot water at the outlet is directly collected into a well-insulated vertical storage tank and water at inlet is taken directly from the overhead storage tank. Small header tank enhanced efficiencies of the particular water heating system. Operating hot storage tank is store $11.25MWhr$ annually in account of charging fluid and loss to environment.
- Paper determine techno-economic advantage which is 28,957.5kg estimated amount CO_2 emissions and 9,477kg/yr of water vapor to atmosphere is avoided.
- Also auxiliary heating is made inside the hot water storage tank in compensation of overall heat loss so that water maintain demand temperature for a longer duration of time and it can be used in the night time when there is no availability of solar radiation.
- The economic analysis of the system was done with an initial total investment of 96,761ETBirr and a life cycle savings of 26,904ETBirr/yr. The economic performance of the system has proved that the proposed solar water heating system is feasible because it gives a positive analytic result and source of startup cost can determine by company option. The payback period 3.6 years is determined by saved of fuel cost.

A 3-D numerical simulation was carried out to investigate about the heat transfer characteristics of TPCT-HP on the basis of analytical design. Various heat transfer fluids were examined at constant operating condition, model and filling ratio in order to assess the performance of heat transfer equipment. Powerful CFD tool ANSYS soft wear in FLUENT with the VOF transient model method can successfully compute the complex evaporation and condensation phenomena inside the thermosiphon. A two-phase closed thermosiphon is considered when charged with

three working fluids water, Al and Cu nanofluid. The synthesized nanofluid characterized 0.5 and 4.1vol% of Cu and Al nanoparticle with water respectively.

From the result visualization it is found that the CFD simulation was able to reproduce the operation of the thermosyphon at $4kPa$ operating pressure for $40sec$ duration with 50% filling ratio of evaporator section. Water had higher fluid temperature at condenser section when it compared with nanofluids. It indicates smallest heat transfer capability. The pool boiling in the evaporator section flow vector to top and condensed liquid film in the condenser section flow vector to bottom. Vapor volume fraction is higher at end of simulation for water case. The pressure drop in water shown at evaporator section bottom part and for nanofluids at interface of two phase which enhance evaporation process when compared with base fluid. Transient performance analysis conclusions are the following.

- Higher thermal conductivity, latent heat of vaporization and lower specific heat of nanofluids has a very important role on the enhancement of heat transfer. Heat transfer performance and thermal efficiency of employed nanofluids were higher than the base fluid.
- The heat transfer average fluid temperature decreasing at the condenser section increases heat transfer and sustainability of closed mechanism. Cu-water has lower temperature value than Al-water and water is next to it.
- The optimum mixture density is kept the continuity of heat transfer and prevent dry-out interior fluid domain. Cu-water and Al-water is optimum but base fluid exposed to drying out.
- Decreasing of evaporator and condenser section thermal resistance with time enhancement of heat transfer. At evaporator section heat transfer coefficient increased by 25.2% and 37.9% for Cu-water and Al-water nanofluid respectively when its compared with base fluid.
- Condenser heat transfer coefficients of Cu-water nanofluid are greater than those of other heat transfer fluids. The average heat transfer coefficient of Cu-water nanofluid is about 30.95% and 78.55% higher than those of Al-water nanofluid and water respectively. Al-water nanofluid also increased by 47.6% from base fluid.

- The overall thermal resistance for TPCT-HP is decreased by about 51.86% for Cu nanofluid, whereas it is reduced by 42.75% for Al-water nanofluid compared with water.

Therefore, using Cu-water nanofluid for heat transfer in TCPT-HP provides a simple and economical technique to enhance the performance of TPCT-HP. This would offer an efficient solar thermal energy conversion.

7.2 Recommendations and Future Work

Recommendation and future work on the presented research is

- Cu-water Nano fluid for different heat removal systems in many applications.
- Can use for solar air heating and cooking by using different working fluid
- For higher Temperature demand and better performance add simple compound parabolic collector integrate with it.
- Experimental investigation can done using presented design.
- Can optimize the condenser geometry, internal and external surface roughness of TPCT-HP for better heat transfer performance.
- Effects of nano particle in pool boiling phenomena can investigate in the future.

Bibliography

WorldBank. Ethiopian economic overview. Technical report, World Bank, 2016.

V K Jain and S N Srinivas. Inspiring success stories. In *Empowering rural Indian the RE way*. Ministry of New and Renewable Energy, Government of India, Block No. 14, CGO Complex, Lodhi Road, New Delhi – 110 003, 2012.

Soteris Kalogirou. *Solar Energy Engineering - Processes and Systems*. Elsevier, 2009.

Yirga Belay Muna. Estimation of solar panel orientation with different tilt angles at haramaya university. Msc thesis, HARAMAYA UNIVERSITY, School of Graduate Studies, Department of Physics, Haramaya, Ethiopia, June 2014.

A.W Culp. *Principles of Energy Conversion*. McGraw Hill, New York, 2 edition, 1991.

Prof. Zekai , Sen. *Solar energy fundamentals and modeling techniques : atmosphere, environment, climate change and renewable energy*. Springer, Verlag, London, 2008.

Ahmed F. Zobaa and Ramesh C. Bansal. *HAND BOOK OF RENEWABLE ENERGY*, chapter Chapter 12, Non-grid Solar Thermal Technologies, page 267. World Scientific Publishing Co. Pte. Ltd., 2011.

Dawit Hailu Mazengia. Ethiopian energy systems potentials, opportunities and sustainable utilization. Master's thesis, Sustainable Development, Uppsala University, Uppsala, Sweden, September 2010.

EEPCo. Current energy supply. Technical report, Ethiopian Electric Power Corporation, <http://www.eepco.gov.et>, 2016.

- DFIP. Water storage and hydropower: supporting growth, resilience and low carbon development. A dfid evidence-into-action paper, Department for International Development, UKAID, 2009.
- Dalelo A. Rural electrification in ethiopia: Opportunities and bottlenecks. Technical report, Dalelo, Rural Electrification in Ethiopia: Opportunities and Bottlenecks, 2013.
- F. Drake and Y. Mulugetta. Assessment of solar and wind energy resources in ethiopia. *Solar Energy*, 57(3):205–217, 1996.
- Jargstorf. Information for project appraisal: Ethiopia. PN 97.2019.4-001.09, Wind Energy Programme BTERNA, 2004.
- Yidnekachew Messele and Ababayehu Assefa. Thermal analysis, design and experimental investigation of parabolic trough solar collector. *Advances in Intelligent Systems and Computing*, 2015.
- Aidan Duffy Lacour Ayompe. Thermal performance analysis of a solar water heating system with heat pipe evacuated tube collector using data from a field trial. *Solar Energy*, 001(90):17–28, April 2013.
- S. R Sanjeev Kumar S. Siva Kumar, K. Mohan Kumar. Design of evacuated tube solar collector with heat pipe. *Solar Energy*, 4:12641–12646, 2017.
- Amanda L. Fuentes-Silva Martín Picón-Núñez, Guillermo Martínez-Rodríguez. Targeting and design of evacuated-tube solar collector networks. *Chemical Engineering Transactions*, 52, 859-864:859–864, 2016.
- William Lteif Michel Hayek, Johnny Assaf. Experimental investigation of the performance of evacuated tube solar collectors under eastern mediterranean climatic conditions. *Energy Procedia*, 6:618–626, 2011.
- Anunaya saraswat Avadhesh Yadav. An experimental study on evacuated tube collector for steam generation in india. *Energy and Power Engineering*, 10(5), 2016.

- Saad Mekhilef Omid Mahian M.A. Sabiha, R. Saidur. Progress and latest developments of evacuated tube solar collectors. *Renewable and Sustainable Energy Reviews*, 51:1038–1054, July 2015.
- Roonak Daghigh and Abdellah Shafieian. Theoretical and experimental analysis of thermal performance of a solar water heating system with evacuated tube heat pipe collector. *Applied Thermal Engineering*, 2016.
- Kedar Bhojak Raghurajsinh B., Parmar. Performance of an evacuated tube collector with heat pipe technology. *International Journal of Engineering Research and General Science*, 2016.
- Bale V. Reddy Behnaz Rezaie and Marc A. Rosen. Thermodynamic analysis and the design of sensible thermal energy storages. *INTERNATIONAL JOURNAL OF ENERGY RESEARCH*, 41:39–48, 2017.
- N.Nallusamy S.A.Vijay Padmaraju, M.Viginesh. Comparitive study of sensible and latent heat storage systems integrated with solar water heating unit. *Solar Energy Technology*, 2008.
- Saitoh T.S Hoshi, A. Screening of high melting point phase change materials (pcm) in solar thermal concentrating technology based on cflr. *Solar thermal*, 04(023), 2004.
- Lane GA. Encapsulation of heat of fusion storage materials. In *Proceedings of 2nd Southeastern Conference on Application of Solar Energy*, 1976.
- Hussam Jouhara Bandar Fadh, Luiz C. Wrobel. Numerical modelling of the temperature distribution in a two-phase closed thermosyphon. *Applied Thermal Engineering*, 60:122 – 131, 2013.
- Ammar Abdulaziz Alsairafi Asghar Alizadehdakhel, Masoud Rahimi a. Cfd modeling of flow and heat transfer in a thermosyphon. *Heat and Mass Transfer*, (37):312–318, 2010.
- Dr. Yarasu Ravindra B. Patil Aniket D. Factors affecting the thermal performance of two phase closed thermosyphon: A review. *International Journal of Emerging Technology and Advanced Engineering*, 2(9):2250–2459, 2012.
- Hussam Jouhara Bandar Fadhl, Luiz C. Wrobel. Cfd modelling of a two-phase closed thermosyphon charged with r134a and r404a. *Applied Thermal Engineering*, 2014.

Raya K. Al-Dadah Saad M. Mahmoud Richard Hood Ahmed A. Alammam, Fadhel N. Al-Mousawi. Enhancing thermal performance of a two-phase closed thermosyphon with an internal surface roughness. *Cleaner Production*, 185:128–136, March 2018.

Ambrosini and Ferreri J.C. Stability analysis of single-phase thermosyphon loops by finite difference numerical methods. *Nuclear Engineering and Design*, 201(1):11–23, 2000.

Dr.M.Manzoor Hussain Syed Khader Bashad Moh Naseemaa, S. Nawazish Mehdi and Abdul Samade. Heat enhancement of heat exchanger using aluminium oxide(Al_2O_3), copper oxide(CuO)nano fluids with different concentrations. *Materials Processing and Characterization*, 2018.

Vajjha Ravikanth S. and Debendrak. Das. Measurements of specific heat and density of aluminium oxide nanofluid. *Mesoscopic, Nanoscopic and Macroscopic Materials*, 2015.

K. Kadrigama Adnan M. Hussein, R.A. Bakar and K.V. Sharma. Experimental measurement of nanofluids thermal properties. *International Journal of Automotive and Mechanical Engineering (IJAME)*, 2013.

D. Gangacharyulu Amarinder Singh and Summet Sharma. Study of heat transfer of aluminium oxide in water and ethylene glycol based nanofluid in single pass multi cross flow heat exchanger. *International Journal of Research and Technology*, 2016.

Shijo Thomas and Sobhan C.B. Heat transfer measurement in aluminium oxide nanofluid using rectangular thermosyphon loop. *International Conference on Heat Transfer, Fluid Mechanics and Thermodynamics*, 2014.

Azizah Mohd Rohni Jawad Raza and Zurni Omar. Numerical investigation of copper-water (Cu-water) nanofluid with different shapes of nanoparticles in a channel with stretching wall: Slip effects. *Mathematical and Computational Applications*, 2016.

Chun Che Fung Derek Fawcett Wisut Chamsa-ard, Sridevi Brundavanam and Gerrard Poinern. Nanofluid types, their synthesis, properties and incorporation in direct solar thermal collectors: A review. *nanomaterials*, 2017.

John H. Lienhard IV and John H. Lienhard V. *HEAT TRANSFER TEXT BOOK*. Phlogiston Press Cambridge, Massachusetts, U.S.A., 2008.

JULES L. ROUBORT WENHUA YU, DAVID M. FRANCE and STEPHEN U. S. CHOI.

Review and comparison of nanofluid thermal conductivity and heat transfer enhancements. *Heat Transfer Engineering*, 29(5):432–460, 2008.

Devendiran Dhinesh Kumar and Valan Arasu Amirtham. A review on preparation, characterization, properties and applications of nanofluids. *Renewable and Sustainable Energy Reviews*, 60(2016):21–40, 2016.

Sayantana Mukherjee and Somjit Paria. Preparation and stability of nanofluids-a review. *Journal of Mechanical and Civil Engineering (IOSR-JMCE)*, 9(2):63–69, September 2013.

Ngoc Viet Nguyen Thanh Tu Vu Thi Ngoc Mai Pham Thi Hai Yen Doan Manh Ha Nguyen Tien Duc Pham, Hoang Hiep Nguyen and Thi Mai Viet Ngo. Adsorptive removal of copper by using surfactant modified laterite soil. *Journal of Chemistry*, 2017.

Dr. S. M. Lawankar Nikhil S. Nagulkar. Study of properties of nanofluids and its effect. *International Research Journal of Engineering and Technology (IRJET)*, 04(06), June 2017.

J C Jarque J E Julia L Hernández R Mondragón, C Segarra and R Martínez-Cuenca. R mondragón1, c segarra1, j c jarque1, j e julia2*, l hernández2 and r martínez-cuenca2. In *European Thermal Sciences*, 2012.

Ravikanth S. Vajjha and Debendra K. Das. Measurements of specific heat and density of Al_2O_3 nanofluid. *Mesoscopic, Nanoscopic, and Macroscopic Materials*, 2015.

Addisu Bekele. Large scale application of solar water heating system in ethiopia. Master's thesis, MECHANICAL ENGINEERING, 2007.

Marut Dutt. R.K. Wanchoo Neetu Rani, Hema Setia. Natural convection heat transfer from inclined cylinders: A unified correlation. *Physical and Mathematical Sciences*, 2014.

Michael Dale. A comparative analysis of energy costs of photovoltaic, solar thermal, and wind electricity generation technologies. *Applied Sciences*, 2013.

Tagelsir Hasan Hassan Abdalla Mohamed Abdalla and Mohamed Eltayeb Mansour. Performance of wet and dry bagasse combustion in assalaya sugar factory - sudan. *Innovative Energy and Research*, 2018.

J.SUDHAKAR and P.VIJAY. Control of moisture content in bagasse by using bagasse dryer. *International Journal of Engineering Trends and Technology*, 2013.

N. R. Kannake G. C. Nalamwar and S. S. Sontakke. Study and fabrication of vacuum tube collector solar water heater. *International Journal of Engineering and Innovative Technology (IJEIT)*, 2(1), July 2013.

Emission Estimation Technique Manual.

Jayathi Y. Murthy. *Numerical Methods in Heat, Mass, and Momentum Transfer.* Springer Inc., 2002.

Department of Aerospace Engineering University of Maryland John D. Anderson. *COMPUTATIONAL FLUID DYNAMICS: The basis with application.* McGraw-Hill, Inc., 1995.

Inc ANSYS. *ANSYS Meshing User's Guide.* SAS IP, Inc., January 2016.

ANSYS Inc. *ANSYS Fluent Theory Guide.* SAS IP, Inc., 2016.

Appendix A

Physical Property of Matter

Saturated water

Temp. $T, ^\circ\text{C}$	Saturation Pressure $P_{\text{sat}}, \text{kPa}$	Density $\rho, \text{kg/m}^3$		Enthalpy of Vaporization $h_{\text{fg}}, \text{kJ/kg}$	Specific Heat $c_p, \text{J/kg}\cdot\text{K}$		Thermal Conductivity $k, \text{W/m}\cdot\text{K}$		Dynamic Viscosity $\mu, \text{kg/m}\cdot\text{s}$		Prandtl Number Pr		Volume Expansion Coefficient $\beta, 1/\text{K}$
		Liquid	Vapor		Liquid	Vapor	Liquid	Vapor	Liquid	Vapor	Liquid	Vapor	
0.01	0.6113	999.8	0.0048	2501	4217	1854	0.561	0.0171	1.792×10^{-3}	0.922×10^{-5}	13.5	1.00	-0.068×10^{-3}
5	0.8721	999.9	0.0068	2490	4205	1857	0.571	0.0173	1.519×10^{-3}	0.934×10^{-5}	11.2	1.00	0.015×10^{-3}
10	1.2276	999.7	0.0094	2478	4194	1862	0.580	0.0176	1.307×10^{-3}	0.946×10^{-5}	9.45	1.00	0.733×10^{-3}
15	1.7051	999.1	0.0128	2466	4185	1863	0.589	0.0179	1.138×10^{-3}	0.959×10^{-5}	8.09	1.00	0.138×10^{-3}
20	2.339	998.0	0.0173	2454	4182	1867	0.598	0.0182	1.002×10^{-3}	0.973×10^{-5}	7.01	1.00	0.195×10^{-3}
25	3.169	997.0	0.0231	2442	4180	1870	0.607	0.0186	0.891×10^{-3}	0.987×10^{-5}	6.14	1.00	0.247×10^{-3}
30	4.246	996.0	0.0304	2431	4178	1875	0.615	0.0189	0.798×10^{-3}	1.001×10^{-5}	5.42	1.00	0.294×10^{-3}
35	5.628	994.0	0.0397	2419	4178	1880	0.623	0.0192	0.720×10^{-3}	1.016×10^{-5}	4.83	1.00	0.337×10^{-3}
40	7.384	992.1	0.0512	2407	4179	1885	0.631	0.0196	0.653×10^{-3}	1.031×10^{-5}	4.32	1.00	0.377×10^{-3}
45	9.593	990.1	0.0655	2395	4180	1892	0.637	0.0200	0.596×10^{-3}	1.046×10^{-5}	3.91	1.00	0.415×10^{-3}
50	12.35	988.1	0.0831	2383	4181	1900	0.644	0.0204	0.547×10^{-3}	1.062×10^{-5}	3.55	1.00	0.451×10^{-3}
55	15.76	985.2	0.1045	2371	4183	1908	0.649	0.0208	0.504×10^{-3}	1.077×10^{-5}	3.25	1.00	0.484×10^{-3}
60	19.94	983.3	0.1304	2359	4185	1916	0.654	0.0212	0.467×10^{-3}	1.093×10^{-5}	2.99	1.00	0.517×10^{-3}
65	25.03	980.4	0.1614	2346	4187	1926	0.659	0.0216	0.433×10^{-3}	1.110×10^{-5}	2.75	1.00	0.548×10^{-3}
70	31.19	977.5	0.1983	2334	4190	1936	0.663	0.0221	0.404×10^{-3}	1.126×10^{-5}	2.55	1.00	0.578×10^{-3}
75	38.58	974.7	0.2421	2321	4193	1948	0.667	0.0225	0.378×10^{-3}	1.142×10^{-5}	2.38	1.00	0.607×10^{-3}
80	47.39	971.8	0.2935	2309	4197	1962	0.670	0.0230	0.355×10^{-3}	1.159×10^{-5}	2.22	1.00	0.653×10^{-3}
85	57.83	968.1	0.3536	2296	4201	1977	0.673	0.0235	0.333×10^{-3}	1.176×10^{-5}	2.08	1.00	0.670×10^{-3}
90	70.14	965.3	0.4235	2283	4206	1993	0.675	0.0240	0.315×10^{-3}	1.193×10^{-5}	1.96	1.00	0.702×10^{-3}
95	84.55	961.5	0.5045	2270	4212	2010	0.677	0.0246	0.297×10^{-3}	1.210×10^{-5}	1.85	1.00	0.716×10^{-3}
100	101.33	957.9	0.5978	2257	4217	2029	0.679	0.0251	0.282×10^{-3}	1.227×10^{-5}	1.75	1.00	0.750×10^{-3}

Saturated air

Temp. $T, ^\circ\text{C}$	Density $\rho, \text{kg/m}^3$	Specific Heat $c_p, \text{J/kg}\cdot\text{K}$	Thermal Conductivity $k, \text{W/m}\cdot\text{K}$	Thermal Diffusivity $\alpha, \text{m}^2/\text{s}$	Dynamic Viscosity $\mu, \text{kg/m}\cdot\text{s}$	Kinematic Viscosity $\nu, \text{m}^2/\text{s}$	Prandtl Number Pr
-150	2.866	983	0.01171	4.158×10^{-6}	8.636×10^{-6}	3.013×10^{-6}	0.7246
-100	2.038	966	0.01582	8.036×10^{-6}	1.189×10^{-5}	5.837×10^{-6}	0.7263
-50	1.582	999	0.01979	1.252×10^{-5}	1.474×10^{-5}	9.319×10^{-6}	0.7440
-40	1.514	1002	0.02057	1.356×10^{-5}	1.527×10^{-5}	1.008×10^{-5}	0.7436
-30	1.451	1004	0.02134	1.465×10^{-5}	1.579×10^{-5}	1.087×10^{-5}	0.7425
-20	1.394	1005	0.02211	1.578×10^{-5}	1.630×10^{-5}	1.169×10^{-5}	0.7408
-10	1.341	1006	0.02288	1.696×10^{-5}	1.680×10^{-5}	1.252×10^{-5}	0.7387
0	1.292	1006	0.02364	1.818×10^{-5}	1.729×10^{-5}	1.338×10^{-5}	0.7362
5	1.269	1006	0.02401	1.880×10^{-5}	1.754×10^{-5}	1.382×10^{-5}	0.7350
10	1.246	1006	0.02439	1.944×10^{-5}	1.778×10^{-5}	1.426×10^{-5}	0.7336
15	1.225	1007	0.02476	2.009×10^{-5}	1.802×10^{-5}	1.470×10^{-5}	0.7323
20	1.204	1007	0.02514	2.074×10^{-5}	1.825×10^{-5}	1.516×10^{-5}	0.7309
25	1.184	1007	0.02551	2.141×10^{-5}	1.849×10^{-5}	1.562×10^{-5}	0.7296
30	1.164	1007	0.02588	2.208×10^{-5}	1.872×10^{-5}	1.608×10^{-5}	0.7282
35	1.145	1007	0.02625	2.277×10^{-5}	1.895×10^{-5}	1.655×10^{-5}	0.7268
40	1.127	1007	0.02662	2.346×10^{-5}	1.918×10^{-5}	1.702×10^{-5}	0.7255
45	1.109	1007	0.02699	2.416×10^{-5}	1.941×10^{-5}	1.750×10^{-5}	0.7241
50	1.092	1007	0.02735	2.487×10^{-5}	1.963×10^{-5}	1.798×10^{-5}	0.7228
60	1.059	1007	0.02808	2.632×10^{-5}	2.008×10^{-5}	1.896×10^{-5}	0.7202
70	1.028	1007	0.02881	2.780×10^{-5}	2.052×10^{-5}	1.995×10^{-5}	0.7177
80	0.9994	1008	0.02953	2.931×10^{-5}	2.096×10^{-5}	2.097×10^{-5}	0.7154
90	0.9718	1008	0.03024	3.086×10^{-5}	2.139×10^{-5}	2.201×10^{-5}	0.7132
100	0.9458	1009	0.03095	3.243×10^{-5}	2.181×10^{-5}	2.306×10^{-5}	0.7111

Solid materials

Composition	Melting Point, K	Properties at 300 K				Properties at Various Temperatures (K), $k(\text{W/m}\cdot\text{K})/c_p(\text{J/kg}\cdot\text{K})$					
		ρ kg/m ³	c_p J/kg·K	k W/m·K	$\alpha \times 10^6$ m ² /s	100	200	400	600	800	1000
Aluminum:											
Pure	933	2702	903	237	97.1	302	237	240	231	218	
						482	798	949	1033	1146	
Alloy 2024-T6 (4.5% Cu, 1.5% Mg, 0.6% Mn)	775	2770	875	177	73.0	65	163	186	186		
						473	787	925	1042		
Alloy 195, Cast (4.5% Cu)		2790	883	168	68.2			174	185		
Copper:											
Pure	1358	8933	385	401	117	482	413	393	379	366	352
						252	356	397	417	433	451
Commercial bronze (90% Cu, 10% Al)	1293	8800	420	52	14		42	52	59		
							785	160	545		
Phosphor gear bronze (89% Cu, 11% Sn)	1104	8780	355	54	17		41	65	74		
							—	—	—		
Cartridge brass (70% Cu, 30% Zn)	1188	8530	380	110	33.9	75	95	137	149		
							360	395	425		
Constantan	1493	8920	384	23	6.71	17	19				
Stainless steels:											
AISI 302		8055	480	15.1	3.91			17.3	20.0	22.8	25.4
								512	559	585	606
AISI 304	1670	7900	477	14.9	3.95	9.2	12.6	16.6	19.8	22.6	25.4
						272	402	515	557	582	611
AISI 316		8238	468	13.4	3.48			15.2	18.3	21.3	24.2
								504	550	576	602

Appendix **B**

Data collection sheet

Location data

Sit Name	Altitude (m)	Latitude	Longitude	Surrounding condition		
				Ordinary Ground	Gravel Roof	Forestry
Wonji-Shoa						

Contact at Metrology

1. Contact one

Name: **Position:**

Phone:

Email:

2. Contact two

Name: **Position:**

Phone:

Email:

Meteorological data

Month	Daily Global Solar Radiation in Horizontal (kWh/m ² /day)	Daily Difusive Solar Radiation in Horizontal (kWh/m ² /day)	Amb. pr. (kpa)	Amb. Temp (°C)		Wind Vel. (m/s)	Abs. Humidity (kg w. v/kg d. a)	Av. Sunshine day	Max. Av. Sunshine day	Sunrise hr	Sunset hr
				T max	T min						
Jan											
Feb											
Mar											
Apr											
May											
June											
July											
Aug											
Sept											
Oct											
Nov											
Dec											

Flow demand pattern and fuel type data

Flowrate Measure Attempt (L/sec)	Working hour (hr.)											
	1	2	3	4	5	6	7	8	9	10	11	12
1												
2												
3												
4												
5												
6												
7												
8												
9												
10												

Fuel Source for Water Heating Property and Type Data

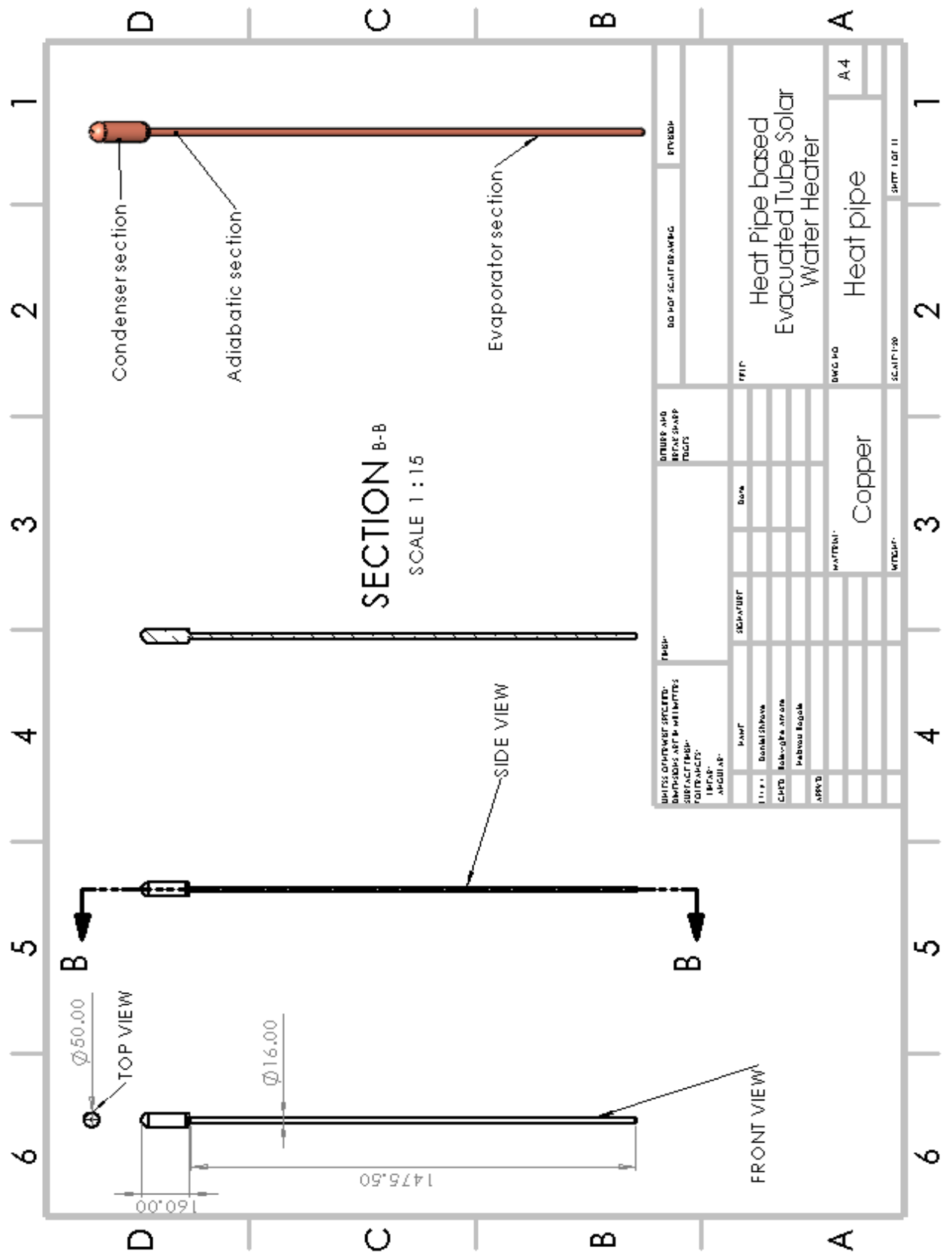
Fuel source	Alternative use of fuel	Use of fuel unit/day	Total hot water production	Total electric production

For biomass use

Moisture content (%)	Emission content	Combustion Technology

Appendix **C**

Drawing sheet

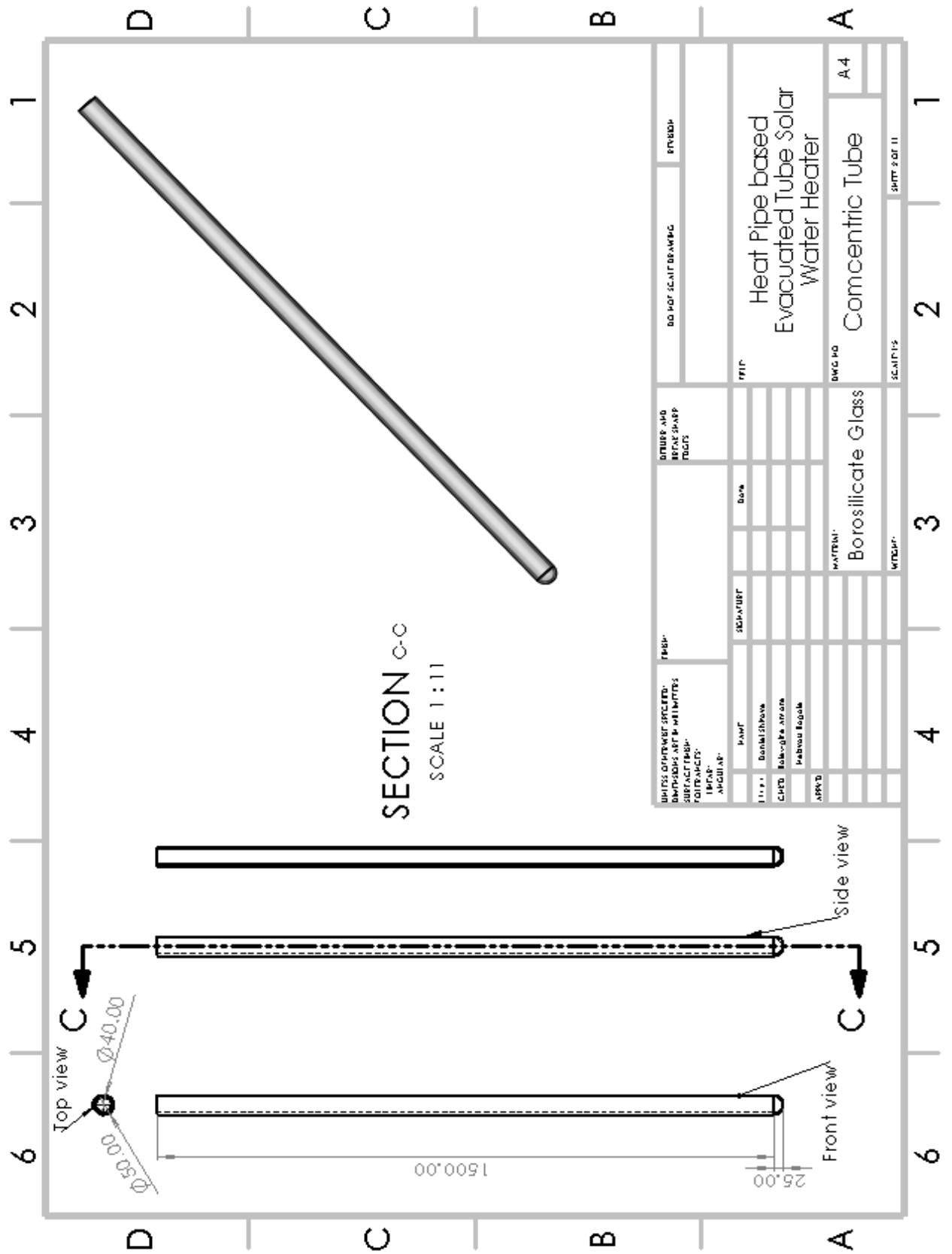


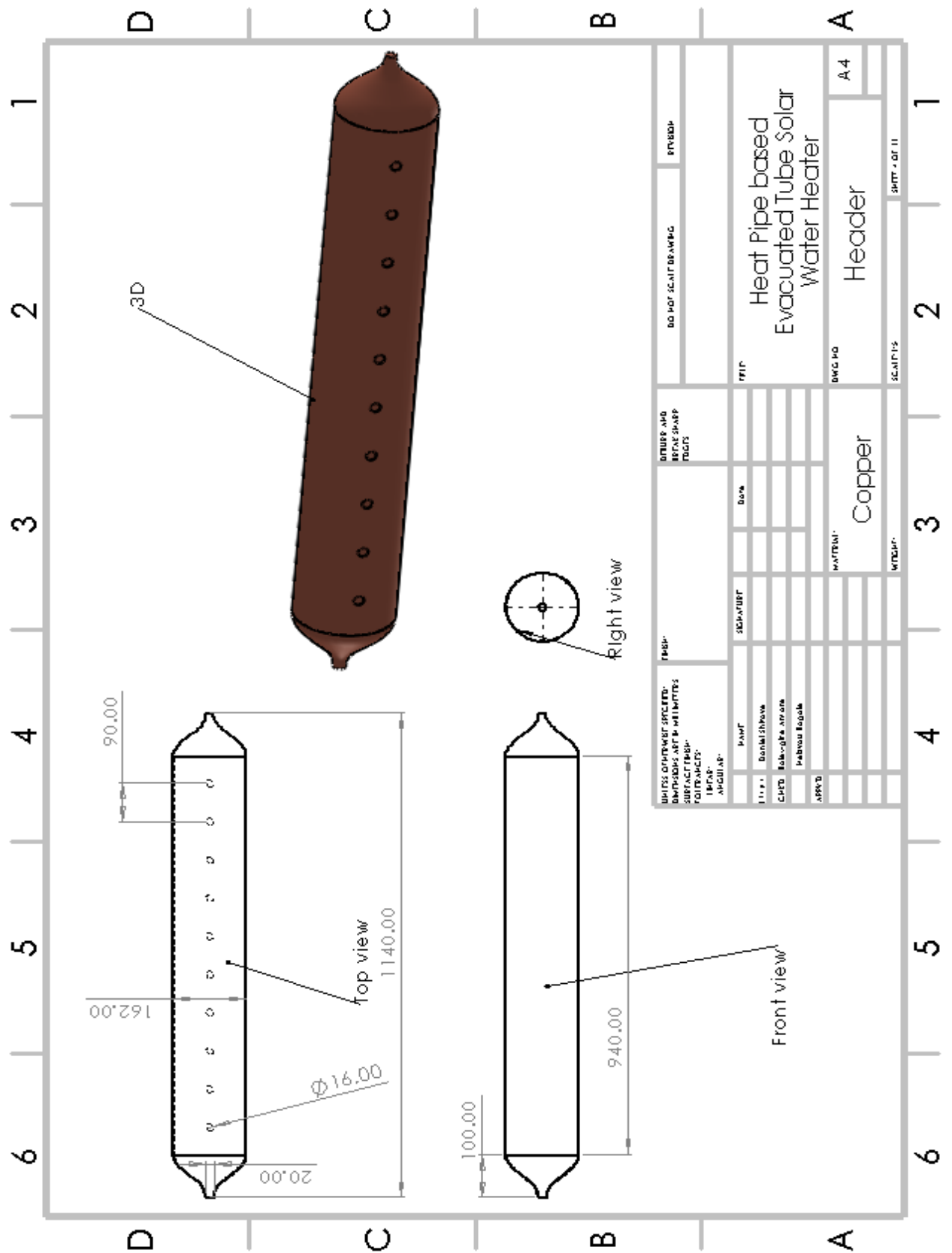
DATE	DESCRIPTION	BY	CHECKED	APPROVED	SCALE	SHEET NO.	TOTAL SHEETS
11.11.2023	DESIGN	DANISH KHAN			1:15	01	01
12.11.2023	CAD	HABIBU RAGHA					
13.11.2023	APPROVAL						

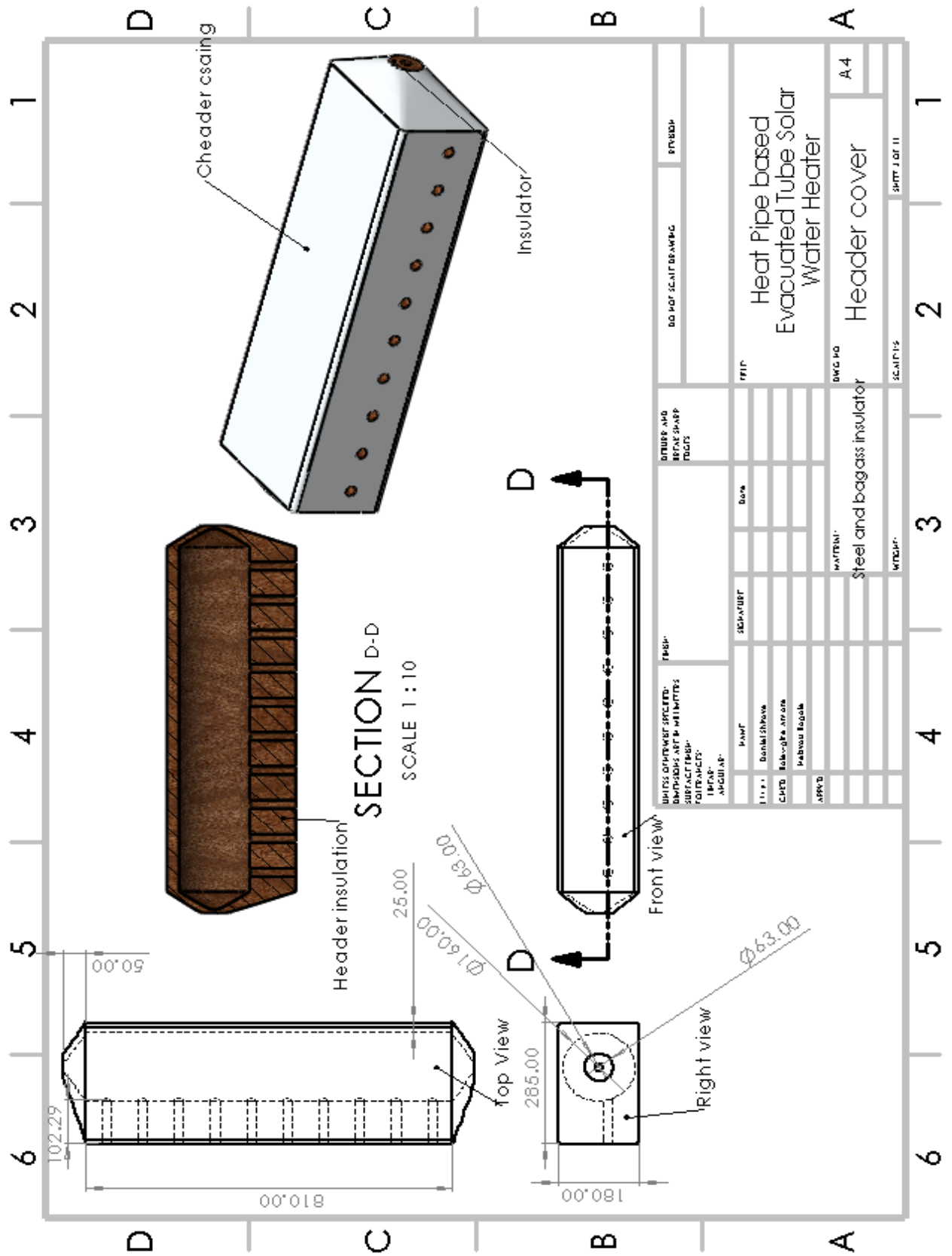
ITEM NO.	DESCRIPTION	QUANTITY	UNIT	REMARKS
01	CONDENSER SECTION	1	SECTION	
02	ADIABATIC SECTION	1	SECTION	
03	EVAPORATOR SECTION	1	SECTION	

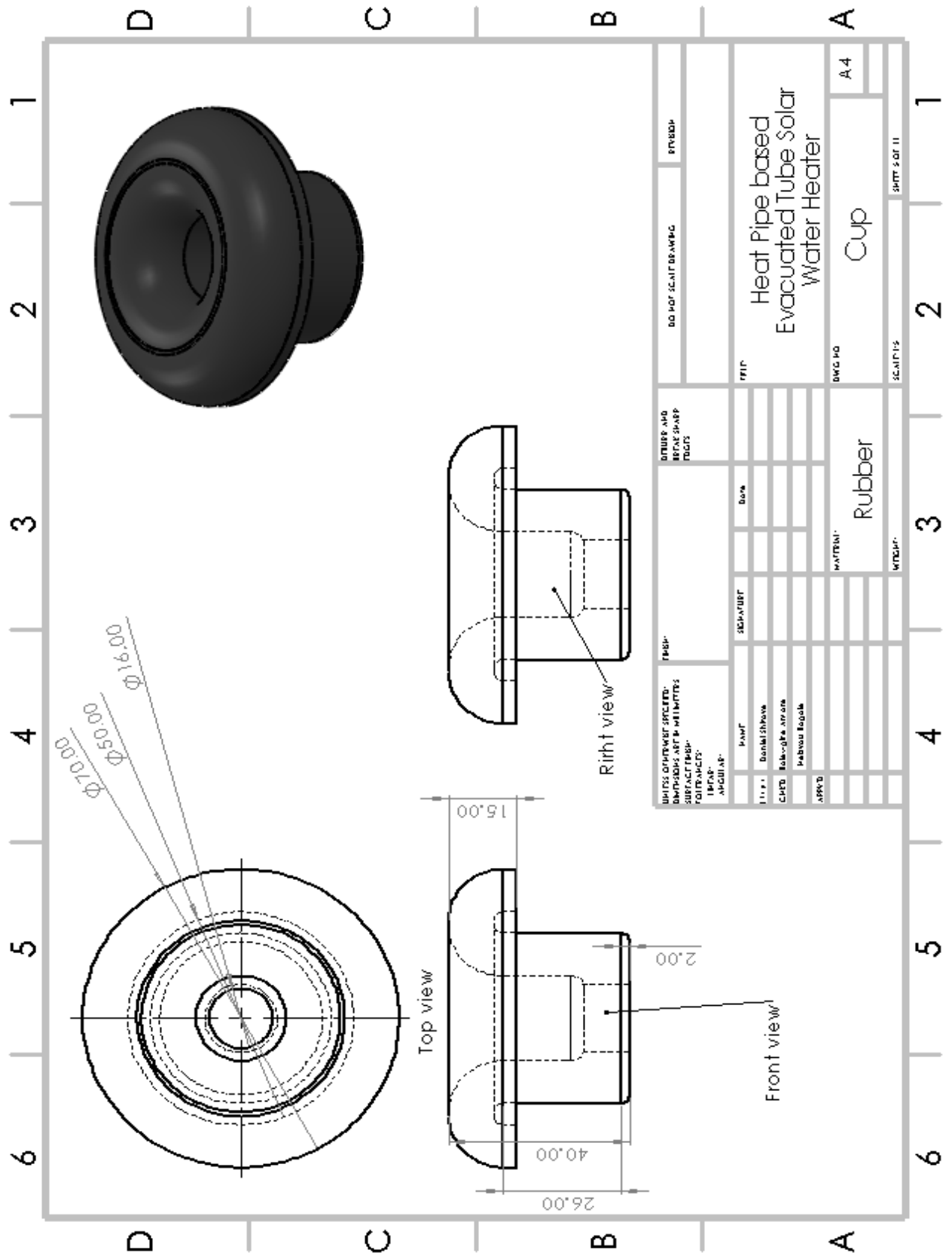
ITEM NO.	DESCRIPTION	QUANTITY	UNIT	REMARKS
01	COPPER TUBE	1	SECTION	

ITEM NO.	DESCRIPTION	QUANTITY	UNIT	REMARKS
01	COPPER TUBE	1	SECTION	









DATE: 01/05/2017		TIME: 10:30		BY: DR. S. K. SINGH		FOR: DR. S. K. SINGH	
DESIGNER: DR. S. K. SINGH		CHECKER: DR. S. K. SINGH		DATE: 01/05/2017		TIME: 10:30	
PROJECT: Heat Pipe based Evacuated Tube Solar Water Heater		PART: Cup		MATERIAL: Rubber		SCALE: 1:1	
NO.	REV.	DATE	BY	REASON	APPROVED	DATE	BY
1	0	01/05/2017	DR. S. K. SINGH	ISSUED FOR MANUFACTURE	DR. S. K. SINGH	01/05/2017	DR. S. K. SINGH

